NASA CONTRACTOR REPORT

NASA CR

NASA CR-1671

APPLICATIONS OF HOLOGRAPHY TO VIBRATIONS, TRANSIENT RESPONSE, AND WAVE PROPAGATION

by D. A. Evensen and R. Aprahamian

Prepared by
TRW SYSTEMS GROUP
Redondo Beach, Calif.
for Langley Research Center

1. Report No. NASA CR-1671	2. Government Accession No.	3. Recipient's Catalog No.
4. Title and Subtitle Applications of Holography to Vibrations, Transient Response, and Wave Propagation		5. Report Date December 1970
		6. Performing Organization Code
7. Author(s) D. A. Evensen and R. Aprahamian		8. Performing Organization Report No. AM 70-11
		10. Work Unit No. 124-08-14-08
9. Performing Organization Name and Address TRW Systems Group One Space Park Redondo Beach, California 90278		11. Contract or Grant No. NAS1-8361
		13. Type of Report and Period Covered Contractor Report
12. Sponsoring Agency Name and Address National Aeronautics and Space Administration Washington, D. C. 20546		14. Sponsoring Agency Code

15. Supplementary Notes

Technical Film Supplement L-1081 available on request.

16. Abstract   This report is concerned with the application of holographic techniques to three areas of applied mechanics:

   o   High-frequency Vibrations of Beams and Plates

   o   Transient Response Studies

   o   Studies of Transverse Wave Propagation

Time-average holography was used to record over 30 vibration modes of a cantilever beam, and stored-beam (real-time) interferometry was used to identify over 100 modes of an 8" x 10" simply-supported plate. The resonant frequencies involved ranged from 9 cps to 100,000 cps. Experimental and theoretical results for mode shapes and resonant frequencies are given for both the beam and the plate.

The transient response of a 20" cantilever beam was determined using the technique of stored-beam (real-time) holographic interferometry combined with high-speed motion picture photography. The resulting displacement-time histories are compared with analytical results for the response problem.

The transverse wave propagation study was conducted using pulsed laser holography. Interferograms were obtained of a bending wave propagating in a long beam. Experimental plots of the bending displacement vs. distance along the beam were obtained, and these data were compared with analytical results for the problem.

Wherever possible, detailed comparisons were made between theory and experiment. and in virtually all cases the agreement was favorable. A technique of extending holography to measure large-amplitude vibrations is presented, and some potential applications of holography to applied mechanics are discussed.

17. Key Words (Suggested by Author(s)) Time average, real time, pulse holography High-frequency vibration Timoshenko theory Plate and beam experiments	18. Distribution Statement Unclassified - Unlimited

19. Security Classif. (of this report) Unclassified	20. Security Classif. (of this page) Unclassified	21. No. of Pages 145	22. Price* $3.00

FOREWORD

This contract was administered in the Structural Dynamics Branch, Dynamics Loads Division, LaRC, with John S. Mixson as the technical monitor. In addition to his routine duties as monitor, Mr. Mixson supplied analytical results for the transient response test and the wave propagation study which greatly improved our understanding and confidence in the experimental data.

Other contributors to this study include Drs. L. O. Heflinger, R. F. Wuerker, and R. E. Brooks of TRW's Physical Research Center, who provided helpful technical advice on many occasions. Robert Haborak was primarily responsible for the success of the movie which was produced as part of this contract, and J. E. Wright did an outstanding job in technical support of the experiments. The work was performed in the Advanced Technology Department of the Applied Mechanics Laboratory, TRW Systems Group.

APPLICATIONS OF HOLOGRAPHY TO VIBRATIONS, TRANSIENT RESPONSE, AND WAVE PROPAGATION

David A. Evensen

and

Robert Aprahamian

TRW Systems Group

SUMMARY

Holography is a lensless imaging technique which allows the reconstruction of three-dimensional images. A related technique, called holographic interferometry, allows one to measure static or dynamic displacements on the order of a wavelength of light. The present report is concerned with the application of these holographic techniques to three areas of applied mechanics: (i) high-frequency vibrations of beams and plates, (ii) transient response measurements, and (iii) studies of transverse wave propagation.

High-Frequency Vibrations

Time-average holography was used to identify over 30 transverse vibration modes of a cantilever beam. The fundamental frequency of the beam was 9 cps, and the highest mode identified was at 100,000 cps. Photographs of beam vibration modes are included herein. Similar tests were run using 8" x 10" simply-supported plate, and stored-beam holographic interferometry was used to identify the plate vibration modes in real time. The fundamental frequency of the plate was 162 cps, and over 100 modes were identified using holography at frequencies up to 76,768 cps. Photographs were made of selected modes, and several are included herein. The experimental patterns for the vibrating plate are readily interpreted, and the rapid, graphic display of the mode shapes in real-time makes these holographic techniques very attractive. To emphasize these features of holography, a 10-minute sound movie entitled "Vibration Analysis Using Holographic Interferometry" was produced. Motion-picture film supplement L-1081 has been prepared and is available on loan. A request card and a description of the film are included at the back of this document.

The high-frequency vibration studies demonstrated that holography is a new and useful tool for vibration analysis. At frequencies of 50,000 cps and above, vibration patterns were obtained for modes which had not been observed by any other means. The experimental data agreed well with vibration theories which include rotatory inertia and shear effects; the experiments provided verification of these theories at high frequencies.

A possible drawback with the use of time-average holography for some applications is a restriction to small amplitude vibrations. For large vibration amplitudes, the interference fringes can crowd together and become difficult to interpret. In addition, time-average holography requires that the optical system be isolated from background noise and vibration. Exploratory studies reported herein indicate that these two difficulties can be overcome by the use of pulsed laser holography. This conclusion is supported by recent work using pulsed holography for large amplitude vibrations of noisy subjects.

Transient Response

The transient response of a 20" cantilever beam was determined by using the technique of stored-beam (real-time) holographic interferometry combined with high-speed motion picture photography. A stored-beam hologram of the cantilever beam was set up, and the beam was subjected to a transverse impact at the tip. A high-speed motion picture camera was placed behind the hologram to record the motion of the interference fringes caused by the impact. The data contained on the movie film was reduced frame-by-frame yielding the displacement-time history of several stations along the length of the beam. The experimental results were compared with analytical solutions for the transient response, and generally good agreement was obtained.

The transient response test demonstrated the feasibility of a new measuring technique which had not been used previously. This technique has the advantages that no sensor need be attached to the structure, and that data can be easily recorded over a large are of the structure. Displacement-time histories of individual points on the structure can be obtained subsequent to viewing the overall response. A disadvantage of the method is that each movie frame must be examined individually, which turned out to be a laborious task. This disadvantage can be partially overcome by using a photocell-and-counter technique, but this approach is still under development.

Wave Propagation

The transverse wave propagation study was conducted using pulsed laser holography. A bending wave was initiated in a long beam by impacting it in the center with a ballistic pendulum. Interferograms of the bending pulse were obtained at three distinctly separated times, and changes in the pulse shape were readily detected at the different times. Experimental plots of the bending displacement vs. distance along the beam were obtained, and these results were in good agreement with analytical results for the problem.

The wave propagation study provided the first photographs of a bending wave propagating in a beam. Previous experiments using strain gages or displacement pickups gave the response of the beam (at one point) as a function of <u>time</u>. The present results provide the displacement as a function of the distance along the beam (at a particular time). Further

studies of wave propagation problems using holography appear quite promising, and pulsed laser holography will provide the basic experimental technique for these studies.

1.0 INTRODUCTION

Holography is a lensless imaging process which allows the reconstruction of three-dimensional images of diffuse objects (Refs. 1,2). A related technique, known as holographic interferometry (Ref. 3), allows the experimenter to measure static or dynamic displacements on the order of a wavelength of the light used to make the holograms (Ref. 4). This new experimental technique represents a powerful tool for studying problems in experimental mechanics. Holographic interferometry has been applied to such problems as wave propagation (Ref. 5), static stress measurements (Ref. 6), and aerodynamic flow (Ref. 7,8). It was first applied to vibration analysis by Powell and Stetson (Ref. 9) in 1965, and it has been extensively applied to steady-state vibrations since then (Refs. 10, 11, 12, 13).

The basic motivation of these early papers on the applications of holography to vibrations was to demonstrate the feasibility and potential of the technique. The main objective of the present investigation was to exploit this potential in the areas of high-frequency vibrations, transient motions, and the propagation of transverse bending waves. At the start of this work (1968) the following assessment was made with respect to the state-of-the-art concerning high-frequency vibrations:

"With present non-holographic measurement techniques, it is possible to experimentally determine the first 10 - 15 modes or so of a typical beam (or beam-like structure). However, holography promises an increase in measurement capability of two orders of magnitude; thus it appears feasible to determine many more modes than was formerly possible. For example, by using holography it may be possible to determine the first 50 - 100 modes of a beam, instead of only 10 - 15. An analagous situation exists for plates, where it appears that it may be possible to find the first 100 - 300 modes."

"For both beams and plates, shear deformation and rotatory inertia can have a significant influence on the higher vibration modes. Using Timoshenko beam theory, it is possible to estimate the alterations in mode shape due to these effects. By determining the higher vibration modes experimentally (using holography) one would be in a position to make some of the first direct comparisons between theory and experiment involving shear deformation and rotatory inertia."

In retrospect, now that the work has been completed, it is safe to say that holography lived up to our expectations.

The work reported herein is divided into five main parts, as follows:

 o Holography and Holographic Interferometry

 o Steady-State Vibration Tests

o   Transient Response Tests

o   Wave Propagation Study

o   Suggestions for Future Experiments

The section on holography is intended to explain the fundamentals of the technique to vibration engineers and others not already familiar with the subject.   The steady-state vibration tests include the results of high frequency experiments on a 30-inch cantilever beam and an 8" x 10" simply-supported rectangular plate.   The fundamental frequency of the beam was 9 cps, and over thirty additional transverse modes were identified; the corresponding resonant frequencies ranged from 500 cps to over 100,000 cps.   The fundamental frequency of the simply-supported plate was 162 cps, and more than 100 plate modes were identified using stored-beam interferometry, at frequencies as high as 76,768 cps.   Many of these plate modes were recorded on time-average holograms, and photographs from several of the holograms are included herein.   The experimental patterns for the vibrating plate are readily interpreted, and they are even more graphic than the well-known Chladni sand figures.   The resonant frequencies and mode shapes show good agreement with the theory, providing rotatory inertia and shear effects are included for the higher modes.   In addition to being described herein, the results of the beam vibration studies are detailed in Reference 14, and the plate results are reported in Reference 15.

Transient response tests were run using a 20-inch cantilever beam and stored-beam holography.   In this technique, live interference fringes were formed when the beam was subjected to a transverse impact at the tip. The rapid movement of the interference fringes was recorded using a high-speed motion picture camera.   By analyzing the motion of the fringes on the movie film, the deflection time-history of the tip of the beam was determined.   The experimental time-history showed excellent agreement with the calculated response of the beam; some of these transient results were reported in Reference 16.   The wave propagation study was conducted using pulsed laser holography and a beam of rectangular cross-section approximately 6 feet long.   A transverse bending wave was initiated in the beam by impacting it transversely with a ballistic pendulum.   Double-exposure holograms were made using a pulsed laser, which was triggered to illuminate the beam as the bending wave propagated along it.   The very short pulse width of the laser (on the order of 10^{-8} sec.) was sufficient to effectively "freeze" the motion of the stress wave.   Interferograms were made with the wavefront at three successive locations along the beam.   From these interferograms, the lateral deflection of the beam was determined as a function of position along the beam.   These deflection plots were very similar to analytical results for the problem.

The suggestions for future experiments include static applications such as shell buckling and two-dimensional strain measurements as well as further work in vibrations.   The suggestions presented are accompanied by preliminary data or references which appear promising for future applications of holography.

5

2.0 HOLOGRAPHY AND HOLOGRAPHIC INTERFEROMETRY

Introduction and Background

The term "holography" is used to describe a means of recording the amplitudes and phases of waves, such as light waves or sound waves. Holography originated with Gabor (Ref. 1) who pointed out the possibility of recording (on a piece of photographic film) the <u>amplitudes and phases</u> of coherent, monochromatic light waves transmitted through a transparent object. By then projecting light through the photographic film (which is called a "hologram") it is possible to reproduce a <u>three-dimensional image</u> or the original object.

The reproduction of images as Gabor suggested became practical with the advent of the laser as a source of monochromatic, coherent light. In 1964, Leith and Upatnieks (Ref. 2) demonstrated that a three-dimensional image of an opaque object could be reconstructed in a manner similar to that proposed by Gabor. Figure 1 shows a typical set-up of the apparatus used in the Leith and Upatnieks holographic method.
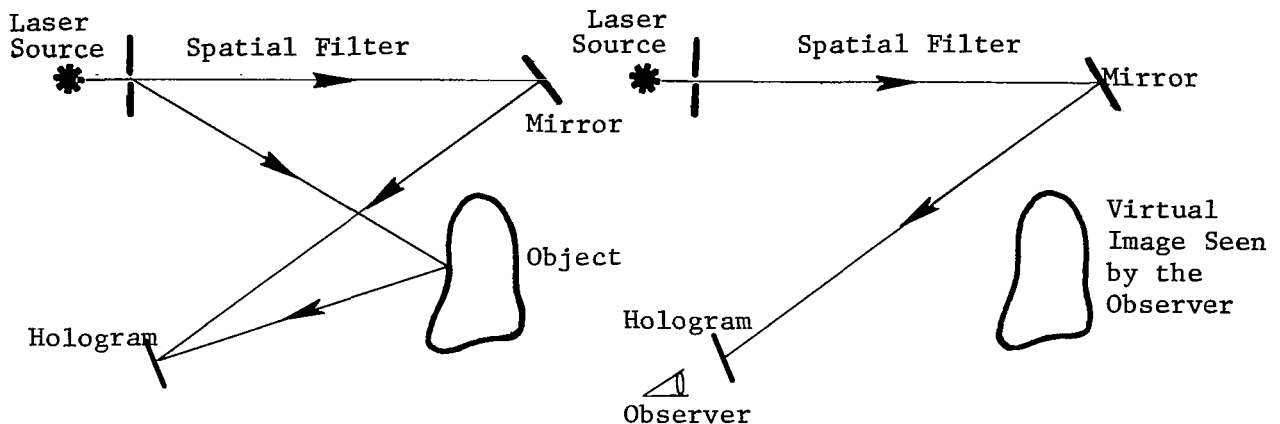
Figure 1 - Left: Image Recording Process

Right: Image Retrieval

6

In making the hologram, the light waves from the object (object beam) interact with the light from the mirror (reference beam). When the light from the mirror is _in phase_ with the light from the object, the waves add; conversely, the waves cancel one another when they are out of phase. This type of interaction results in variations in the intensity of the light striking the photographic film (these are _spatial_ variations in intensity, in the plane of the hologram.) Since photographic film reacts to the intensity of light impinging on it, the exposed film gives a permanent record of the interaction of the two light beams.

To reconstruct the image of the object from the hologram, the developed photographic film is illuminated with any monochromatic light source, e.g., the original laser. Now the light interacts with the _hologram_, and the result is a three-dimensional image of the original object. Such a reconstructed image can be quite impressive, to say the least. For example, Heflinger, Brooks, and Wuerker of TRW Systems have made a hologram of a bullet in flight (Ref. 3). With the usual schlieren photographs of a bullet, the shock waves appear as _lines_ in the picture. From the hologram, however, one is able to see the _conical_, _three-dimensional nature of_ the shock waves.

The reconstruction of images in this fashion can be described mathematically as follows.

In the formation of the hologram, let the light coming from the object be denoted by

$$O = A_1 e^{i\phi_1} \tag{2-1}$$

where A_1 is the real amplitude and ϕ_1 is the phase. The harmonic factor $e^{i\nu t}$ has been omitted for convenience in Equation (2-1), and A_1, ϕ_1 are to be evaluated at the plane of the hologram. In a similar fashion, the light from the reference beam which reaches the plane of the hologram can be described by

$$R = A_2 e^{i\phi_2} \tag{2-2}$$

The amplitude of the light impinging on the hologram is the sum of the object beam plus the reference beam, which gives

$$U = O + R = A_1 e^{i\phi_1} + A_2 e^{i\phi_2} \tag{2-3}$$

The hologram, which is a photographic plate, responds to the _intensity_ of the light. The light intensity in the plane of the hologram is given by

$$I = UU^* = A_1^2 + A_2^2 + A_1A_2e^{i(\phi_1-\phi_2)} + A_1A_2e^{(\phi_2-\phi_1)} \qquad (2-4)$$

where U* denotes the complex conjugate of U. Since the photographic film responds to the intensity, I, a recording of Equation (2-4) is made by the hologram.

When the hologram is re-illuminated by the reference beam (and the object removed from the scene) the light transmitted by the hologram is given by L = R (transmittance) = R(1-KI) where K is a constant; i.e.,

$$L = A_2e^{i\phi_2}\left(1 - K[A_1^2 + A_2^2 + A_1A_2e^{i(\phi_1-\phi_2)} + A_1A_2e^{i(\phi_2-\phi_1)}]\right) \qquad (2-5)$$

Or, multiplying out the individual terms,

$$L = [1-K(A_1^2 + A_2^2)]A_2e^{i\phi_2} - KA_1A_2^2e^{i\phi_1} - KA_1A_2^2e^{i(2\phi_2-\phi_1)} \qquad (2-6)$$

The first term in Equation (2-6) is equivalent to the original reference beam $A_2e^{i\phi_2}$, but it has been modified by the scalar $1 - K(A_1^2 + A_2^2)$. The second term contains $A_1e^{i\phi_1}$, and as such it is equivalent to the light coming from the original object (multiplied by the scalar $- KA_2^2$). Thus it is the second term which gives rise to the reconstructed image of the original object. The third term in Equation (2-6) represents a conjugate wave, and it may be regarded as emanating from a fictitious but identical object situated in a different plane.

This brief discussion of the mathematics behind the holographic process contains only the bare essentials and neglects many of the technical details involved. The reader interested in the details of the process may want to consult recent text books (Refs. 17-19) or the original papers (Refs. 1, 2); a more complete discussion of some useful equations related to holography is given in Appendix A.

Holographic Interferometry and Pulsed Laser Holography

Although image reconstruction was one of the first applications of holography, a technique that has more potential from a research standpoint is "double-exposure holography," which is one form of holographic interferometry (Ref. 3). The essential ideas are as follows: first make a hologram of the object you wish to examine; then subject the object to loads which cause it to deform, and expose the same hologram for a second time. Now when this "double-exposed hologram" is developed and then

illuminated, two images are produced: one is from the undeformed body, the other from the deformed body. These light waves (which form the two images) interact with one another, thereby creating interference fringe patterns. By analyzing the fringe patterns, one can determine the surface deformations of the body, which were caused by the applied load. Haines and Hildebrand (Ref. 4) give expressions which show how to relate the interference fringes with the surface deformations of the object. An extensive mathematical description of holographic interferometry was presented recently in Ref. 20.

Holographic interferometry is exemplified by pulsed laser holography, which was used herein to record a transverse wave propagating along a beam. First the laser was pulsed once to expose the hologram showing a stationary beam. Then a stress wave was initiated in the beam, and a second pulse of the laser was timed to expose the hologram when the wave had traveled part way along the beam. The resulting double-exposed hologram was developed and its fringe pattern was analyzed to obtain the shape of the bending wave. A detailed discussion of these results is given in Section 5, and they are mentioned here as an illustration of pulsed laser holography.

Pulsed laser holography can be applied to vibration problems, and such applications are discussed in Section 6. The more usual technique (for steady-state vibrations) is time-average holography, which is discussed in the next section.

Time-Average Holography

To understand time-average holography, it is instructive to consider the ordinary time-exposure photography of a vibrating object, such as a swinging pendulum. As the pendulum swings back and forth, its velocity is a maximum at the bottom of the swing and goes to zero when the pendulum reaches its maximum displacement. In a time exposure of the swinging pendulum, then, the film is exposed primarily where the velocity is zero (at the extremes of the swing) and is exposed very little where the velocity is a maximum. A time-averaged hologram of a vibrating object is directly analogous to the time exposure of the pendulum. First, the object to be studied is set into vibration in one of its resonant modes. Then a hologram is made by exposing the photographic plate for a "long" period of time (e.g. several vibration periods). Because of the sinusoidal nature of the vibration, the hologram is exposed primarily when the amplitude of vibration is at its maximum (and the velocity is zero). The result is a hologram which yields a fringe pattern that represents peak-to-peak displacement in a normal mode. By analyzing the fringe pattern from such a time-average hologram it is possible to measure the surface displacements of the vibrating body. An analysis of fringe patterns from time-average holograms was first presented by Powell and Stetson (Ref. 9), who considered the case where the vibrations were normal to the surface being examined. The analytical results involve the roots of J_o (the zero-order Bessel function) and are discussed in Section 3.0.

9

Stored-Beam Holography

Stored-beam holography provides the experimenter with a visual means of detecting and identifying vibration modes in real-time, and it was used in the present study. This type of holography gives rise to "live" interference fringes, which shift and change as the object of interest moves and deforms. In the live fringe method, a hologram of the undeformed, stationary object is made and developed. This hologram is then very carefully put back in its original position, i.e., it is put back in the photographic plate holder where it was originally held. The hologram is then illuminated by the laser and reconstructs an image of the undeformed object superimposed on the real object. Now suppose the object being studied is allowed to deform: then the light from the deformed body interacts with the stored image of the undeformed body (produced by the hologram) and a live interference fringe pattern is formed.

When this live fringe technique is applied to an object which is vibrating sinusoidally in a normal mode, the fringe pattern appears to be stationary to the experimenter. In actuality, the fringe pattern shifts and changes rapidly, but the human eye acts as a time-averaging device and the fringe pattern seen by the observer is much like that from a time-average hologram. A discussion of vibration analysis in real-time using the stored-beam technique is given in Ref. 21. Other studies using real-time holography are given in Ref. 22.

Another technique which uses stored-beam principles is stroboscopic holographic interferometry (Ref. 23). In this technique, the laser beam is flashed periodically in synchronization with the vibration being observed. A common procedure is to use a variable speed motor with a disc mounted on it to interrupt the laser beam periodically. A hologram of the stationary, undeformed object is also used in the stroboscopic method. Although this technique was not used herein, it does have application to vibration analysis and may be of interest to some readers; see Refs. 10, 23, and 24.

3.0 STEADY-STATE VIBRATION TESTS

Summary

This section contains a description of the steady-state vibration tests which were conducted on a cantilever beam and a simply-supported rectangular plate. The beam tests are discussed first, followed by the plate results. In both cases, the experimental set-up is presented and followed by the test procedure. Some analytical considerations are required to interpret the experimental results, and a section is devoted to each. The discussion concludes with a comparison of analysis with the experiments. Experimental mode shapes are compared with analytical curves, and frequency vs. mode number results are presented.

Beam Vibration Modal Survey

Experimental Set-Up. - The beam which was tested was an aluminum (6061-T6) cantilever 30 inches long, 1 inch wide, and one-quarter of an inch thick. The supported end was clamped to a steel support block in such a fashion that the beam vibrated in a horizontal plane. The support block was 8 inches long, 5 inches high, and 6 inches wide; it weighed approximately 65 lbs. and was simply placed on the granite table, not cemented down.

With this arrangement, the fundamental frequency of the beam was found to be 9 cps. In order to provide a diffuse optical surface, the beam was subjected to a liquid honing process. Liquid honing is a process similar to shot-peening or sand-blasting, and it is commercially available at many machine shops and specialty companies. The resulting surface has a diffuse, satin finish, which can be uniformally illuminated without highly reflective "hot spots."

The apparatus used to make the holograms of the cantilever is shown schematically in Figure 2. Figure 3 is a photograph of the actual equipment and layout. The light, 0, emitted by the laser is directed to a beam splitter BS by means of the mirror, M1. Three beams of light are emitted from the beam splitter and designated as 01, 02, and R. Two of these, 01 and 02, are primary beams, which are used to illuminate the cantilevered specimen. They are directed by means of mirrors, M2 and M3, respectively, through a double set of diffusers, D1 and D2, onto the cantilever. The third beam of light, R, is due to internal reflections in the beam splitter. It is weak in intensity compared to 01 and 02 and is ideal to use as a reference beam. It is directed by mirrors M4 and M5 to a spatial filter, SF. The spatial filter consists of a 60X lens and a 6 micron pinhole. The 60X lens brings the light, R, to a focus. However, due to imperfections inherent in such a high power lens, the focal point is not really a "point," but rather a "zone." The micron pinhole is adjustable to allow only the "cleanest" light in the focal zone to pass. Other small imperfections in the light, e.g. due to higher modes in the laser cavity, are also

11
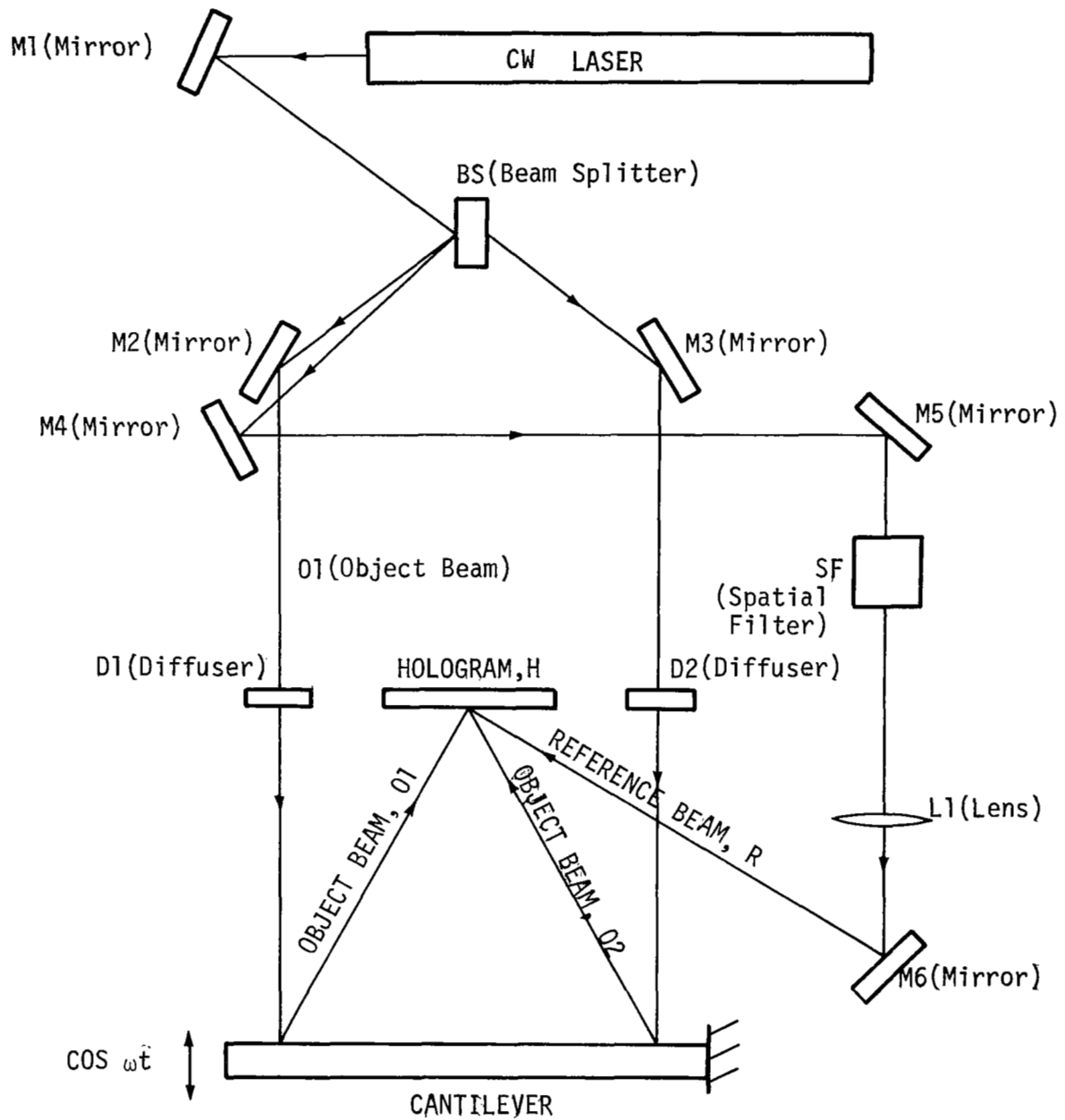
Figure 2 - The Apparatus Used in Making Holograms of
the Cantilever Beam
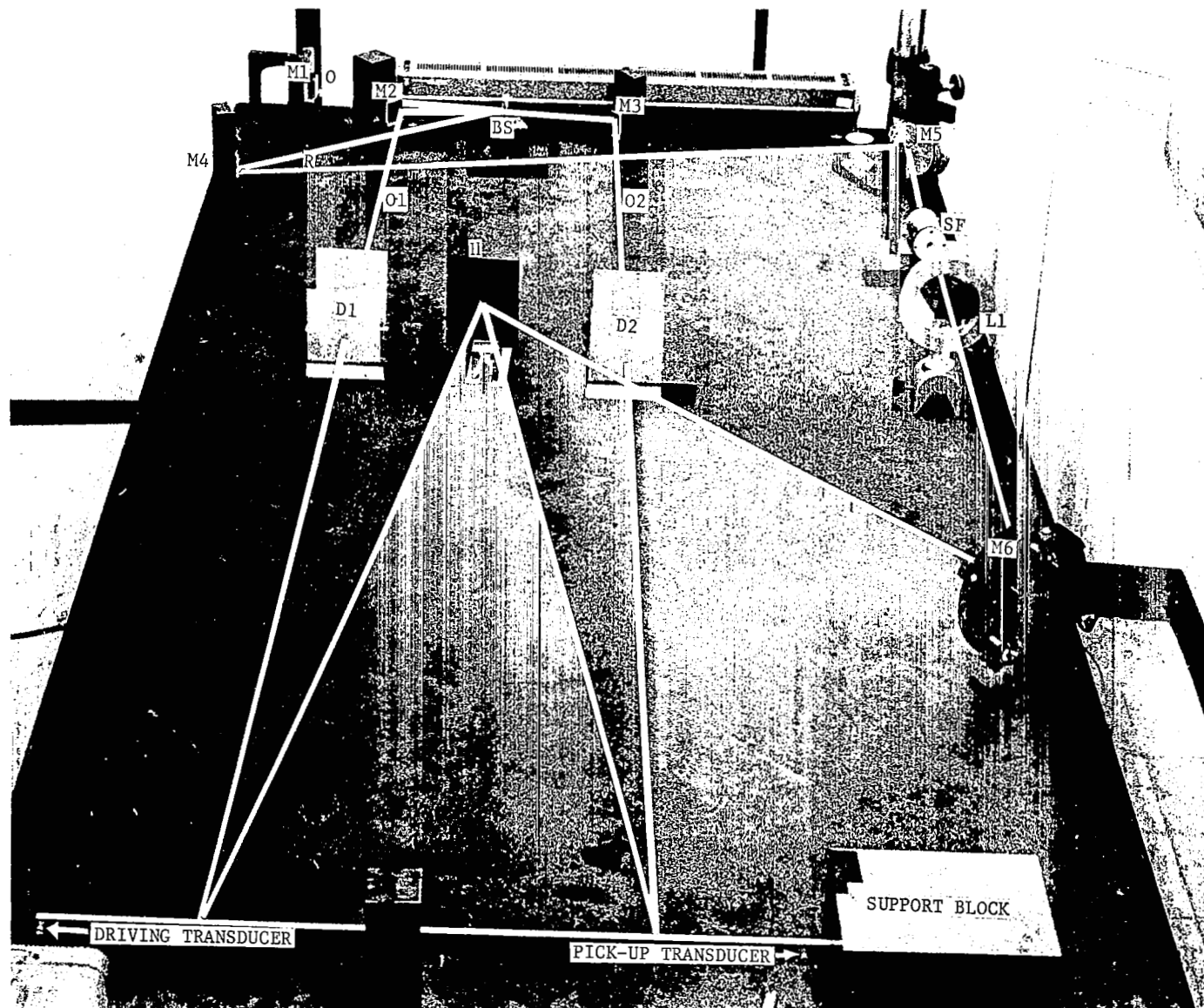
Figure 3 - Actual Equipment Used to Make Holograms

removed by the spatial filter. Upon leaving the spatial filter, the light is collimated by means of the lens, L1, and the collimated light is directed by the mirror, M6, to strike the high resolution photograph plate, H. It is vitally important that the total path lengths of beams 01, 02, and R (measured from the beam splitter to the hologram) do not differ from each other by an amount greater than the "coherence length" of the laser. If this condition is not satisfied, the beams of light, 01 and 02, will not interact properly with the reference beam, R, to produce interference patterns at the photographic plate; in this case, no hologram will result. For the 15 milliwatt helium-neon laser used in the experiments, the "coherence length" was approximately 25 cm. (10 in.).

The optical equipment and the cantilever beam were placed on a large (8,000 lbs.) granite table that was shock-isolated from the laboratory surroundings. (The granite table is shown in Figure 3.)

The cantilever was excited to resonance by means of a piezoelectric crystal transducer connected to a standard oscillator-amplifier set-up. This driving transducer was cemented to the tip of the beam, and a similar pick-up transducer was mounted near the root. The pick-up transducer was connected to an oscilloscope which monitored the response of the beam. An electronic counter was used to accurately determine the excitation frequency. The transducers and some of the electronic equipment are shown in Figures 3 and 4.

The driving transducer was cylindrical in shape, approximately 5/16 of an inch in diameter and 3/8 of an inch long. It was made by cementing two disc-shaped piezoelectric (ceramic) crystals together, and a thin metal disc was then cemented to the top. This resulted in a "stack" of wafers or discs, as shown in Figure 5. The complete transducer weighed approximately 4 grams when assembled.

When a sinusoidal voltage was applied to the transducer, the ceramic crystals would alternately expand and contract, causing the metal disc to move back and forth along the axis of the transducer. A sinusoidal force resulted (due to the inertia of the metal disc) which was transmitted to the beam and used to excite it to resonance.

OSCILLATOR

OSCILLOSCOPE

AMPLIFIER

VOLT METER

BEAM

BEAM SUPPORT STRUCTURE

15
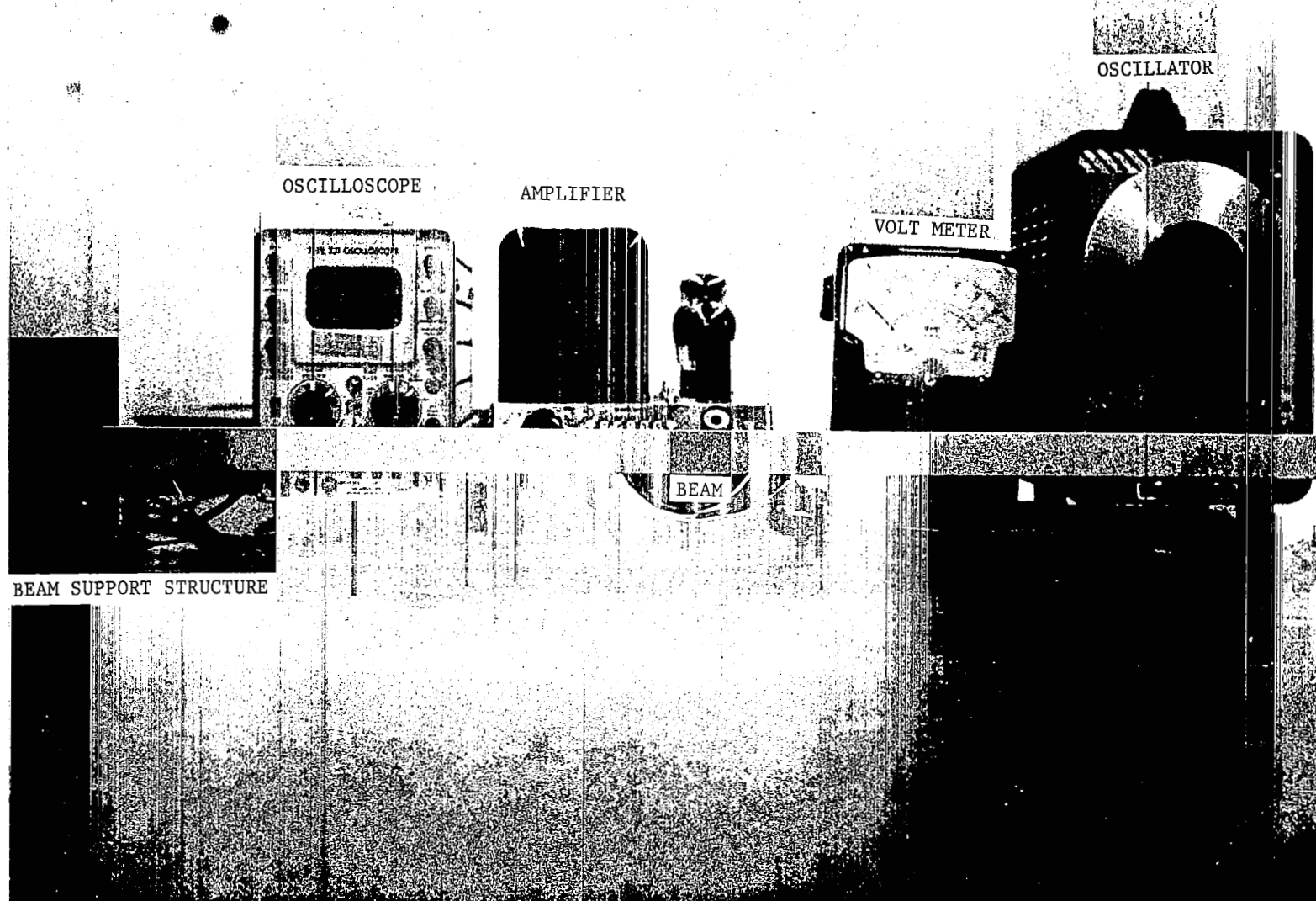
Figure 4 - Close-up of Cantilever Beam and Electronics
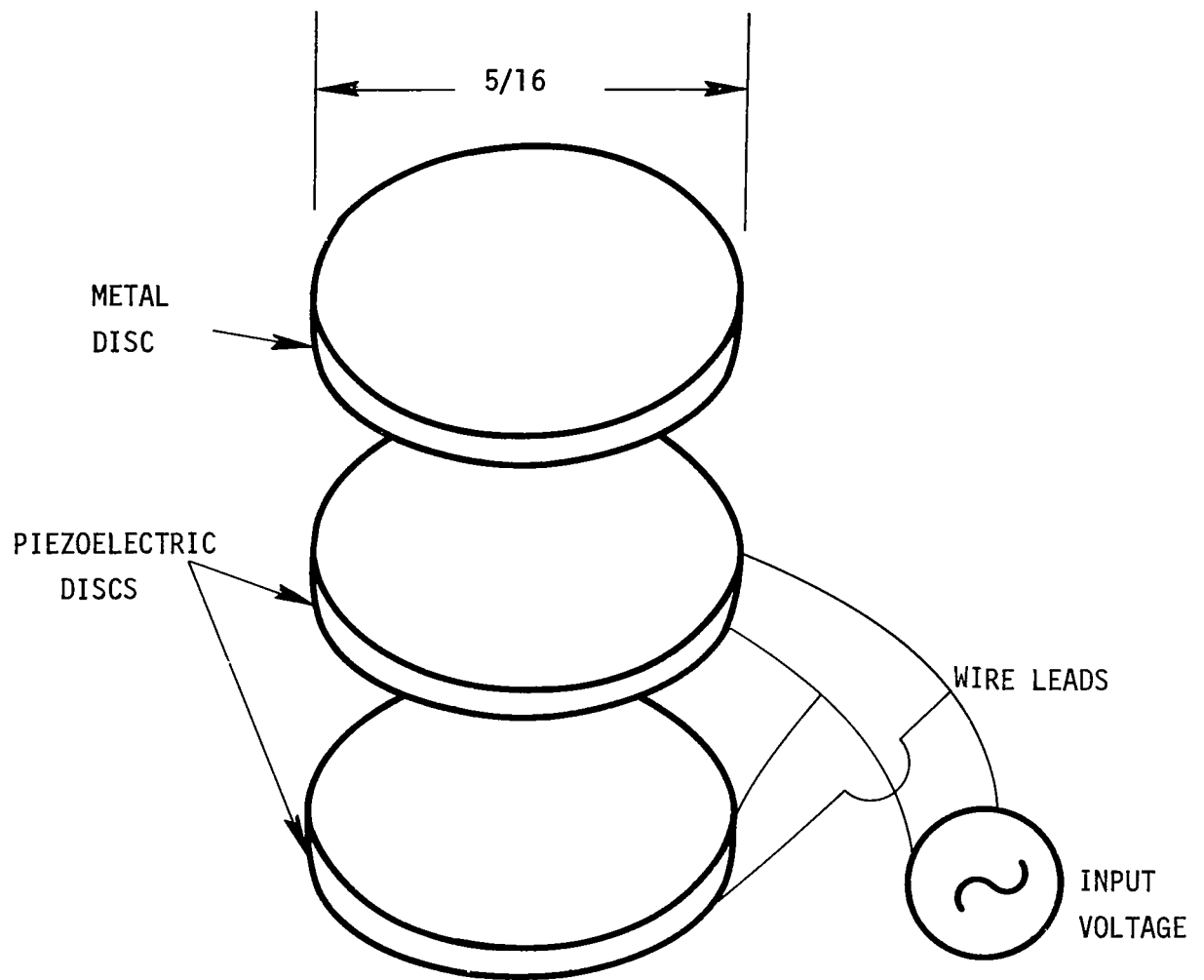
Figure 5 - Schematic of Piezoelectric Transducer

Test Procedure. – The test procedure was simply to tune the oscillator until a large, resonant response was indicated on the oscilloscope. Then the resonant frequency was determined by the counter and recorded. Having found a resonant mode of the beam, the next step was to make a time-average hologram to record the nodal pattern and mode shape. Since the primary purpose was to investigate transverse vibration modes (as opposed to torsional modes) it was necessary to distinguish the type of resonant response. It was readily determined form the oscilloscope that the transverse modes exhibited the usual linear resonance peaks, whereas the torsional modes possessed noticeable nonlinearities in their response. This distinction made it possible to photograph only the desired transverse modes.

Initial attempts to make time-average holograms of the vibrating beam were unsuccessful, due to the presence of undesirable responses of the lower modes of the beam. These low-frequency motions were excited by such things as seismic disturbances and vehicular traffic which were sufficient to move the beam more than one wavelength of the light employed to make the holograms. This problem was overcome by designing a support with a pointed metal stud which could be positioned at a node of the desired mode. This support prevented the low frequency modes from being excited, and successful holograms were made with it in place. A photograph obtained from one such hologram is shown in Figure 6, which will be discussed shortly.

In addition to using the time-averaging technique to record the modes, an attempt was made to employ live fringe interferometry to identify the modes. First, a hologram was made of the unexcited beam. In this case, the auxialiary support stud could not be employed, and consequently the beam was stationary only in the immediate vicinity of the root. Then the developed hologram was put back into the plate holder and the beam was excited by the driving transducer. This arrangement produced live fringes near the root of the beam, and the type of mode (torsional and transverse) could be readily identified by direct visual observation. The live fringe procedure was used to identify a mode at 99,395 cps, and then a time-average hologram was made to record the complete mode shape. A photograph made from this hologram will be discussed in a subsequent section.

Interpretation of the Fringe Patterns – Once the holograms have been made, it is necessary to reconstruct the interference fringe pattern and then to interpret it. Reconstructing the pattern is accomplished by first developing the exposed photographic plate and then illuminating it with the reference beam, R. Figure 6 shows a photograph of a reconstructed image and fringe pattern. The object with the white vertical lines on it is the cantilever beam vibrating in its 21st mode (10,121 cps). For comparison purposes, a 30 inch ruler is shown alongside the beam. The white vertical stripes on the beam represent nodal positions; since they do not move during the vibration, they are brightly exposed on the time-average hologram. The black fringes between consecutive white stripes on Figure 6 can be related to the mode shape of the beam. The curvature of these fringes is attributed to anticlastic behavior of the beam. Such curved

17
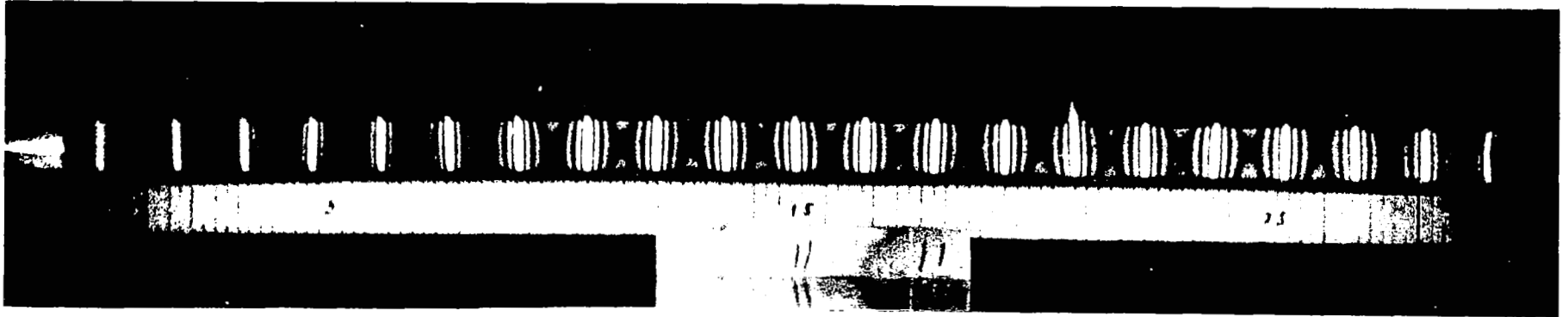
Figure 6 - Photograph of the Image Obtained by Making a Hologram
of the Cantilever Beam Vibrating in its 21st Mode

fringe patterns have been observed previously in the static bending of beams (Ref. 6). For purposes of analysis, the central axis of the beam was used to determine the mode shapes.

The fringe patterns were interpreted by using the analysis presented by Powell and Stetson (Ref. 9). Their results show that the amplitude of vibration for points on the beam which are covered by a fringe can be related to the roots of J_o, the zero-order Bessel function. That is, a fringe is formed where

$$J_o (\Omega_i) = 0 \qquad\qquad (3-1)$$

and Ω_i is defined by

$$\Omega_i = \frac{2\pi}{\lambda} [\cos\theta_1 + \cos\theta_2]A_i \qquad\qquad (3-2)$$

where

    λ is the wavelength of light used to make the holograms

    θ_1 is the angle between the displacement vector of the beam and the line of sight of the observer through the hologram

    θ_2 is the angle between the displacement vector of the beam and the illuminating light source

    A_i is the amplitude of vibration (at fringe i)

The angles θ_1 and θ_2 are shown in Figure 7. A helium-neon laser was used in the experiments, and λ was 6328 Angstroms. At Ω_1, the first root of J_o, we have

$$\Omega_1 = 2.405 = \frac{2\pi}{\lambda} [\cos\theta_1 + \cos\theta_2] A_1$$

or
$$A_1 = \frac{\lambda}{2\pi} \frac{\Omega_1}{(\cos\theta_1 + \cos\theta_2)} = \frac{(4.75 \times 10^{-6} \text{ in.})}{1/2 \ (\cos\theta_1 + \cos\theta_2)} \qquad\qquad (3-3)$$

for the amplitude of vibration at the location of the first fringe. Similarly, the vibration amplitude A_2 corresponds to the second root, Ω_2, etc. Near the center of the beam, the optical arrangement was such that $\theta_1 \simeq \theta_2 \simeq 0$ and the amplitudes are especially easy to compute. The first five fringe numbers and the corresponding vibration amplitudes A_n are given in Table I.
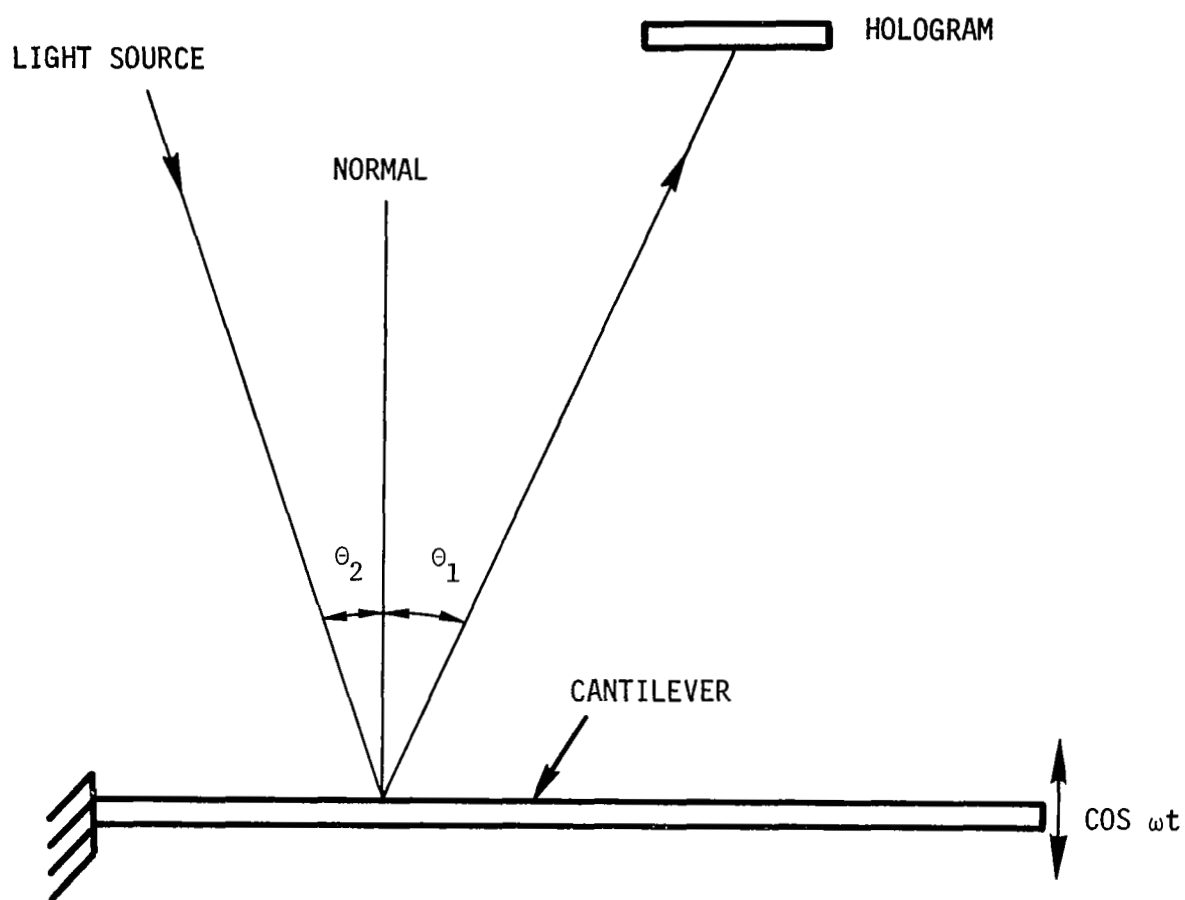
Figure 7 -   Diagram Showing the Angles Θ_1 and Θ_2.

TABLE I

Amplitude Determination for
Time-Average Holograms

Fringe Number	Root, Ω_i	Vibration Amplitude (inches)
1	2.405	4.75×10^{-6}
2	5.520	10.9
3	8.654	17.1
4	11.79	23.3
5	14.93	29.5

An example of fringes near the center of the beam and their interpretation is shown in Figure 8.

Referring to Figure 8, the first fringe (adjacent to a nodal line) occurs at an amplitude of 4.75×10^{-6} inches. The next fringe is formed where the amplitude of vibration is 10.9×10^{-6} inches, etc. As indicated in Figure 8, the values in Table I relate to single amplitude of vibration, not peak-to-peak displacement.

It should be noted that the vibration amplitude must be at least 4.75×10^{-6} inches for a fringe to form; this illustrates the lower limit of sensitivity of the time-average holographic technique.

Experimental Results and Comparisons with Analysis – The experimental results were in the form of time-average holograms which were recorded at the resonant frequencies of the modes involved. Photographs made from typical holograms are shown in Figure 9. Four very high-frequency modes are shown in Figure 10. Appendix B contains additional beam vibration modes and their associated frequencies.

Equations (3-1) and (3-2) were used to determine the shape of the 21st mode from the corresponding hologram. This experimentally determined mode shape was compared with the results of a typical computer program (Ref. 25) which employs Timoshenko Beam Theory; the comparison is illustrated in Figure 11. Discrepancies near the tip are probably due to the effect of the driving transducer.

Additional mode shapes and frequencies were calculated, and these results were compared with the corresponding experimental values. Such a comparison on the basis of frequency versus mode number is shown in Figure

FRINGE PATTERN

BEAM DISPLACEMENT

4.75×10^{-6}

4.75×10^{-6}

10.9×10^{-6}
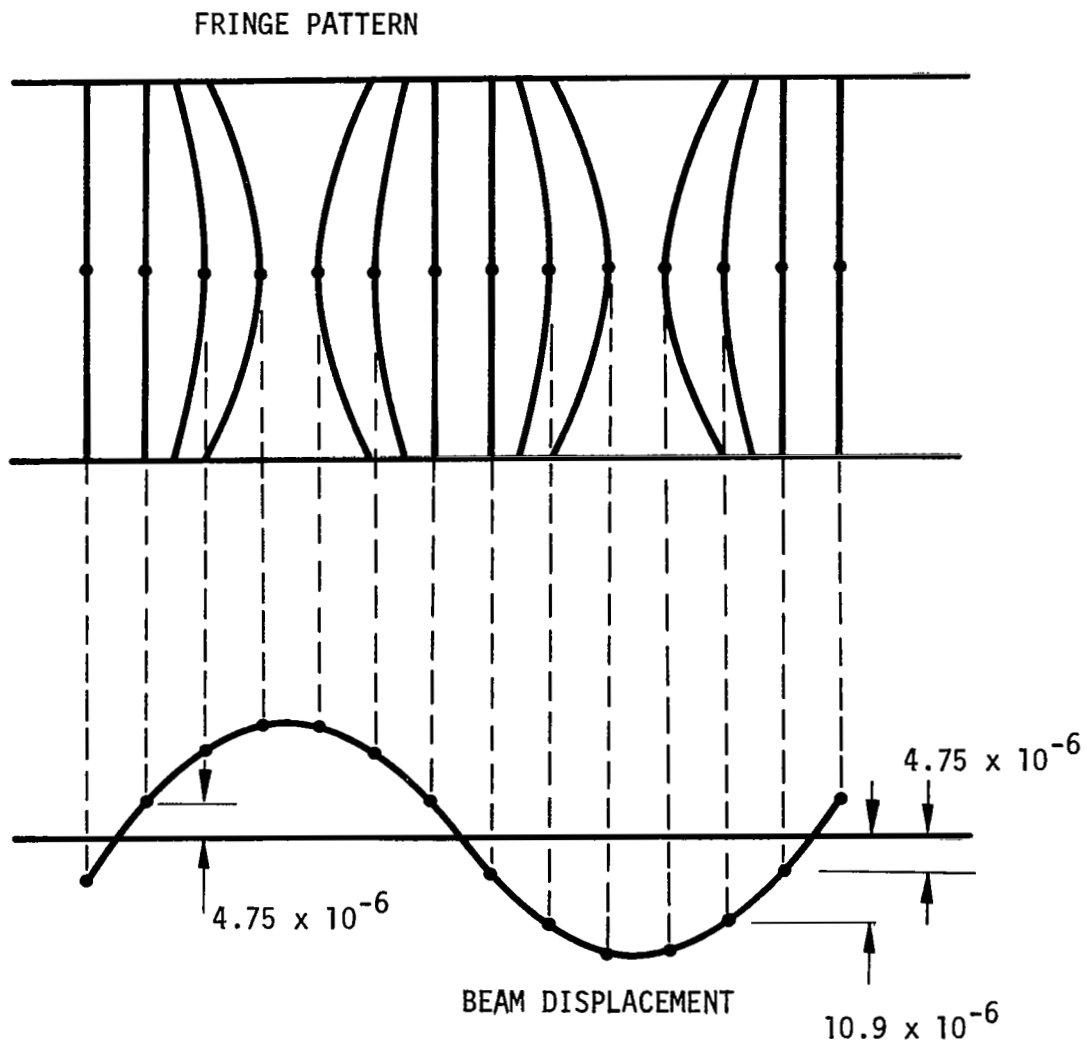
Figure 8 - Typical Fringe Pattern and Corresponding
Vibratory Displacement.

22
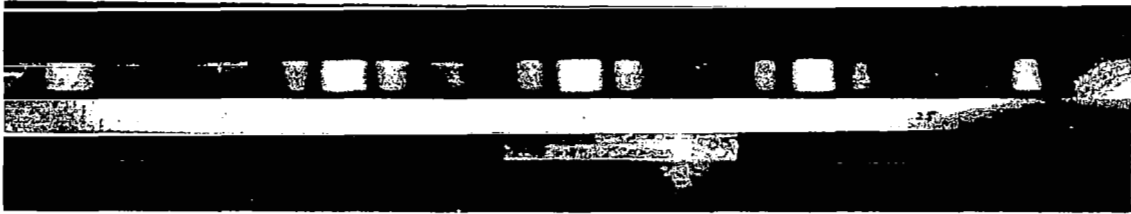
(a) 5th mode, f = 500 cps

(b) 15th mode, f = 5155 cps
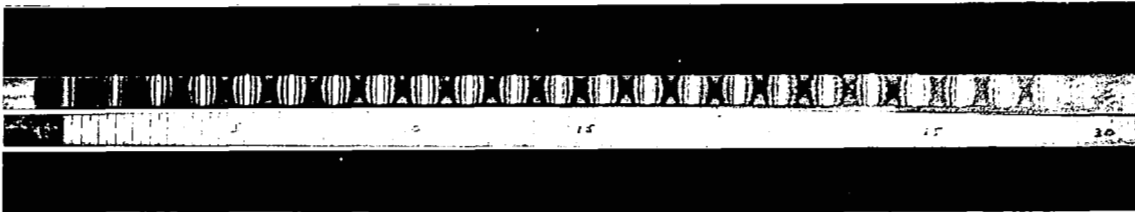
(c) 24th mode, f = 13,148 cps
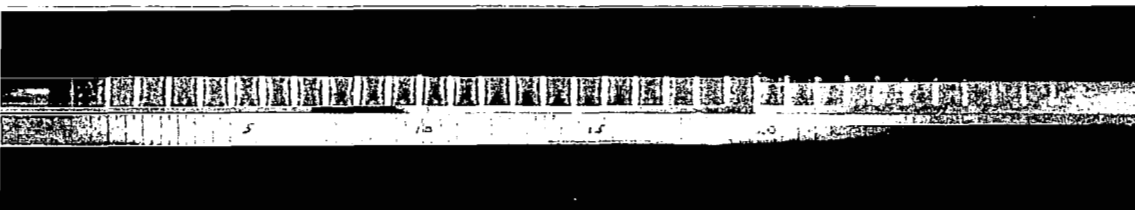
(d) 34th mode, f = 25,665 cps

Figure 9 - Transverse Vibration Modes (Cantilever Beam)

23
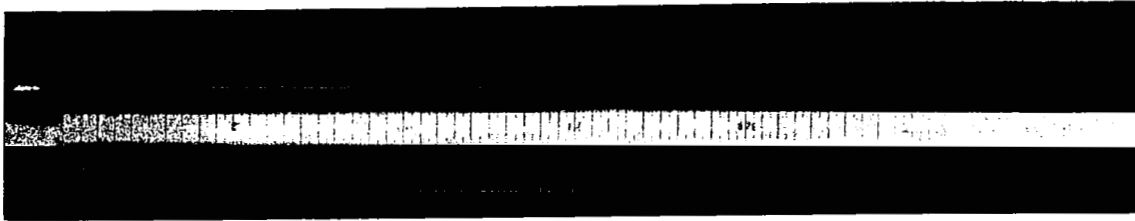
(a)   Plate-type Mode, f = 71,662 cps
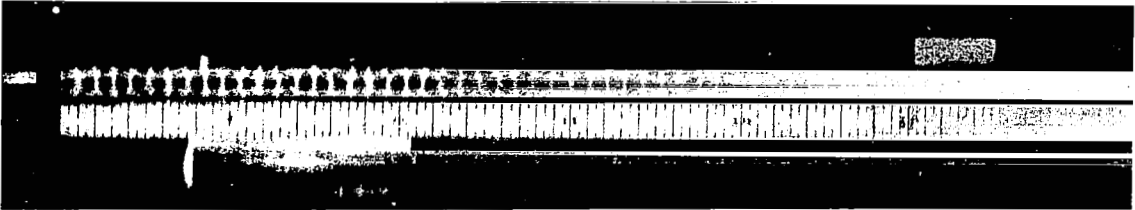
(b)   Plate-type Mode, f = 100,315 cps
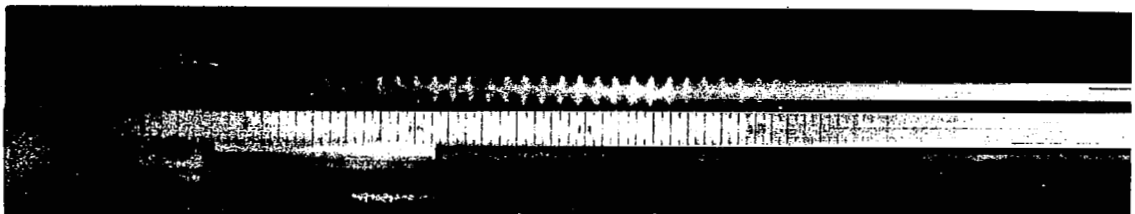
(c)   Torsional Mode, f = 72,846 cps

(d)   Transverse Mode, f = 99,395 cps

Figure 10 - High Frequency Beam Modes
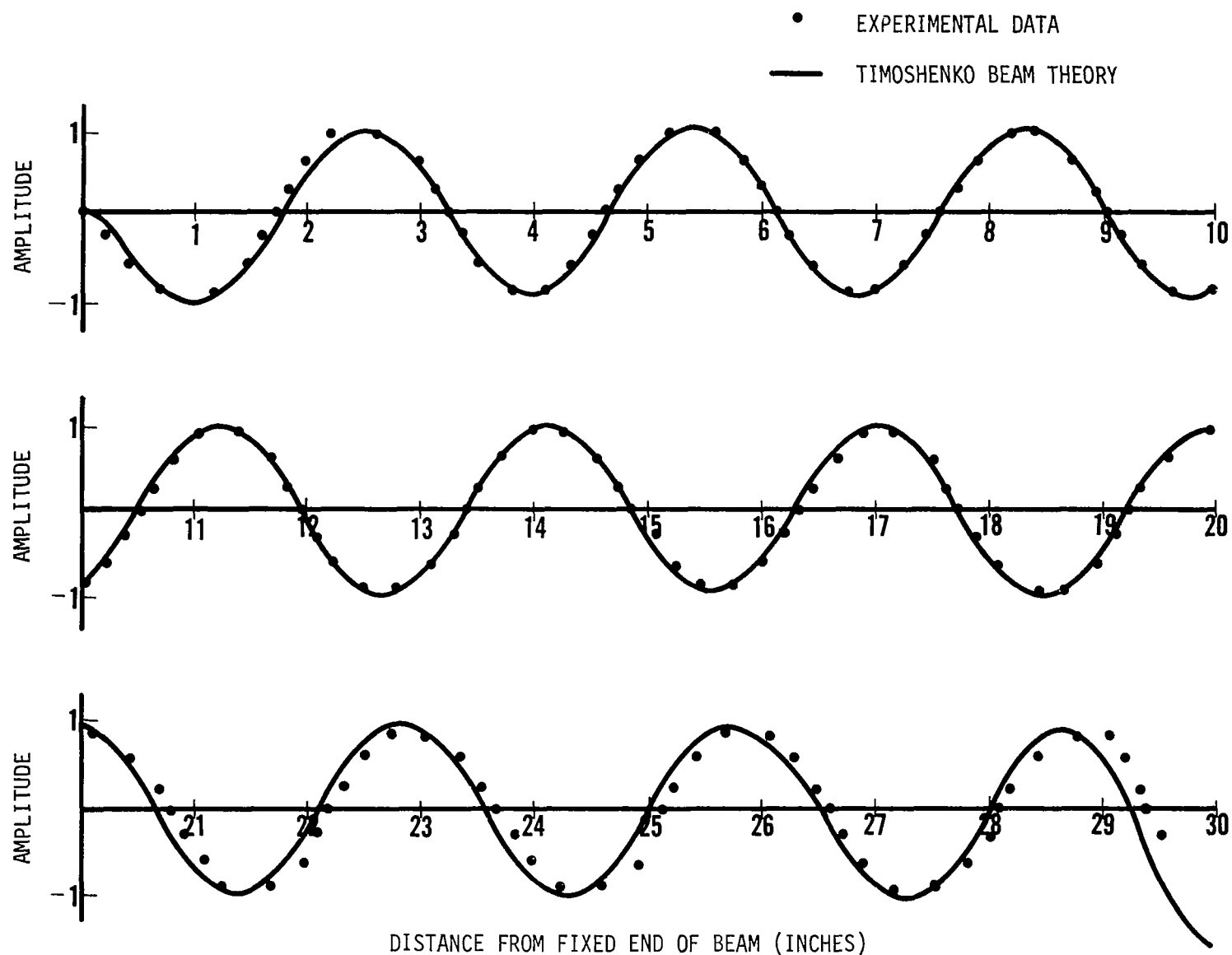
Figure 11 - Comparison of the Experimental and Calculated Shape for the 21st Mode (Cantilever Beam)

12. As illustrated therein, the calculated frequency (based upon Timoshenko Beam Theory) compares very well with the experiments. The data points plotted in Figure 12 are also given directly in Table II.

In order to find the limitations of the experimental technique, holograms were made of the beam vibrating in selected modes up to the 77th, which occurred at a frequency of 99,395 cps (see Figure 10). Other modes between the 34th and 77th were identified and the corresponding frequencies were noted. For these very high modes, the influence of boundary conditions becomes unimportant, and the frequencies can be calculated from the case of a traveling wave in an infinitely long beam. Using Timoshenko Beam Theory the resulting frequency equation is given by (Ref. 26):

$$\varepsilon \left(\frac{c}{c_o}\right)^4 - \left(\frac{c}{c_o}\right)^2 \left[\frac{3}{\pi^2}\left(\frac{d}{\Lambda}\right)^{-2} + 1 + \varepsilon\right] + 1 = 0 \qquad (3-4)$$

where $c_o = \left(\frac{E}{\rho}\right)^{1/2}$ is the bar velocity

c is the phase velocity

Λ is the wavelength of the bending wave

d is the depth of the (rectangular) cross-section

$\varepsilon = \frac{2(1 + \nu)}{R'}$

where ν is Poisson's ratio and R' is 5/6 for a rectangular cross-section.

The wavelength Λ was determined from the holograms, and the frequency, f, was measured directly by the electronic counter. By using the relation $c = f\Lambda$, it was possible to plot (c/c_o) vs Λ/d from the experiments.

These experimental results were compared with the lowest root of equation (3-4) as shown in Figure 13. The close agreement shown in Figure 13 again demonstrates the validity of Timoshenko Beam Theory for the vibration problem at hand. In interpreting Figure 13, note that the low-frequency long-wavelength modes lie near the origin; as one moves out along the curves, away from the origin, the frequencies increase and the wavelengths become shorter.

Although the main objective was to record transverse modes, additional modes were found in which the beam vibrated like a cantilevered plate. Figures 10(a) and 10(b) show modes in which there are two nodal lines parallel to the longitudinal axis of the beam. Several transverse nodal lines are also shown in the photograph, and these modes are classified as "cantilever plate modes." Figure 10(c) shows another related type of vibration pattern, an antisymmetric mode (a torsional mode) with a nodal line along the central axis of the beam. An additional torsional mode is shown in Appendix B.

26
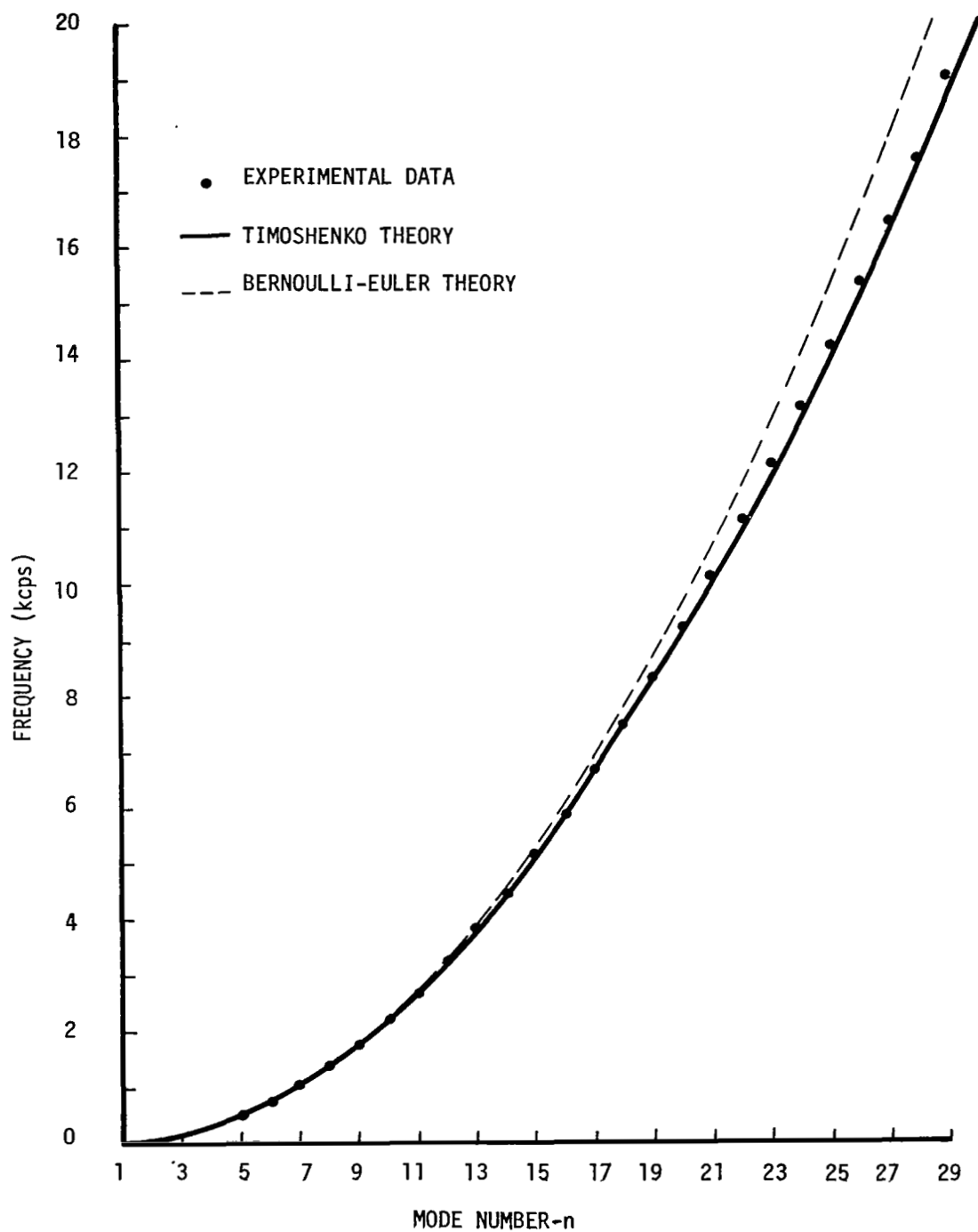
Figure 12 - Natural Frequency as a Function of
Mode Number (Cantilever Beam)

TABLE II

RESONANT FREQUENCIES (CANTILEVER BEAM)

MODE NUMBER	EXPERIMENTAL FREQUENCY (CPS)	CALCULATED FREQUENCIES	
		TIMOSHENKO	BERNOULLI – EULER
1	9	9.06	9.06
2		56.77	56.8
3		158.8	159.0
4		310.9	311.7
5	500	513.2	515.3
6	746	765.2	770.0
7	1044	1066.5	1075.8
8	1385	1416.4	1431.3
9	1777	1814.1	1838.5
10	2214	2259	2297
11	2698	2750	2805
12	3262	3287	3365
13	3843	3868	3976
14	4477	4492	4638
15	5155	5158	5350
16	5870	5866	6113
17	6640	6613	6928
18	7454	7399	7793
19	8308	8223	8709
20	9204	9084	9676
21	10,121	9979	10,693
22	11,106	10,908	11,762
23	12,111	11,870	12,882
24	13,148	12,864	14,052
25	14,200	13,947	15,274
26	15,365	15,364	16,546
27	16,401	16,158*	17,869
28	17,550	17,350*	19,243
29	19,085	18,700*	20,668
30	20,336	19,800*	22,144

*These values were obtained from the frequency equation for the Timoshenko Beam.
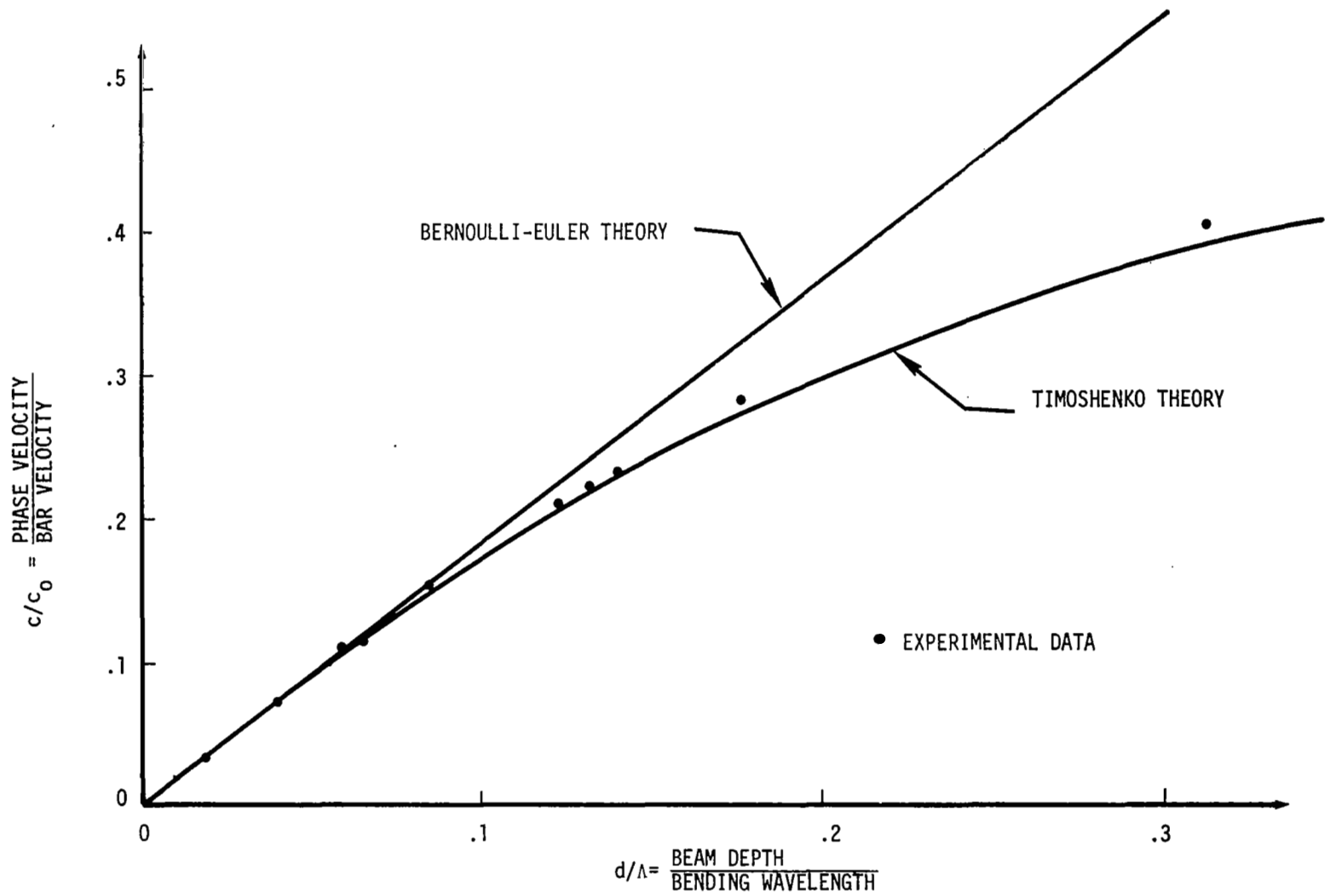
Figure 13 - Phase Velocity as a Function of Wavelength (Cantilever Beam)

In addition to identifying high-frequency transverse, torsional, and cantilever plate modes, it was desired to measure the damping value associated with a high-frequency mode. For this purpose, the 21st mode was excited to resonance and then the excitation was abruptly terminated. The exponential decay of the vibration was monitored by the pickup transducer; a very clean decay trace resulted, which gave a logarithmic decrement value $\delta = 1.59 \times 10^{-2}$. The associated frequency was 10,121 cps, and no indication of "beating" or excitation of adjacent modes was evident.

Plate Vibration Modal Survey

Experimental Set-up. – The plate which was tested was made from 1/16" thick aluminum sheet (6061-T6). The sheet was clamped in a rectangular frame, leaving an 8" x 10" panel in the center which was free to vibrate. Figure 14 shows a photograph of the plate and its clamping frame. Narrow vee grooves were cut at the boundaries of the panel to a depth of 0.024 in. This procedure was used to make the plate boundary conditions approach the case of simple supports. (Details of the plate supports are shown in Figure 15.) The plate was subjected to a liquid honing process in order to provide a diffuse optical surface.

A schematic of the apparatus used to make the holograms is shown in Figure 16. Light from the helium-neon, continuous-wave laser was directed through a spatial filter which expanded the beam sufficiently to simultaneously illuminate a reference mirror and the vibrating plate. Light reflecting from the mirror and the plate exposed the hologram as shown in Figure 16. After the photographic plate (the hologram) was developed, it was accurately repositioned in its holding fixtures, thereby making the system ready to be used for stored beam interferometry. Ideally, one would like to reposition the photographic plate to within a fraction of a wavelength of light. One way to accomplish this end is to develop the hologram in place, without moving it. (Special plate holders are commercially available for this purpose.) The method used herein was to remove the photographic plate, develop it, and put it back in the plate holder. The plate holder used for this purpose is shown in Figure 17. Such plate holders are commercially available or can be made by most well-equipped machine shops.

Time-average holograms were subsequently made with the same apparatus. In all cases, the relative intensities of the object beam and the reference beam were approximately in the ratio of 1:1, and high resolution spectographic plates were used to make the holograms. The optical equipment and the plate specimen were placed on a massive (8,000 lb.) granite table which was shock-isolated from the laboratory surroundings.

The plate was excited to resonance by means of a piezoelectric crystal transducer (see Figure 5) which was connected to a standard oscillatory-amplifier arrangement. The crystal transducer was cemented to the rear surface of the plate. An electronic counter was used to accurately determine the frequency of the signal used to drive the transducer.
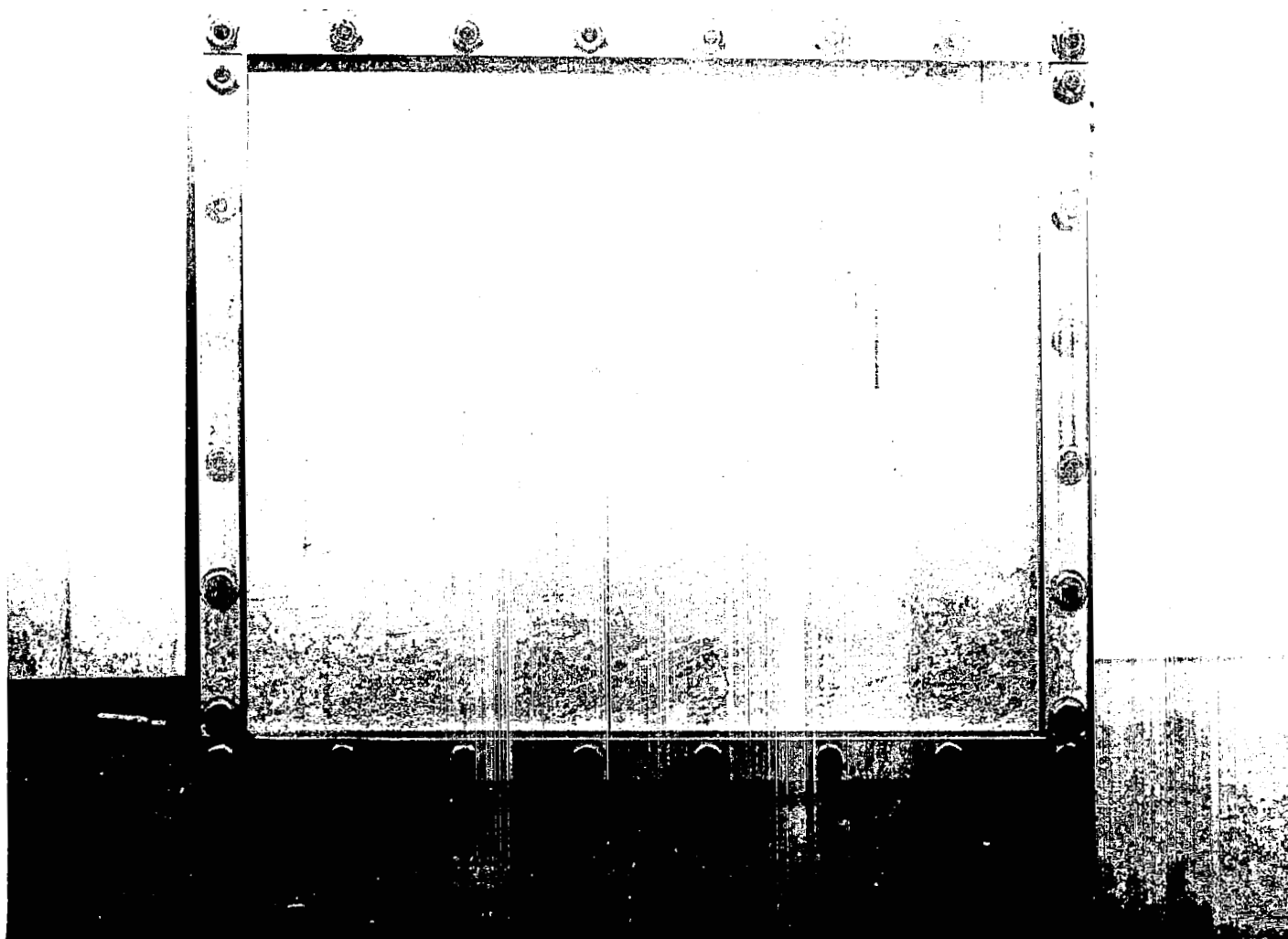
Figure 14 - Aluminum Plate (8" x 10") and Clamping Frame

10"

8"

GROOVE
DETAIL

.024

.0625

CLAMPING
FRAME
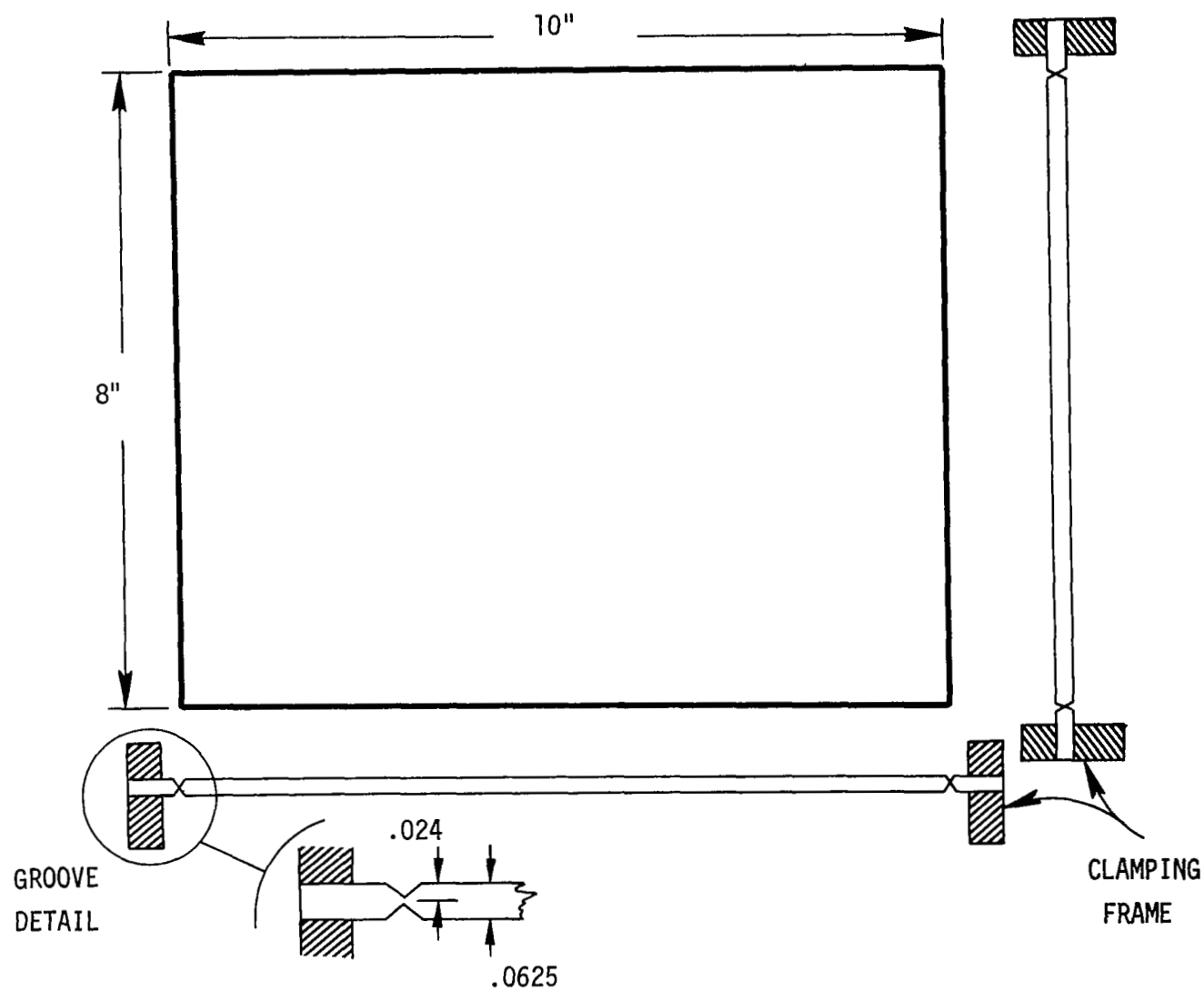
Figure 15 - Details of the Plate Support and Vee-Grooves
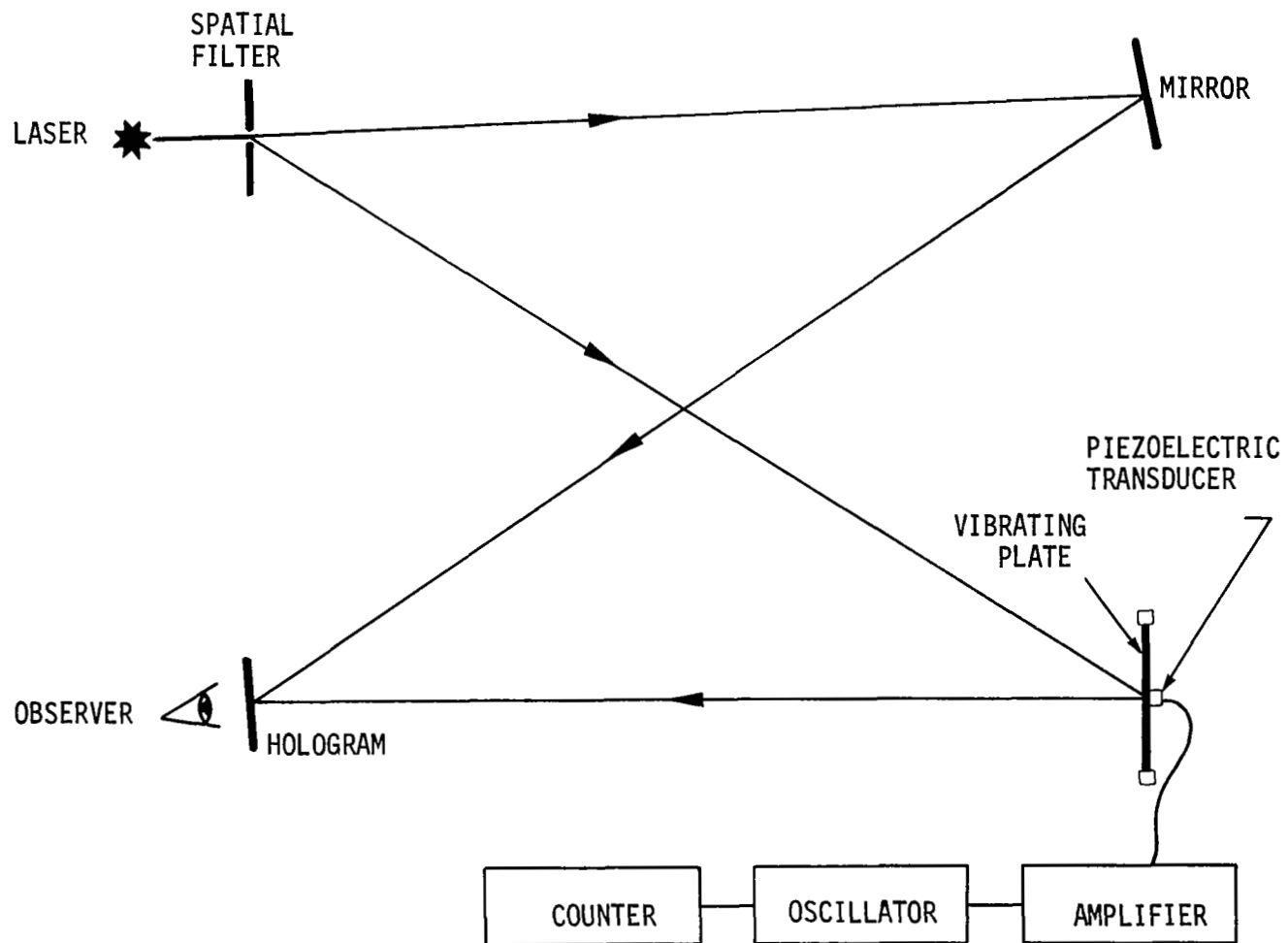
Figure 16 - Schematic of Apparatus used in the Plate Experiments
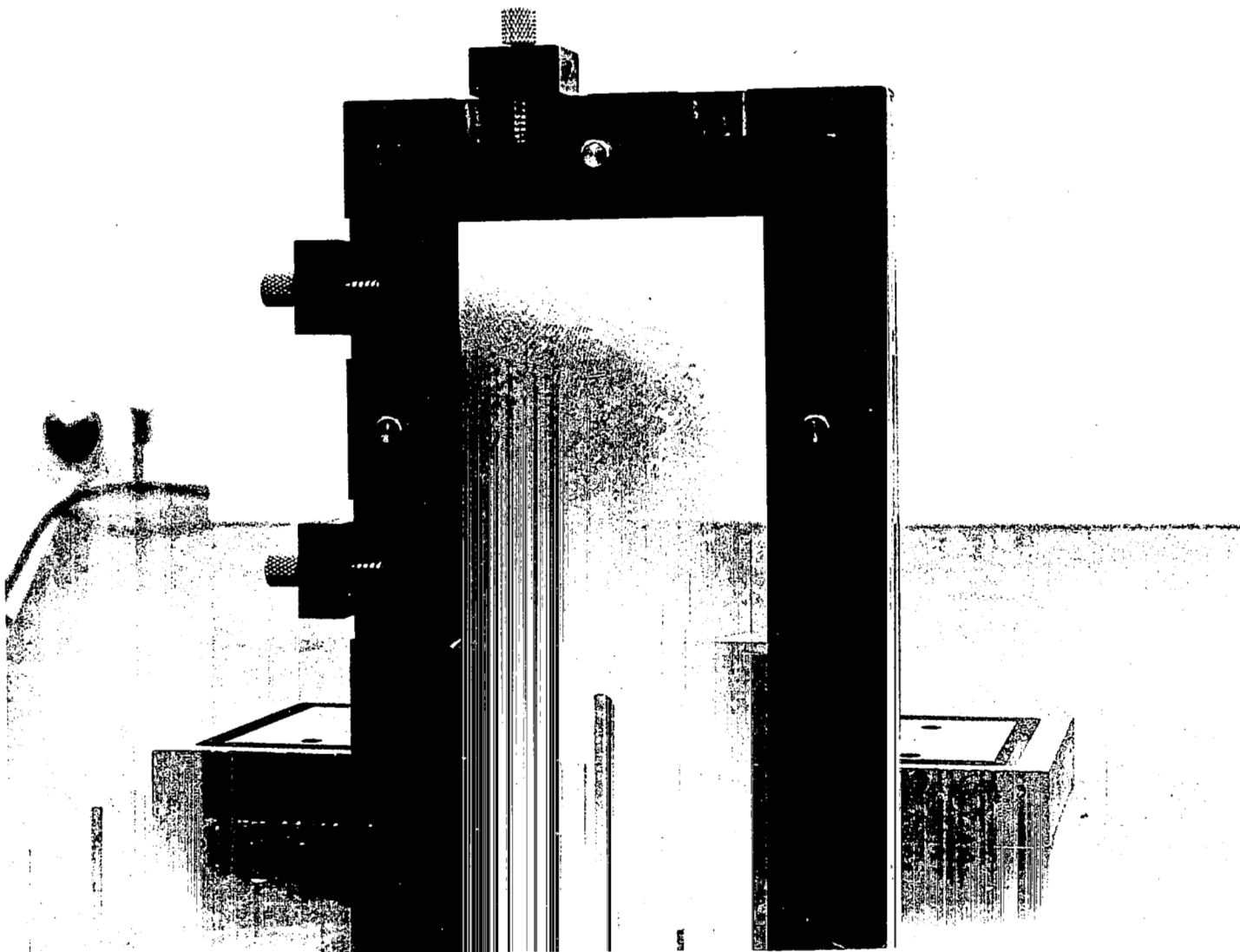
Figure 17 - Photographic Plate Holder

34

Test Procedure. - First a stored beam hologram of the aluminum plate specimen was made and set up. Then the oscillator was slowly tuned until a stationary distinct fringe pattern became visible from the hologram. A time-averaged hologram of the plate was then made and the process continued.

The fringe patterns shown in Figure 18 are from time-average holograms of the vibrating plate. Other typical fringe patterns are shown in Figures 19 and 20. These patterns are very similar to the results observed (in real time) by using stored-beam holography. A photograph made using a stored-beam hologram is shown in Figure 21. The fringe patterns readily allowed the mode numbers of the resonant vibration to be determined, and the corresponding resonant frequency was read from the counter. This procedure allowed rapid identification of the vibration modes, and over 110 modes were found in less than two weeks time. A 35 mm camera was positioned behind the stored-beam hologram to photograph the fringe patterns and thereby record them permanently. A few modes were recorded in this fashion, but the results were not as sharp and clear as was desired. (Compare for example, Figure 21 and Figure 18.) Accordingly, the remaining modes were recorded using time-average holography.

The modes were obtained with the driving transducer mounted in three different locations, including the geometric center of the plate and the center of the northwest quadrant of the plate. The transducer location can be seen in Figure 19, which shows the resulting distortion of the fringe pattern in the center of the plate.

Experimental Results and Comparisons with Analysis. - The results obtained were resonant frequencies and mode shapes for various mode numbers. For a simply-supported plate, classical plate theory gives

$$\Phi_{mn}(x,y) = \sin \frac{m\pi x}{a} \sin \frac{n\pi y}{b} \qquad (3\text{-}5)$$

$$(m = 1,2,3, \ldots \ldots$$
$$n = 1,2,3, \ldots \ldots)$$

as the shape of the m - n th vibration mode; here x and y are coordinates parallel to the sides of the plate, and (a,b) are the lengths of the sides. The corresponding resonant frequency is given by

$$f_{mn} = \frac{1}{2\pi} \left(\frac{D}{\rho h}\right)^{1/2} \left[\left(\frac{m\pi}{a}\right)^2 + \left(\frac{n\pi}{b}\right)^2 \right] \qquad (3\text{-}6)$$

where $D = \dfrac{Eh^3}{12(1-\nu^2)}$ is the plate bending stiffness

and

h   is the plate thickness

ρ is the density of the plate material.

35
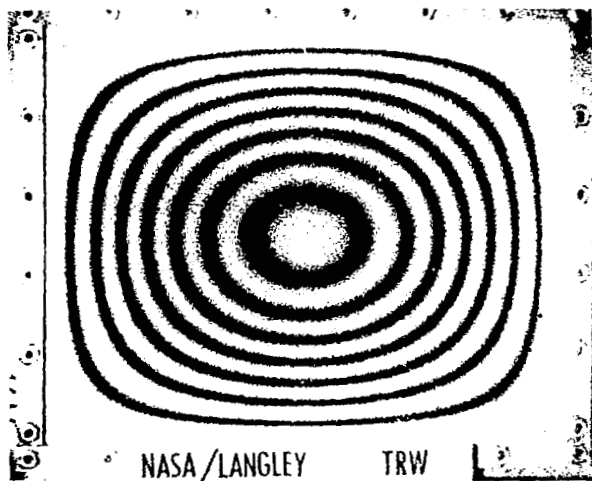
(a) m=1, n=1, f = 162 cps
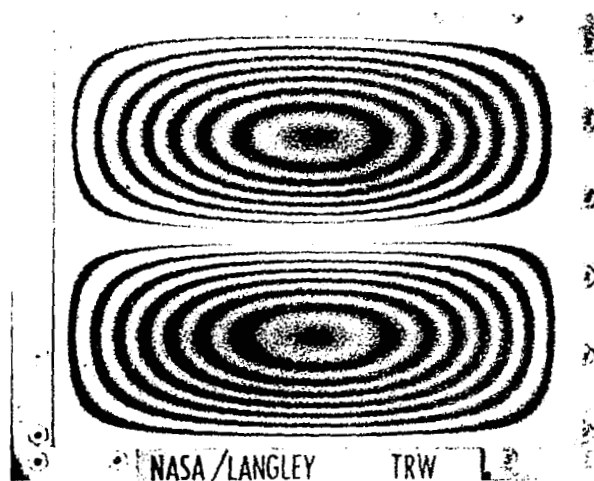
(b) m=2, n=1, f = 425 cps
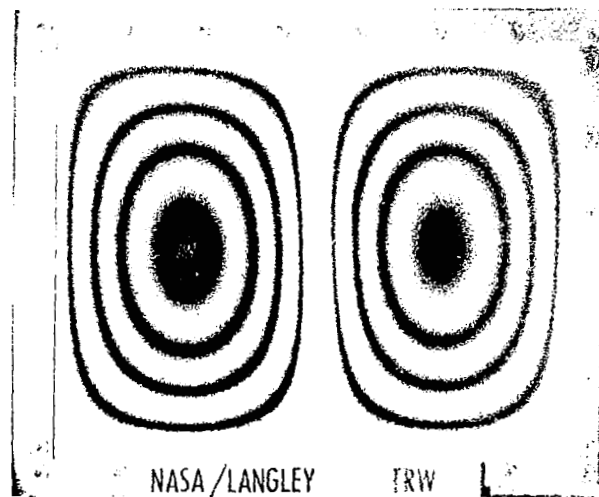
(c) m=1, n=2, f = 357 cps
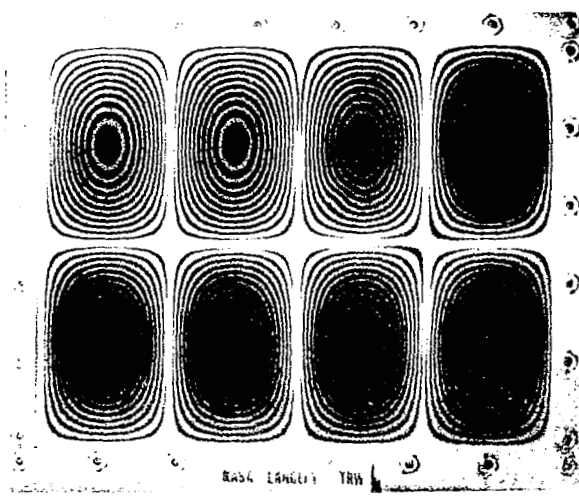
(d) m=2, n=4, f = 1360 cps

Figure 18 - Typical Low-Frequency Plate Modes
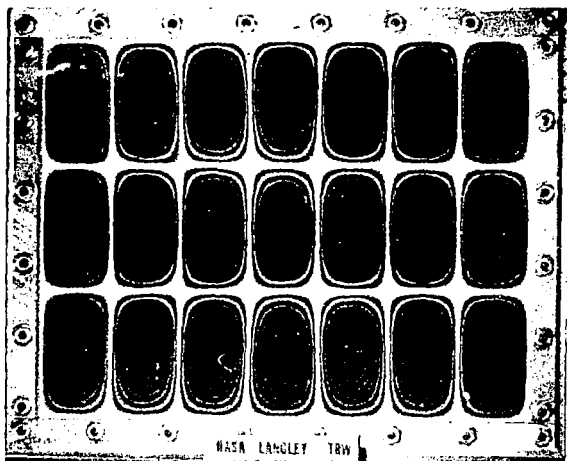
(a) m=3, n=7, f = 5132 cps
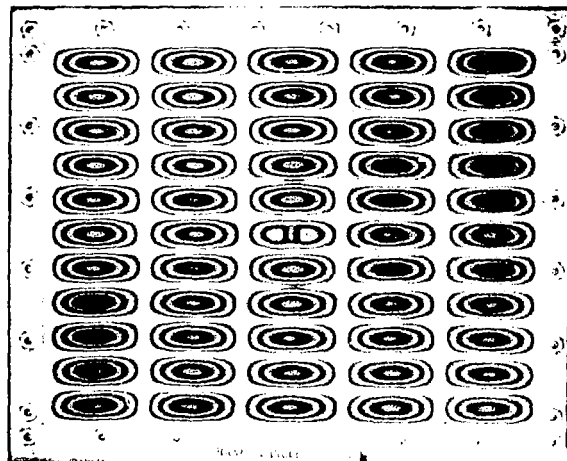
(b) m=11, n=5, f=12,670 cps
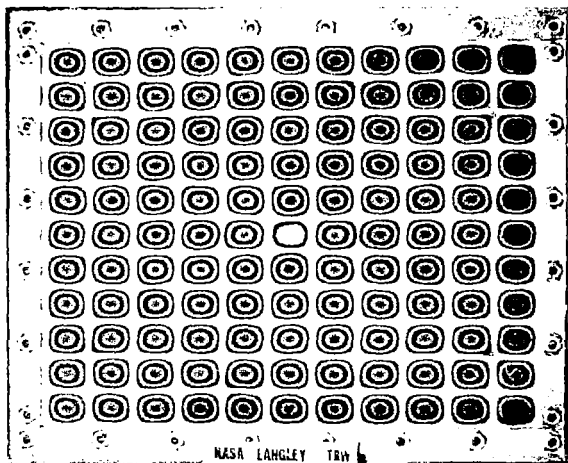
(c) m=11, n=11, f=18,158 cps
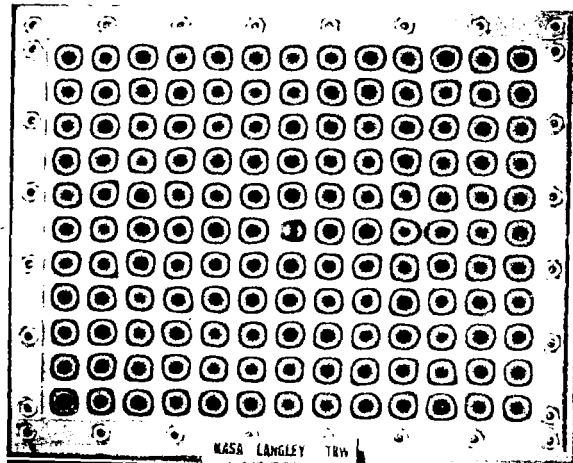
(d) m=11, n=13, f=20,892 cps

Figure 19 - Intermediate Frequency Plate Modes
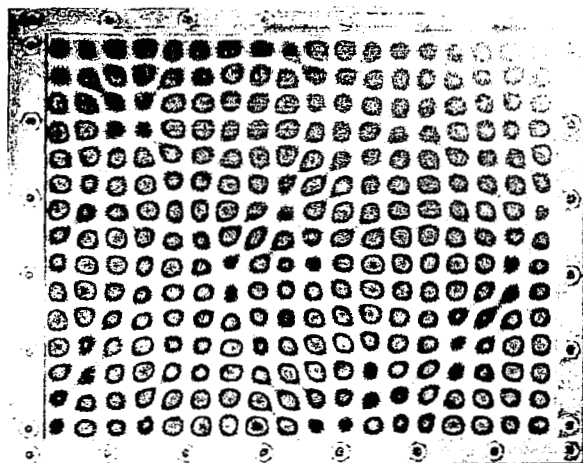
(a) m=15, n=18, f=36,100 cps
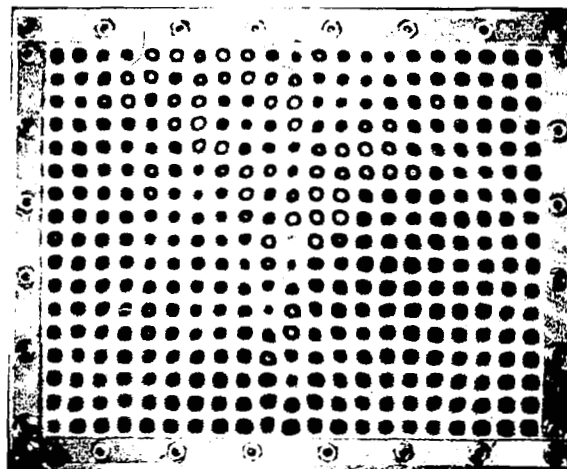
(b) m=17, n=21, f=50,104 cps
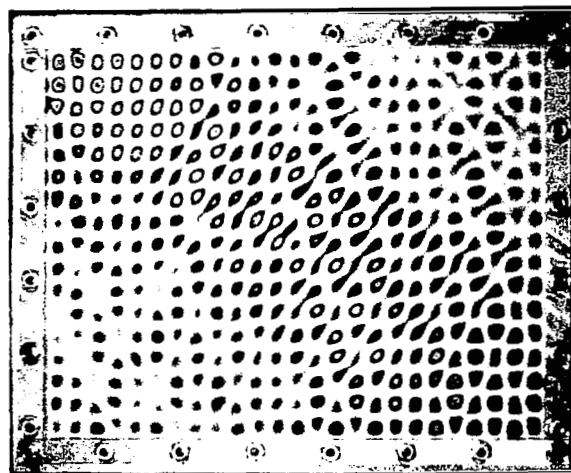
(c) m=17, n=25, f=59,682 cps
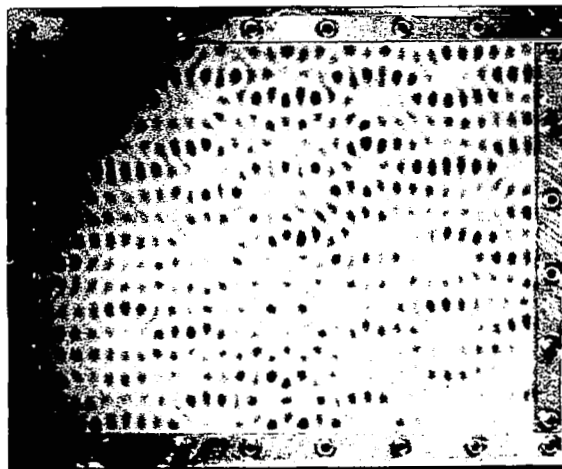
(d) m=17, n=31, f=76,768 cps

Figure 20 - High-Frequency Plate Modes

38
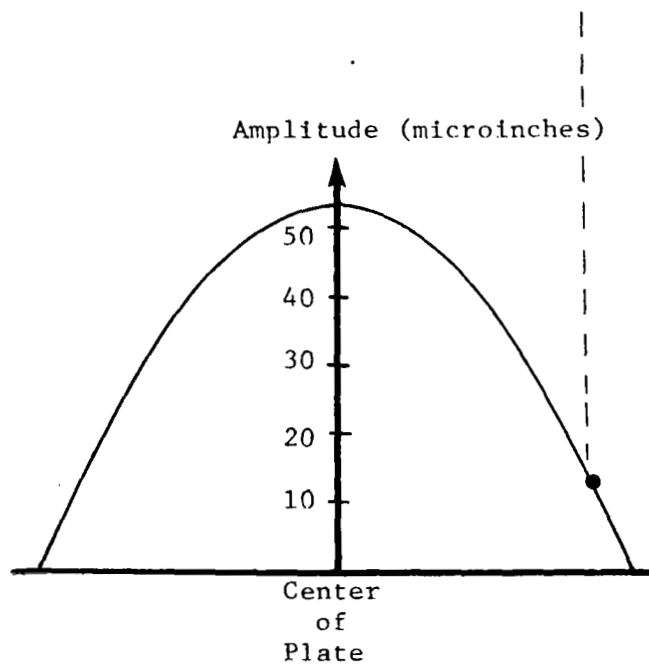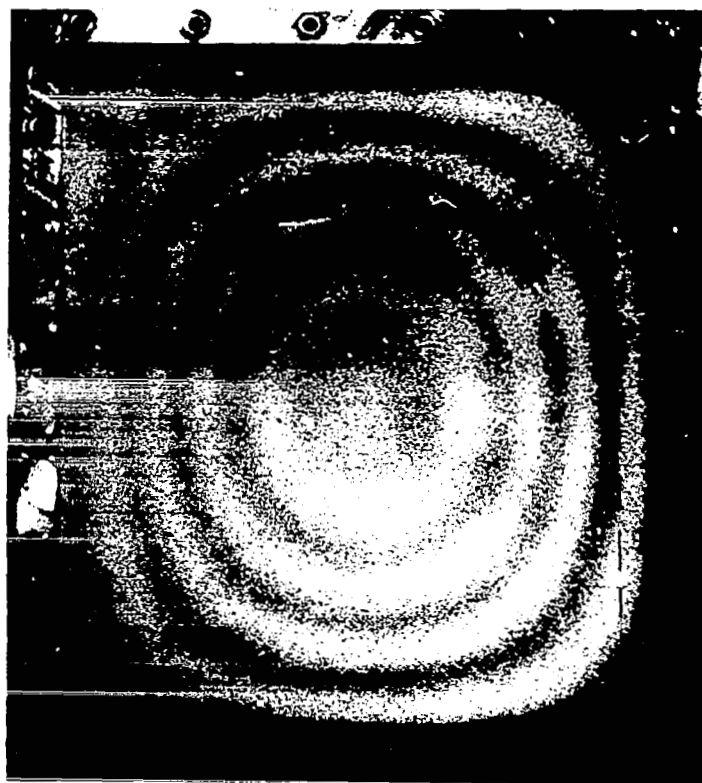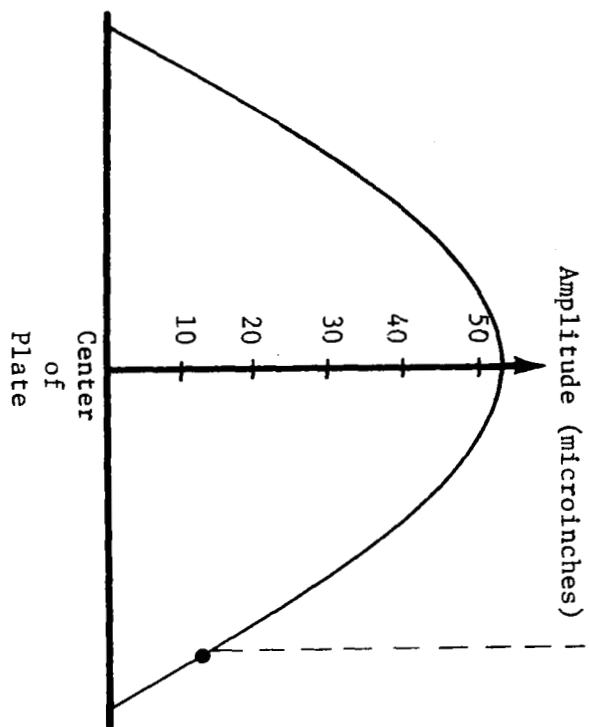
Figure 21 - Fundamental Mode of the 8" x 10" Plate
Using Stored-Beam Holographic Interferometry

39

Table III gives experimental and calculated values of the frequency f_{mn} as a function of the mode numbers m and n. The calculations used the nominal values E = 10 x 10^6 lb/in^2, ρg = 0.1 lb/in^3, a = 8 in., b = 10 in., and h = 1/16 in. A study of the tabulated values indicates that theory and experiment are within 2 - 3% of one another for all but the very low and very high modes. The low modes were influenced by the elastic moment restraints at the boundaries, which were not quite simply-supported. As the mode numbers increase, the effect of the boundary conditions becomes less and less and the experimental frequencies approach the calculations quite closely. Finally, at the very high mode numbers, the effects of rotary inertia and shear become important, and classical plate theory deviates from the experiments.

The results given in Table III are also shown graphically in Figure 22, which illustrates the general agreement just discussed. The figure does not include four very high modes found above 20 kc. In order to improve the calculated results for these three high modes, Mindlin's plate theory (Ref. 27) was used. In terms of the transverse displacement, w, the equation of motion from Ref. 27 is

$$\left(\nabla^2 - \frac{\rho}{G'} \frac{\partial}{\partial t^2}\right)\left(D\nabla^2 - \frac{\rho h^3}{12} \frac{\partial}{\partial t^2}\right) w + \rho h \frac{\partial^2 w}{\partial t^2} = 0 \qquad (3\text{-}7)$$

where ∇^2 is the Laplacian operator,

ρ is the plate density

h is the plate thickness

D is the plate bending stiffness

t denotes time

and G' = κ^2G where G is the shear modulus and κ^2 is a factor to account for shear effects (see Ref. 27).

Using the vibration shape

$$w(x,y,t) = A_{mn} \sin\alpha x \sin\beta y \cos\omega t, \alpha = \frac{m\pi}{a}, \beta = \frac{n\pi}{b} \qquad (3\text{-}8)$$

in equation (3-7), the result is

$$D\left(\alpha^2 + \beta^2\right)^2 - \left(\alpha^2 + \beta^2\right)\left[\frac{\rho h^3}{12} + \frac{\rho D}{G'}\right]\omega^2 - \rho h\omega^2 + \left(\frac{\rho h^3}{12}\right)\left(\frac{\rho}{G'}\right)\omega^4 = 0$$

40

TABLE Ⅲ
PLATE RESONANT FREQENCIES

VALUES ARE GIVEN AS EXPERIMENTAL/THEORETICAL, WHERE CLASSICAL PLATE THEORY WAS USED

m \ n	1	2	3	4	5	6	7	8
1	162/151	357/328	665/623	1071/1036			3058/2984	
2	425/428			1360/1313	1895/1844	2546/2494	3308/3261	4198/4146
3	950/889	1135/1066	1421/1361	1831/1774	2368/2305	3015/2955	3780/3722	4657/4608
4		1790/1712	2074/2006	2481/2420		3668/3600	4421/4368	5306/5253
5	2465/2364	2625/2541	2915/2837	3321/3250	3845/3781	4489/4431	5256/5198	6120/6083
6	3467/3379		3948/3851	4333/4264	4868/4796			
7	4682/4578		5132/5050		6019/5995	6712/6644	7470/7411	8353/8297
8				6931/6846			8839/8795	
9	7647/7529			8487/8415	9026/8946	9628/9595	10414/10362	11295/11248
10					10732/10698	11392/11347	12127/12115	
11					12670/12635		14053/14051	
12						15360/15405		
13			16099/16117		17048/17062	17602/17711	18362/18478	
14						20048/20201		

m \ n	9	10	11	13	14	15	17	18
1	4949/4873		7329/7234	10103/10067			17065/17150	19082/19216
2	5194/5150				12001/11938	13647/13649	17363/17427	
3	5648/5611			10886/10805	12428/12399	14130/14111	17787/17888	19788/19954
4			8669/8618					
5	7147/7087	8255/8208	9493/9448		13863/13874	15558/15586	19181/19363	
6			10496/10462	13238/13295	14789/14889	16502/16601		
7	9353/9300		11676/11661	14464/14494	16005/16088	17676/17800		
8								
9			14566/14612	17327/17445	18788/19039	20524/20751		
10	13969/14004	15080/15125	16276/16364	18997/19198				
11	15871/15940	16932/17062	18158/18301	20892/21134				
12								
13	20164/40367							

m \ n	21	25	31					
17	50104/52683	50682/63543	76768/83376					
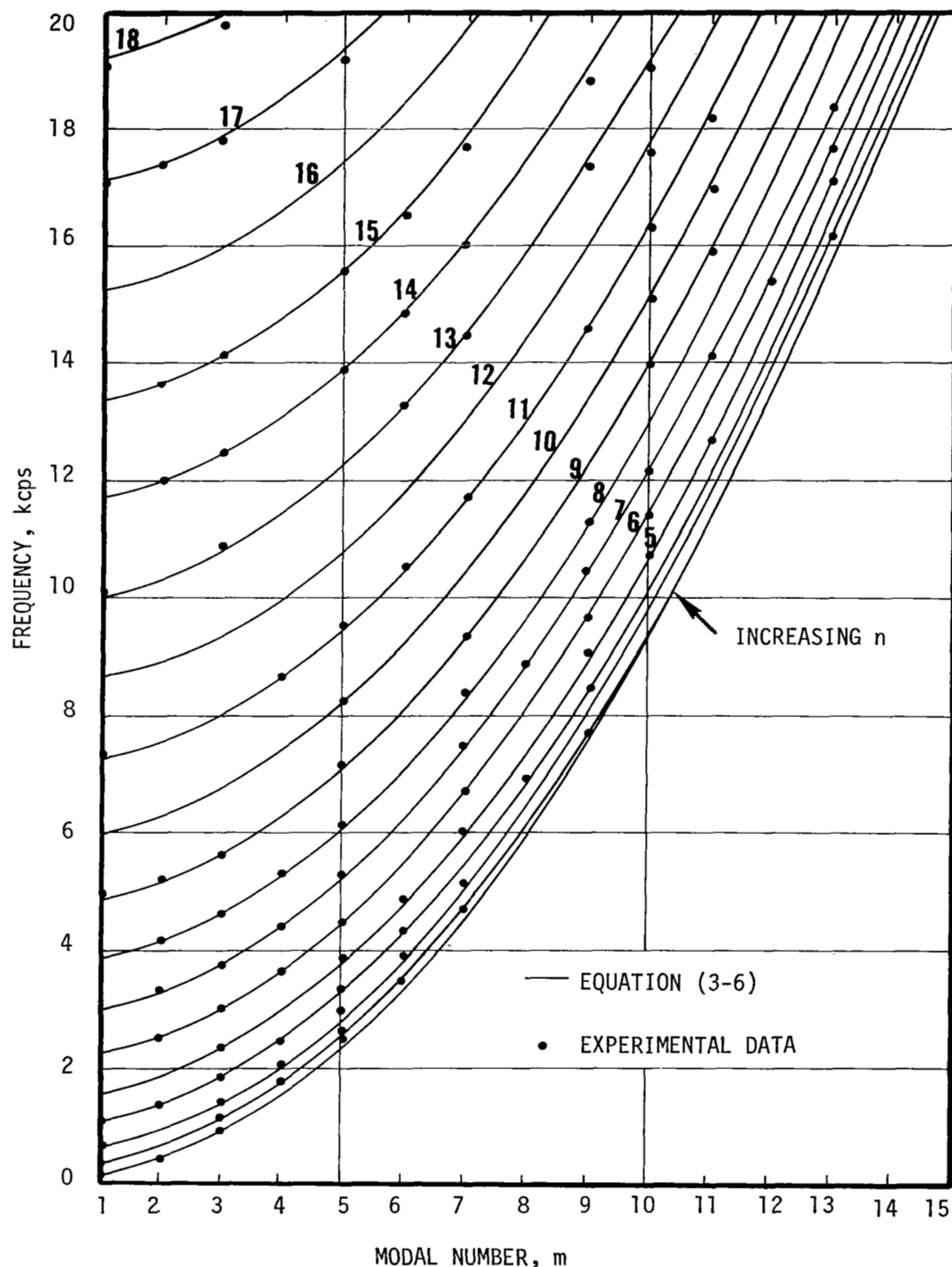
Figure 22 - Plate Resonant Frequency as a Function of
Modal Numbers m and n.

42

for the frequency equation. Now let

$$\alpha^2 + \beta^2 = (\frac{m\pi}{a})^2 + (\frac{n\pi}{b})^2 = (\frac{2\pi}{\Lambda})^2 \qquad (3-9)$$

be used to define a wavelength, Λ, and let $\omega = (\frac{2\pi}{\Lambda})c$ define a wave speed, c. Then equation (3-8) can be put in the form

$$\frac{\pi^2}{3}\left(\frac{h}{\Lambda}\right)^2 \left[\left(\frac{c_p}{c}\right)^2 - 1\right]\left[1 - \frac{c^2}{\kappa^2 c_s^2}\right] = 1 \qquad (3-10)$$

where $c_p^2 = \frac{E}{\rho(1-\nu^2)}$ and $c_s^2 = \frac{G}{\rho}$. The factor κ^2 is a function of Poisson's ratio, and it was determined by using expressions given in (Ref. 27). Values of $\nu = 0.3$ and $\kappa^2 = 0.86$ were used in equation (3-10), and the smallest root (c/c_s) was determined as a function of (h/Λ). This procedure resulted in a calculated curve of nondimensional wave speed as a function of (plate thickness/bending wavelength).

Experimental values for (c/c_s) and h/Λ were obtained using the m and n numbers of the various modes and their corresponding frequencies. In particular, the experimental wavelength was determined from equation (3-9), using a = 8" and b = 10". Similarly, the wave speed was calculated from c = fΛ, where f is the experimental frequency and Λ came from equation (3-9). The experimental data was nondimensionalized using $c_s = (G/\rho)^{1/2}$ 1.219 x 10^5 in/sec. A comparison of the theoretical and experimental values of wave speed as a function of wave length is shown in Figure 23.

All the results plotted in Figure 22 as a one-parameter family of curves can be reduced to the single curve of Figure 23. The straight line in Figure 23 was obtained using classical plate theory, which neglects rotatory inertia and shear effects. The curved line shows Mindlin's plate theory, which includes these effects. The three experimental points at the largest values of h/Λ were obtained from the three very high frequency modes discussed previously. The other points shown in Figure 23 are representative examples of other modes ranging in frequency from 162 to 20,892 cps. Figure 23 demonstrates that classical plate theory agrees with the experiments for values of (h/Λ) less than 0.06. Beyond that point, the experiments agree more closely with Mindlin's plate theory.

The modal numbers m and n were easily determined by viewing the interference fringe patterns. Typical fringe patterns obtained from time

43
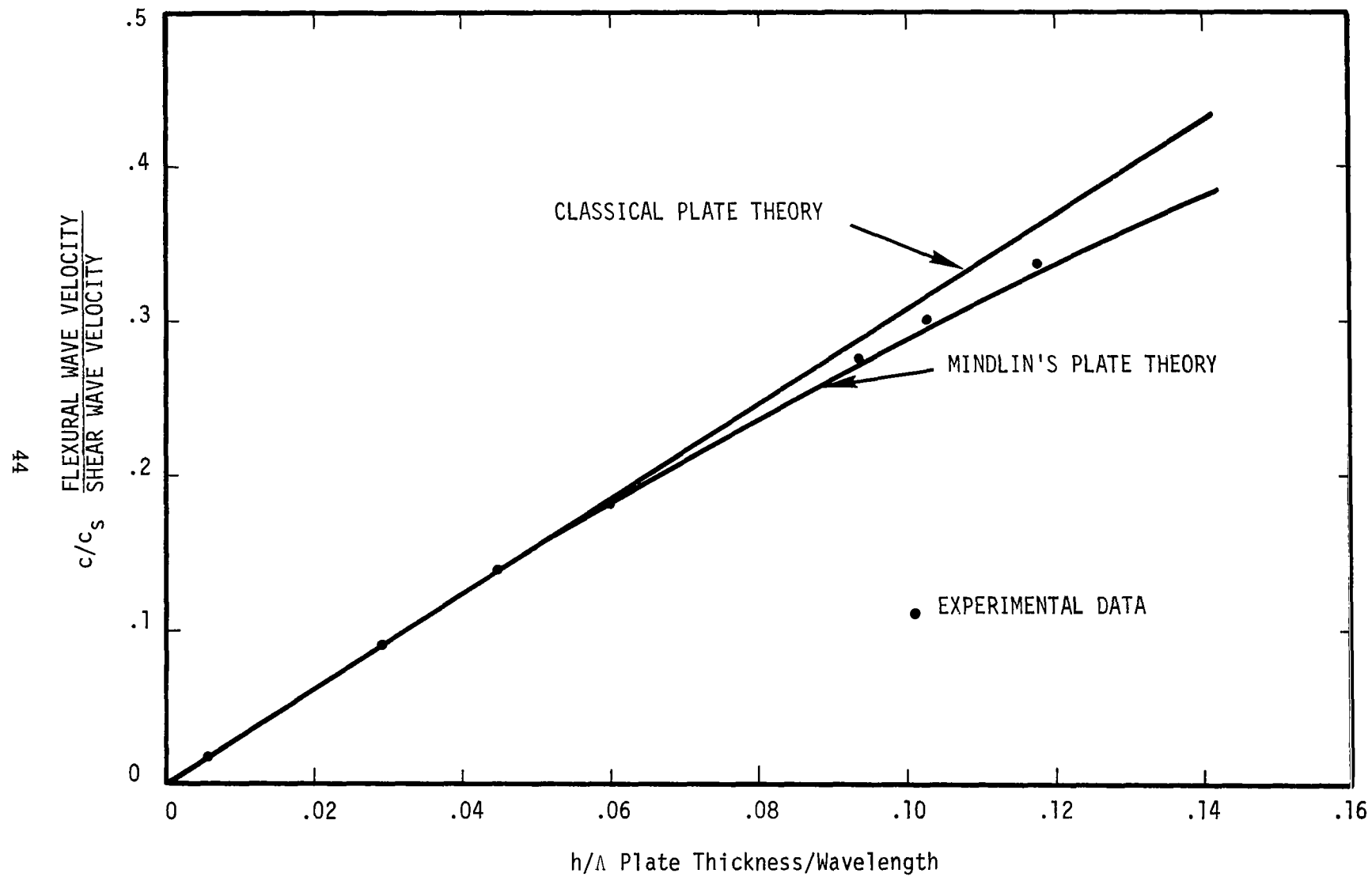
Figure 23 - Wave Velocity Dependence Upon Wavelength (Plate Experiments)

average holograms are shown in Figures 18 through 20. These photographs are very similar to the interference fringe patterns observed visually in real-time by using stored beam holography. The nodal lines show up quite clearly as white areas on the photographs (see Figures 18(d) and 19(a), for example.) Between the nodal lines, the interference fringes form closed "contour lines" encircling each antinode of the vibration shape.

The shape of a vibration mode was determined as follows: First, equations (3-1) and (3-2) were used to find the vibration amplitude corresponding to a particular fringe. Then, by placing a ruler on the photograph and measuring the position of the fringe, it was possible to plot the vibration amplitude at the measured location. This procedure was used to determine several typical mode shapes; examples are shown in Figures 24, 25 and 26, which correspond to photographs 18(a), 18(c), and 18(d), respectively. In cases where the fringes were close together, such as Figure 18(d), a traveling microscope was used to determine the fringe location. As shown in Figures 24 - 26, the experimental mode shape data agreed quite well with the theoretical shape given by equation (3-5). For the first mode, (Figure 18, $m = 1$, $n = 1$), slight deviations from the theoretical mode shape were noted near the boundaries of the plate. These deviations were attributed to the slight elastic moment restraint at the boundaries.

Mode shapes could be determined most easily for the lower modes, in which several concentric fringes enclosed each antinode. The very high modes usually had only a single fringe around each antinode, and consequently the corresponding mode shapes could not be closely resolved. Nevertheless, it is clear from Figures 19 and 20 that the experimental modes possessed the basic "checker-board" character given by equation (3-5). It is also apparent from Figure 27 that the mode shapes were not always perfectly clean and undistorted. Distorted mode shapes, or "compound modes" (such as those shown in Figure 27) were attributed to coupling between two or more modes of nearly equal frequencies. Such distortion due to modal coupling occurred throughout the frequency spectrum. A discussion of measuring compound modes using holographic interferometry was recently presented in Ref. (28).

Additional photographs showing other plate vibration modes are given in Appendix C.
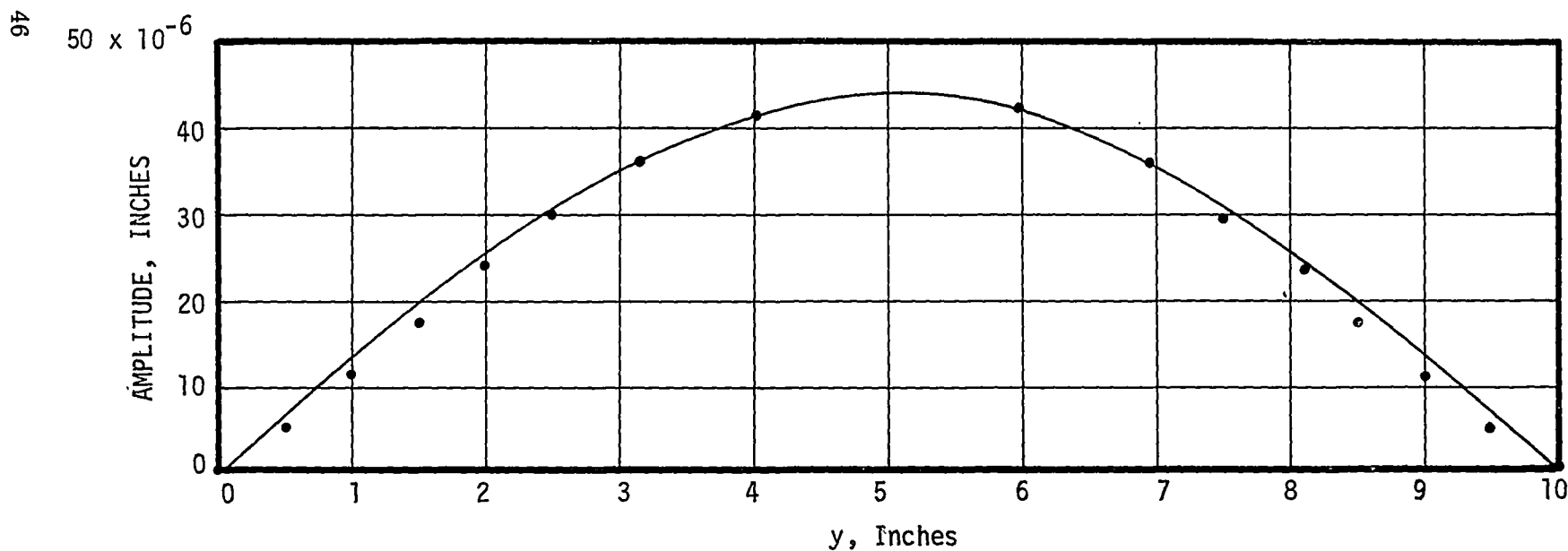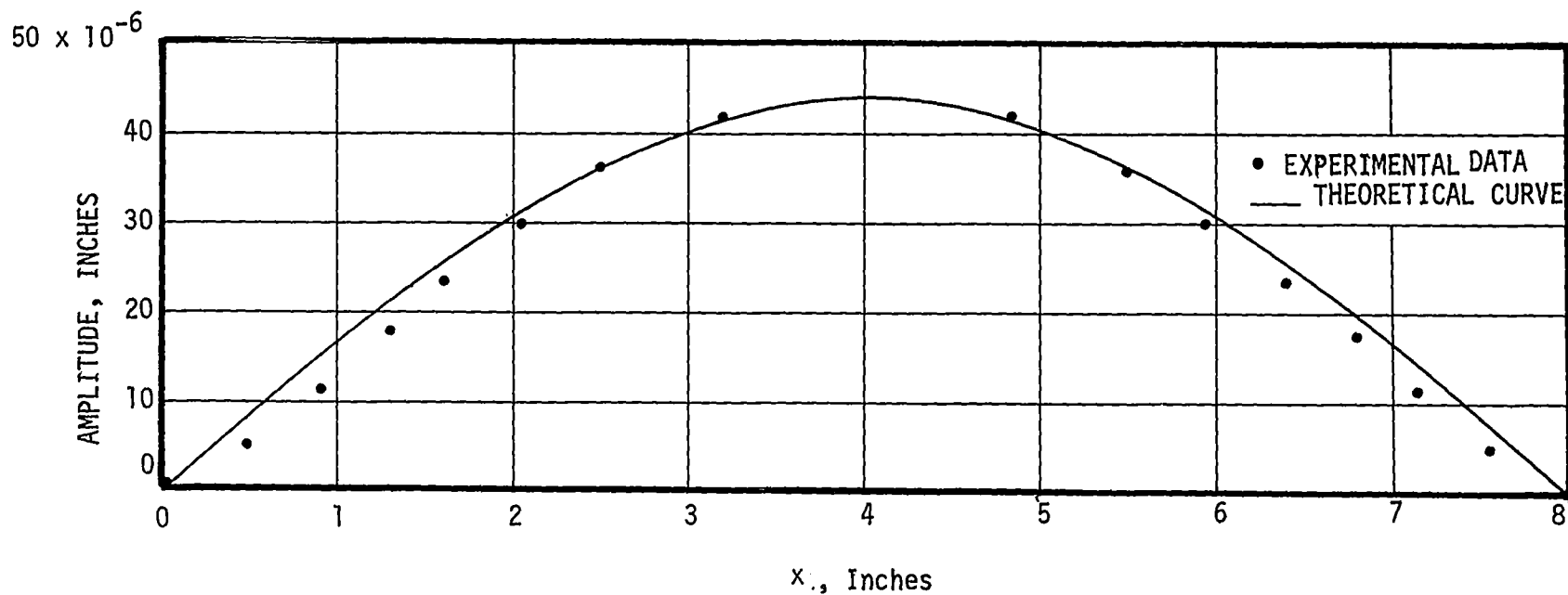
Figure 24 - Calculated and Experimental Mode Shape (1st Mode)
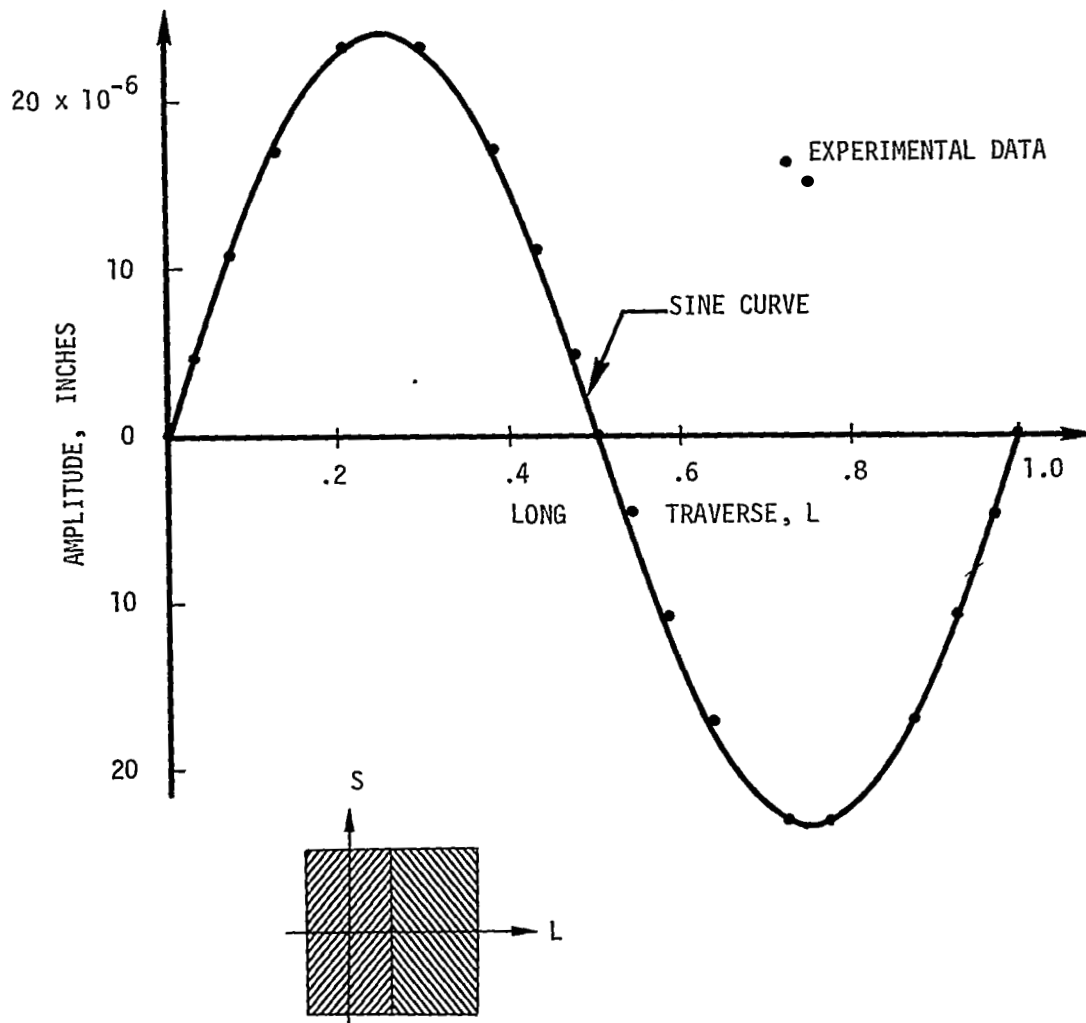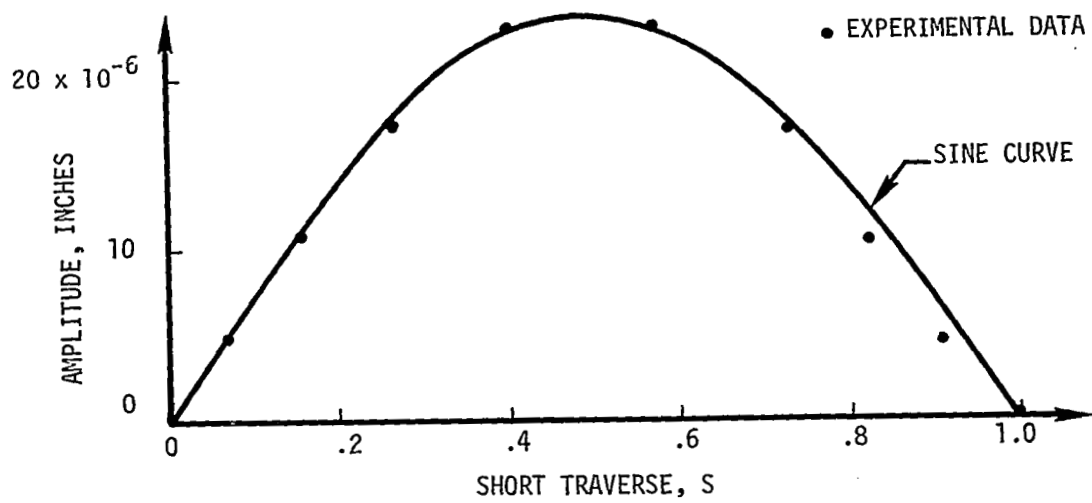
Figure 25 - Mode Shape of the 1x2 Mode

47
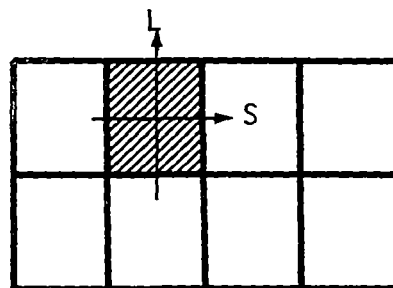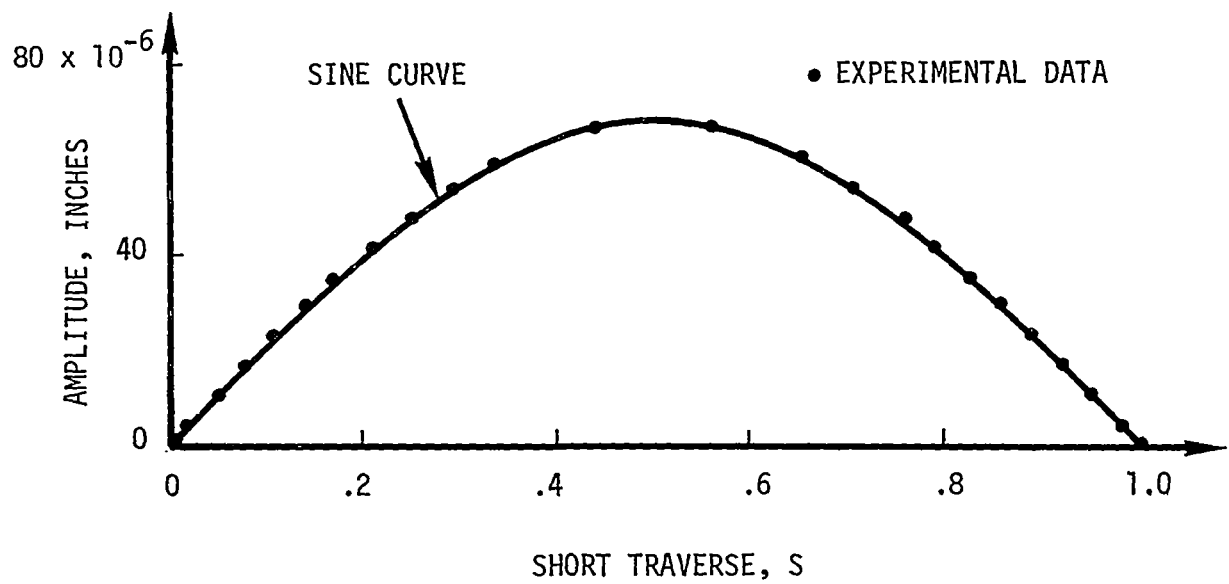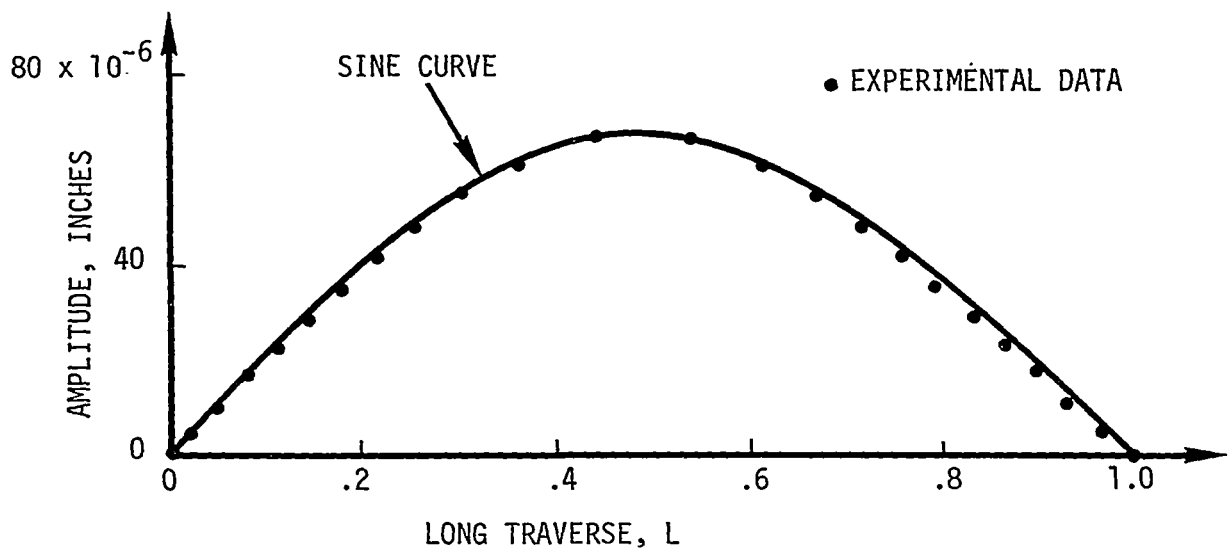
Figure 26 – Mode Shape of the 2x4 Mode
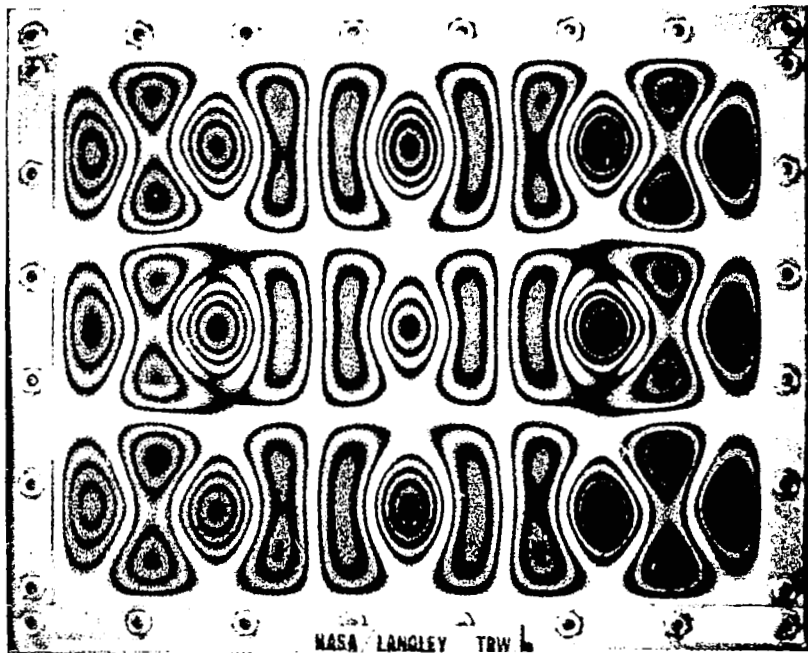
(a) COMPOUND MODE   f = 8000 cps
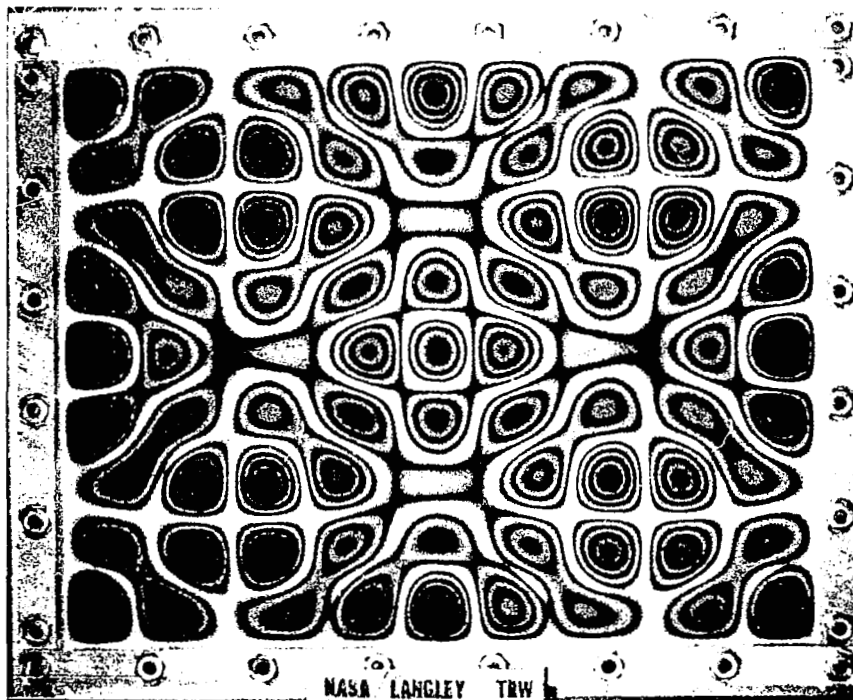
(b) COMPOUND MODE   f = 12,200 cps

Figure 27 - Two Compound Modes

4.0 TRANSIENT RESPONSE TEST

Background and Summary

This test was run to prove the feasibility of using holography to obtain transient response data. A stored-beam hologram of a 20" cantilever beam was set up, and the beam was subjected to a transverse impact impact at the tip. A high-speed motion picture camera recorded the fringe motion, and the movie film was analyzed frame-by-frame to provide displacement-time histories of various points on the beam. A description of the experimental set-up, test procedure, and data reduction process is given in the sections which follow. This portion of the report concludes with a comparison of analytical and experimental results for the response of a cantilever beam to a transverse impact at the tip. The results showed generally good agreement between theory and experiment.

Experimental Set-Up

The cantilever beam used was 20 inches long and made of aluminum (6061-T6). It had a rectangular cross-section, one inch wide by 1/4 inch deep, and it was clamped at the root with a massive steel support block. The beam had a fundamental flexural mode frequency of 19.8 cps. Initially, attempts were made to use a longer beam (with a lower fundamental frequency) but disturbances from background noise prevented the successful production of good quality stored-beam holograms when the longer cantilevers were used. In order to conserve the light from the laser and properly expose the movie film, the surface of the beam was polished to make it highly reflective. A more powerful laser might have allowed use of an unpolished surface.

The experimental arrangement used for the transient test is shown schematically in Figure 28. Figure 29 shows a photograph of the actual set-up for the transient test. Referring to Figure 28, light from the laser is pased through a spatial filter (SF) and then through a converging lens (L). The light is brought to a focus just ahead of a mirror, M; when the light leaves the mirror it expands and is then passed through a collimating lens, CL. Part of the light leaving the collimating lens strikes the beam splitter at point A. Light is reflected from point A on the beam splitter to a two-inch wide mirror M1; it then is reflected to point B on the cantilever beam. Since the beam has a highly polished surface, it reflects the light back along its original path, i.e., back to M1 and then to A. Upon reaching point A, the light passes through the beam splitter and reaches the hologram at point H. This constitutes the object beam for the hologram.

At the same time, part of the light from the collimating lens passed through the beam splitter at point A. This light is sent to a mirror at M1', which reflects it back to the beam splitter again. It is then reflected from the beam splitter to point H on the hologram; this constitutes
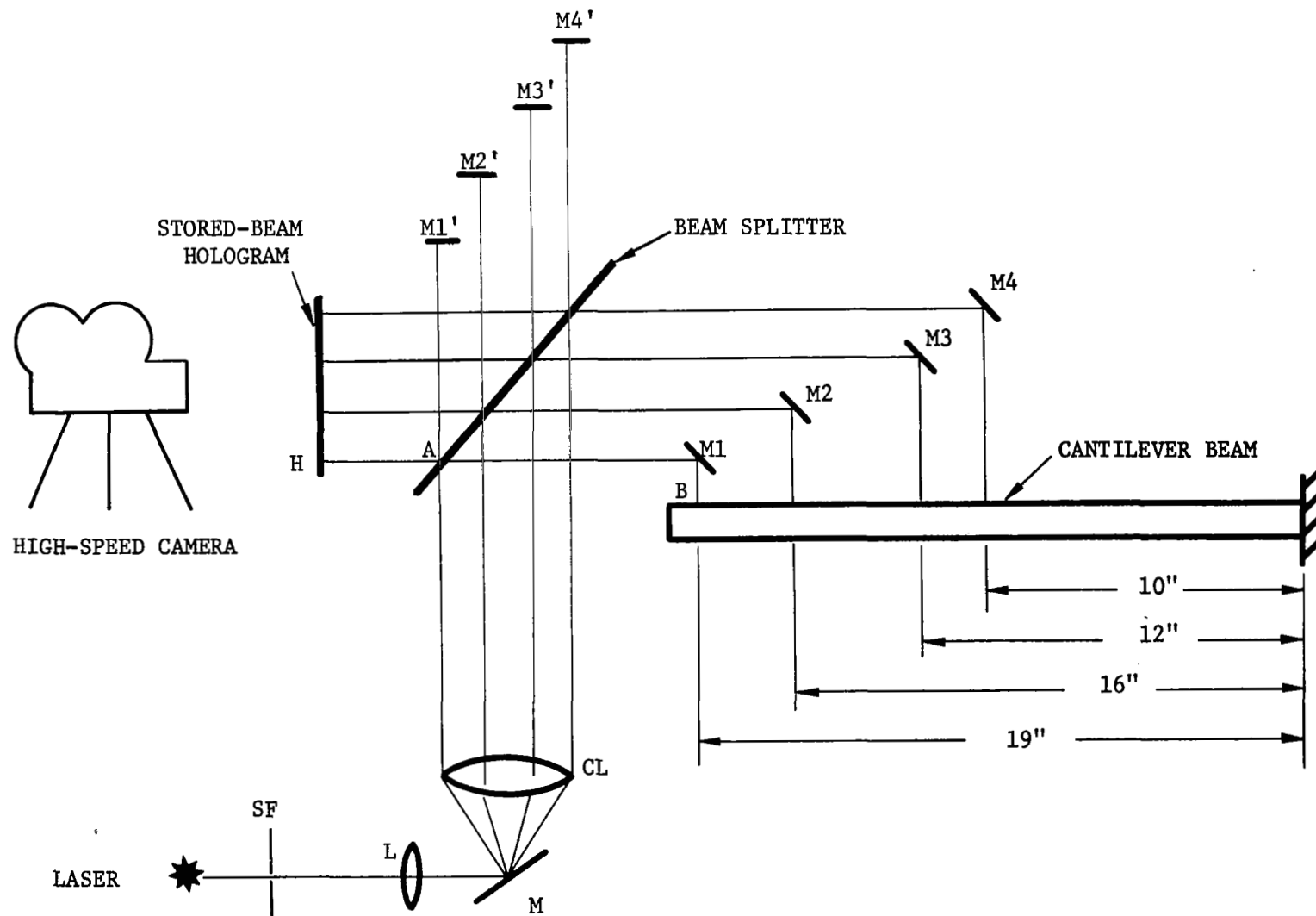
Figure 28 - Optical Arrangement for Transient Response Test
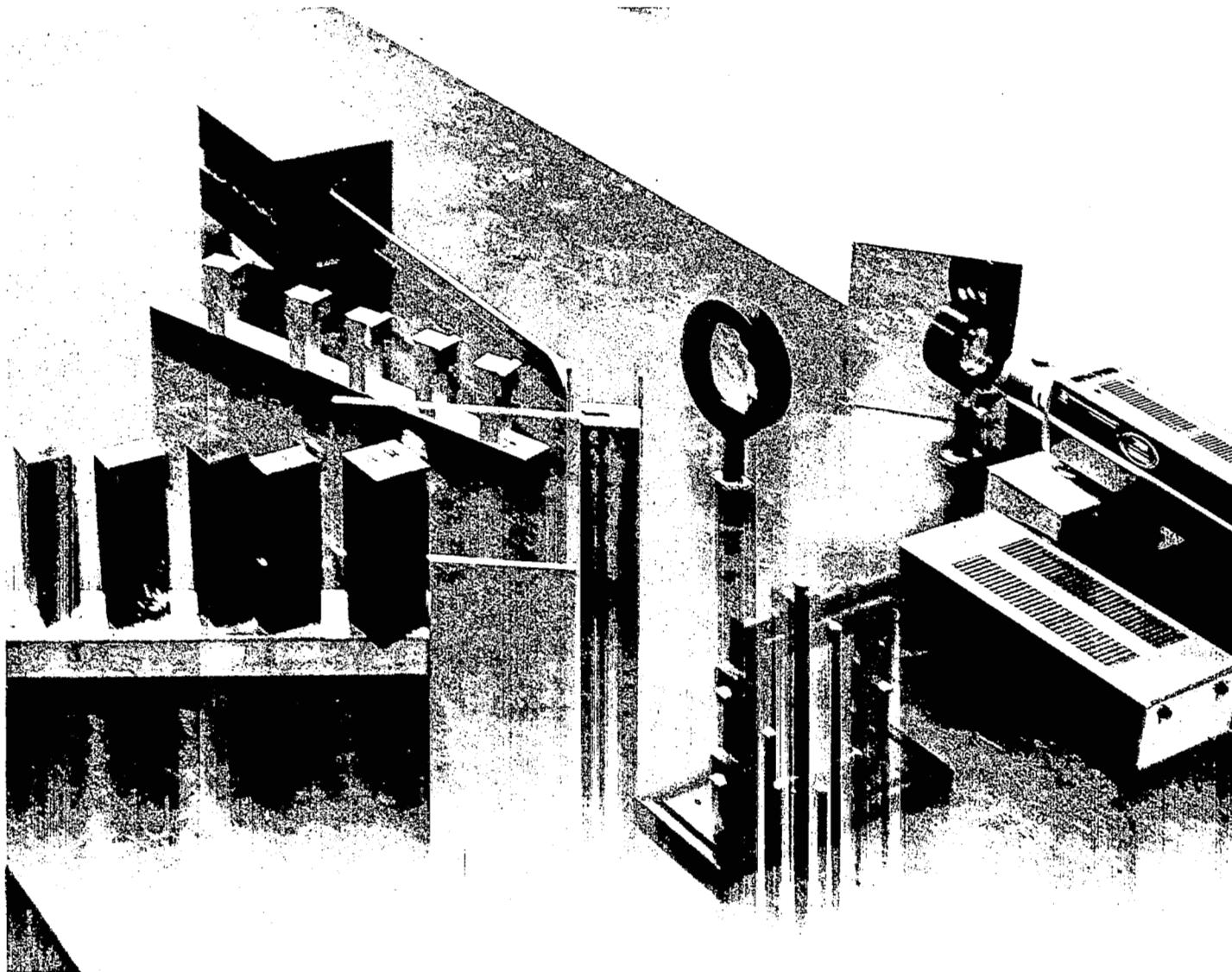
Figure 29 - Actual Set-up (Transient Response Test)

the underlined reference beam for the hologram. In order for successful holograms
to be made, the path length of the object beam (A – M1 – B – M1 – A – H)
must be the same as the reference beam (A – M1' – A – H). In order to
satisfy this requirement, the distance A – M1' was adjusted to be within
one inch of the length A – M1 – B.

The light paths just discussed were sufficient to illuminate a region
nearly two inches long at the tip of the cantilever. Similar arrangements
were made using mirrors (M2, M2') (M3, M3') and (M4, M4') to illuminate one
inch long regions of the beam at the respective distances of 16, 12, and
10 inches from the root. Stored-beam holograms which showed these four
illuminated regions of the cantilever were made with this optical arrange-
ment. The laser output was insufficient to have used a single large
mirror giving a continuous view of the entire beam.

To excite the transient motion, a ballistic pendulum was used to
impart an impulse to the beam. A small (0.016 gram) steel ball was sus-
pended on a 10-inch human hair to make up the ballistic pendulum. The
initial height of the ball was measured using a machinist's scale. A
latch mechanism was used to release the ball without giving it an initial
velocity. The pendulum ball struck a piezoelectric crystal which was
mounted on the beam at one-half an inch from the tip. By monitoring the
output of the transducer with an oscilloscope, the force-time history of
the impulse was determined. The oscilloscope trace showed a half-sine
pulse with a duration of 5 µs. The height to which the pendulum rebounded
(after striking the beam) was recorded using a Polaroid camera which had
the shutter held open. The rebound height was determined from a scale
which was photographed in the background behind the pendulum.

Test Procedure

A small metal support stud was used to apply a slight transverse pre-
load at the tip of the beam. With this support stud in place, a stored
beam hologram was made of the four illuminated spots on the cantilever.
The hologram was bleached (i.e., silver halides contained in the emulsion
were made transparant by a chemical process) and then replaced in the
photographic plate holder. The bleaching process increased the amount
of light transmitted through the hologram. Then the metal support stud
was removed, and the beam returned to its unloaded equilibrium position.
This slight displacement of the beam caused zero-order interference fringes
to appear when the hologram was viewed. Figure 30 is a sketch of the
zero-order fringes and the four illuminated segments of the beam. Small
marks were made on the surface of the beam at intervals of 0.2 inch, and
these marks are illustrated in Figure 30.

With the hologram in position, the high-speed motion picture camera
was aligned and focused to record the interference fringes. The test was
conducted by first turning on the camera and letting it run for about 1
second to come up to speed. (The camera was set for a nominal speed of
4000 frames/sec.) Then the ballistic pendulum was released and allowed
to impact the beam. The motion picture camera recorded the fringe motion

INTERFERENCE FRINGES

x = 10.0   x = 12.0   x = 16.0   x = 18.2   x = 19.0
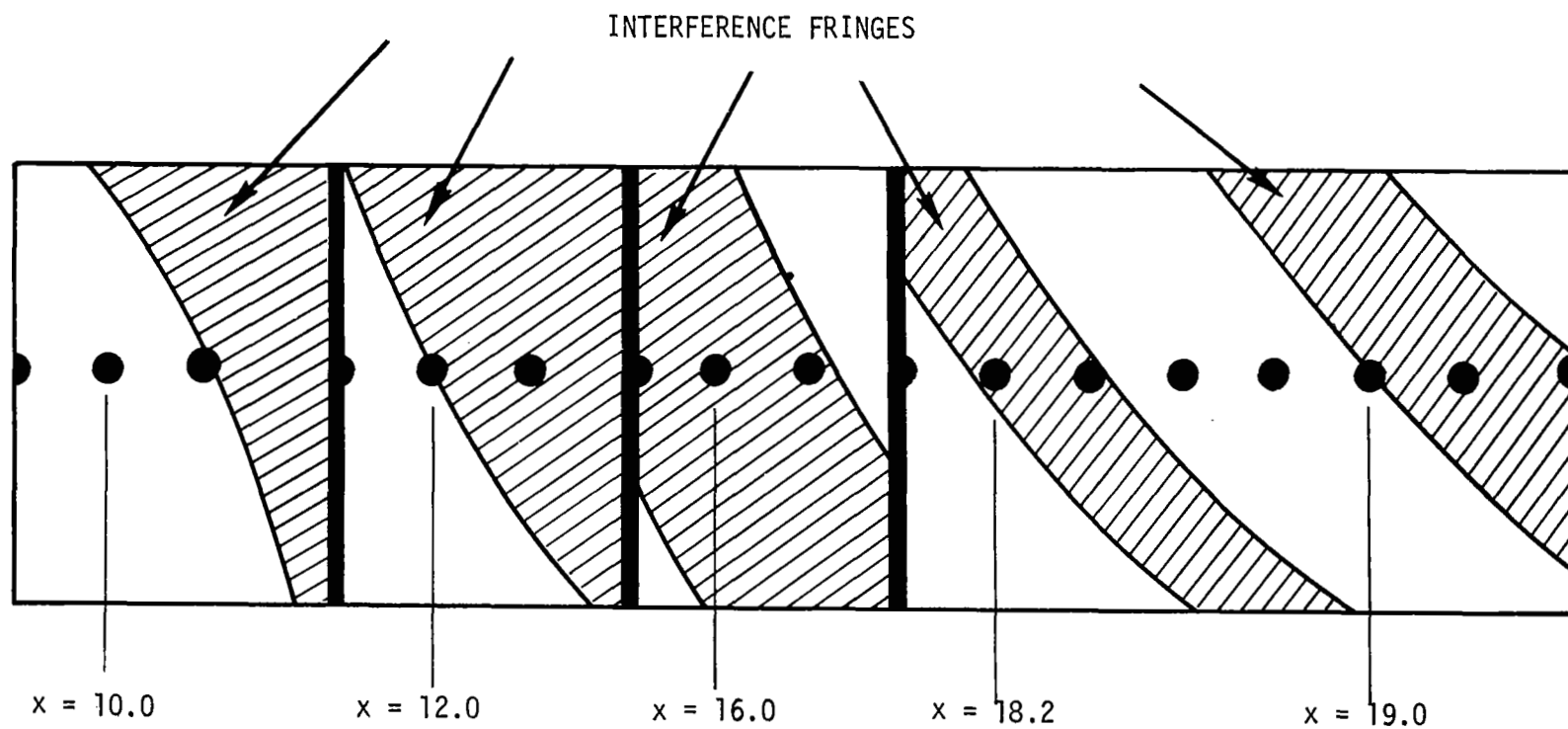
Figure 30 - Sketch of Zero-Order Fringes (Transient Test)

from the initiation of impact until the 400 foot reel of film was ex-
hausted. The Polaroid camera recorded the rebound of the pendulum. The
entire test took less than 5 seconds to complete, once the experiment
had been set up.

Two or three preliminary tests were made to determine the correct f -
stop setting for the high-speed camera, so that the film was exposed
properly. Once these preliminary tests were completed and the film devel-
oped, the final test was made. After the final film was developed, it
was then necessary to reduce the data. The process of obtaining displace-
ment-time histories from the movie film is discussed in the next section.

Reduction of the Film Data

Figure 31 shows photographs of five individual frames from the high-
speed movie results. The illuminated spot at 10" from the root of the
cantilever is in the left of the scene, and the two inch illuminated
segment from 18"-20" appears on the right; the other two illuminated seg-
ments are in the middle of the scene. Frame zero in Figure 31 corresponds
with the zero order fringes sketched in Figure 30. The dots on the beam
which were spaced 0.2 inch apart are partly visible in Figure 31; the
broad fringes would sometimes cover the dots and make them hard to see.
The fact that the fringes are slanted in Figures 30 and 31 is thought to
be due to either slight twisting of the beam when the support stud was
used or inaccurate repositioning of the stored-beam hologram.

To understand how the data was obtained from the movie film, consider
Figure 32, which shows how the fringes formed near the tip of the moving
cantilever beam. Figure 32 is exaggerated drawing which shows the rela-
tionship between the interference fringes and the moving cantilever beam.
The horizontal parallel lines labeled "fringe 0, fringe 1, etc." in Figure
32 are reference lines which control the location of the interference
fringes. These parallel lines have a spacing of $\lambda/2 = 12.45 \times 10^{-6}$ inches
apart, since the displacement between adjacent fringes is $\lambda/2$. The verti-
cal parallel lines in Figure 32 have a spacing of 0.2 inches and refer
to the equally spaced dots on the beam located at 18.0, 18.2, ... inches
from the root of the cantilever. The heavy dashed diagonal lines in
Figure 32 illustrate the position of the cantilever at times which corres-
pond to frames 0, 1, and 2 of the movie film. The field of view of the
movie camera is shown in Figure 32 (for the illuminated region at the tip
of the beam).

Let x denote the distance measured from the root of the cantilever
beam. By viewing Frame 0 of the movie film (Figure 31) and referring to
the marks on the beam, it was noted that the fringe on the right was lo-
cated at x = 19.2 and the adjacent fringe (to the left) was located at
x = 18.35. (These fringe locations correspond to points A and B, respec-
tively, in Figure 32). When the pendulum struck the beam, the tip moved
toward the camera, and the fringes in the movie film (at the tip of the
beam) moved toward the right. Frame 1 (Figure 31) showed that the right
fringe had moved to x = 19.4 and its adjacent partner moved to x = 18.5.
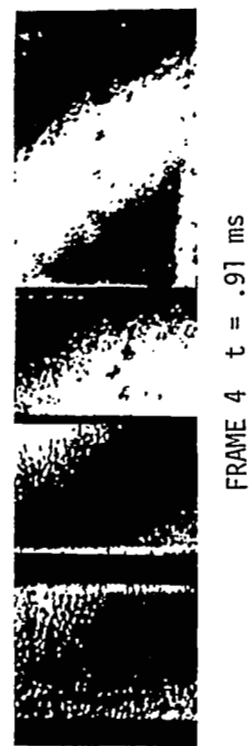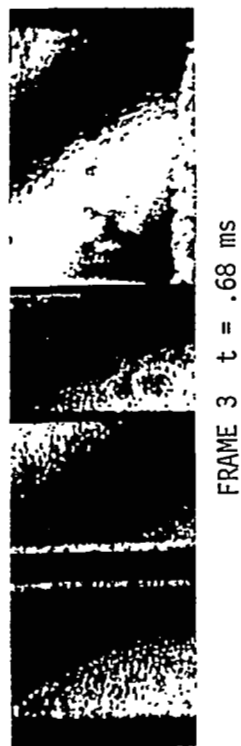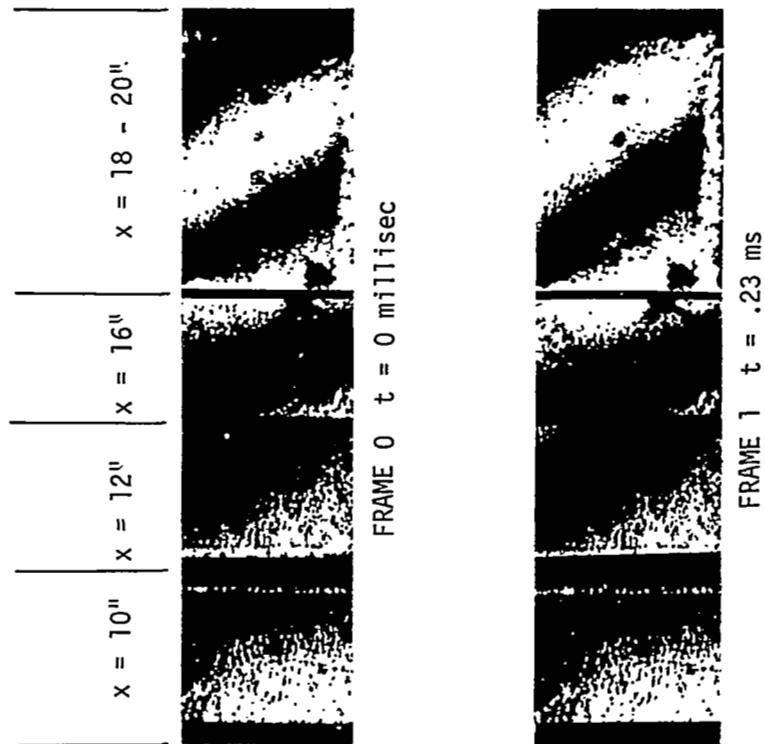(These fringe locations correspond to points A' and B' in Figure 32.)

FRAME 2   t = .45 ms

FRAME 0   t = 0 millisec

x = 10"   x = 12"   x = 16"   x = 18 - 20"

FRAME 3   t = .68 ms

FRAME 1   t = .23 ms

FRAME 4   t = .91 ms

Figure 31 - Frames from High-Speed Movie
(Transient Response, Cantilever Beam)

56

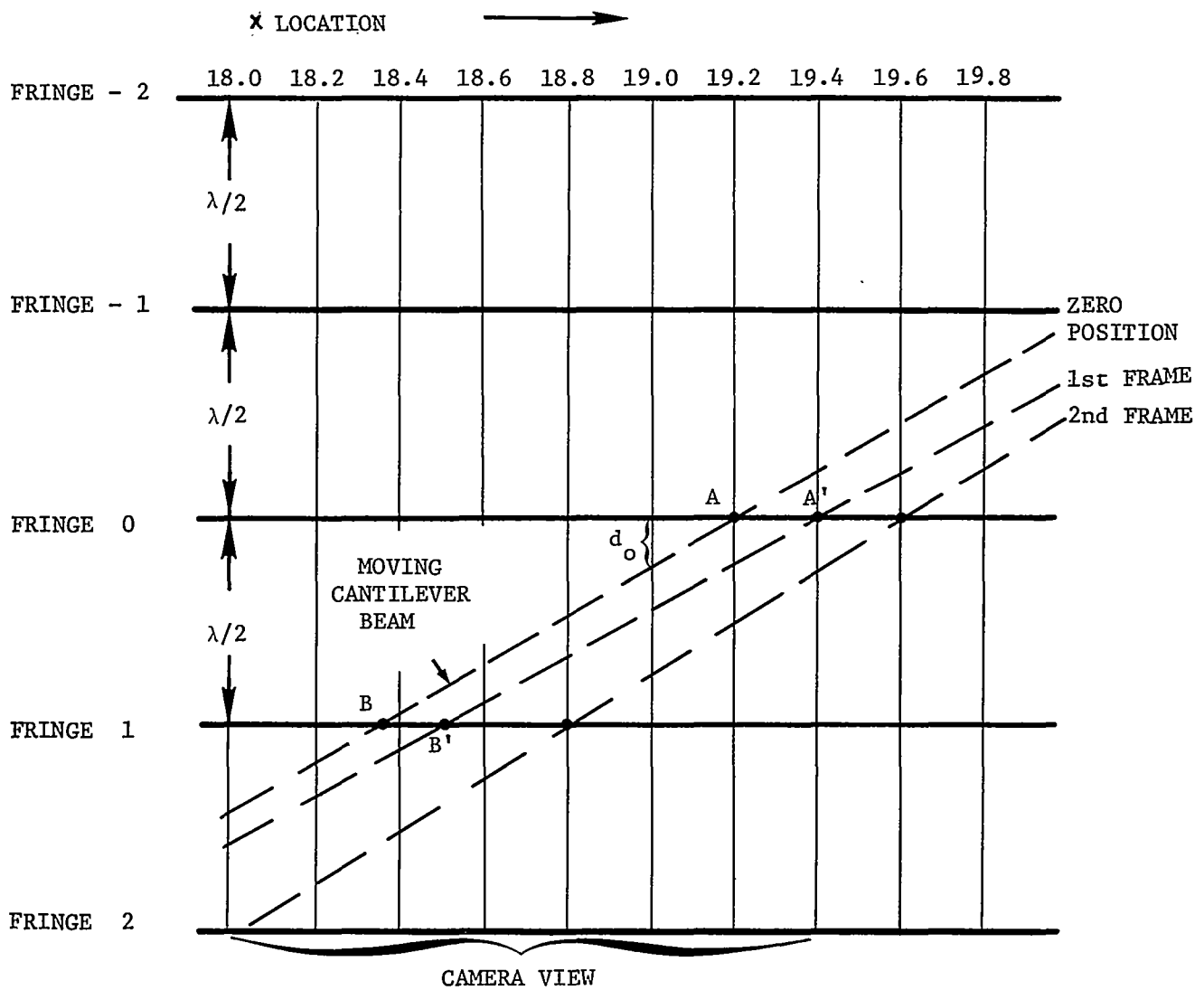from the initiation of impact until the 400 foot reel of film was exhausted. The Polaroid camera recorded the rebound of the pendulum. The entire test took less than 5 seconds to complete, once the experiment had been set up.

Two or three preliminary tests were made to determine the correct f - stop setting for the high-speed camera, so that the film was exposed properly. Once these preliminary tests were completed and the film developed, the final test was made. After the final film was developed, it was then necessary to reduce the data. The process of obtaining displacement-time histories from the movie film is discussed in the next section.

Reduction of the Film Data

Figure 31 shows photographs of five individual frames from the high-speed movie results. The illuminated spot at 10" from the root of the cantilever is in the left of the scene, and the two inch illuminated segment from 18"-20" appears on the right; the other two illuminated segments are in the middle of the scene. Frame zero in Figure 31 corresponds with the zero order fringes sketched in Figure 30. The dots on the beam which were spaced 0.2 inch apart are partly visible in Figure 31; the broad fringes would sometimes cover the dots and make them hard to see. The fact that the fringes are slanted in Figures 30 and 31 is thought to be due to either slight twisting of the beam when the support stud was used or inaccurate repositioning of the stored-beam hologram.

To understand how the data was obtained from the movie film, consider Figure 32, which shows how the fringes formed near the tip of the moving cantilever beam. Figure 32 is exaggerated drawing which shows the relationship between the interference fringes and the moving cantilever beam. The horizontal parallel lines labeled "fringe 0, fringe 1, etc." in Figure 32 are reference lines which control the location of the interference fringes. These parallel lines have a spacing of $\lambda/2 = 12.45 \times 10^{-6}$ inches apart, since the displacement between adjacent fringes is $\lambda/2$. The vertical parallel lines in Figure 32 have a spacing of 0.2 inches and refer to the equally spaced dots on the beam located at 18.0, 18.2, ... inches from the root of the cantilever. The heavy dashed diagonal lines in Figure 32 illustrate the position of the cantilever at times which correspond to frames 0, 1, and 2 of the movie film. The field of view of the movie camera is shown in Figure 32 (for the illuminated region at the tip of the beam).

Let x denote the distance measured from the root of the cantilever beam. By viewing Frame 0 of the movie film (Figure 31) and referring to the marks on the beam, it was noted that the fringe on the right was located at x = 19.2 and the adjacent fringe (to the left) was located at x = 18.35. (These fringe locations correspond to points A and B, respectively, in Figure 32). When the pendulum struck the beam, the tip moved toward the camera, and the fringes in the movie film (at the tip of the beam) moved toward the right. Frame 1 (Figure 31) showed that the right fringe had moved to x = 19.4 and its adjacent partner moved to x = 18.5. (These fringe locations correspond to points A' and B' in Figure 32.)

FRAME 2 t = .45 ms

FRAME 3 t = .68 ms

FRAME 4 t = .91 ms

x = 10"   x = 12"   x = 16"   x = 18 - 20"

FRAME 0 t = 0 millisec

FRAME 1 t = .23 ms

Figure 31 - Frames from High-Speed Movie'
(Transient Response, Cantilever Beam)

Figure 32 - Relative Position of Interference Fringes and Cantilever Beam

By neglecting the curvature of the beam and assuming that it was straight between two adjacent fringes, it was possible to obtain the displacement of the beam (in the tip region) by interpolation. The interpolation scheme can be understood by referring to Figure 33. First of all, the location $x = 19.0$ was chosen as the point where the deflection-time history would be computed. It was thus necessary to determine the "initial offset" at $x = 19.0$, represented by d_o in Figure 33.

The computation of d_o was accomplished by using similar triangles; thus, taking the ratios of corresponding sides (from Figure 33) we have

$$\frac{d_o}{BC} = \frac{19.2 - 19.0}{AC} \tag{4-1}$$

where BC and AC designate the sides of triangle ABC. However, the length $AC = 19.2 - 18.35 = 0.85$ in., and $BC = \frac{\lambda}{2} = 12.45 \times 10^{-6}$ in. Substituting these results into equation (4-1) yields

$$d_o = (\frac{.2}{.85})(12.45 \times 10^{-6}) = 2.93 \times 10^{-6} \text{ in.} \tag{4-2}$$

for the initial offset.

For Frame 1, a similar interpolation scheme was used to compute $d + d_o$, where d is the deflection at $x = 19.0$. Referring again to similar triangles in Figure 33, we have

$$\frac{(d + d_o)}{(\lambda/2)} = \frac{(19.4 - 19.0)}{(19.4 - 18.5)} = \frac{.4}{.9} \tag{4-3}$$

Equation (4-3) gives $(d + d_o) = 5.59 \times 10^{-6}$ in., and the deflection d can found by subtracting the initial offset, d_o. Thus, for the first frame, we have

$$d = (5.59 - 2.93) \times 10^{-6} \text{ in.}$$
$$\tag{4-4}$$
$$d = 2.66 \times 10^{-6} \text{ in.}$$

at the location $x = 19.0$. This interpolation procedure was continued for the first 714 movie frames following the initiation of impact. It was necessary to designate consecutive fringes by number, as indicated in Figure 31, since the fringes would move in and out of the scene as the beam moved back and forth.
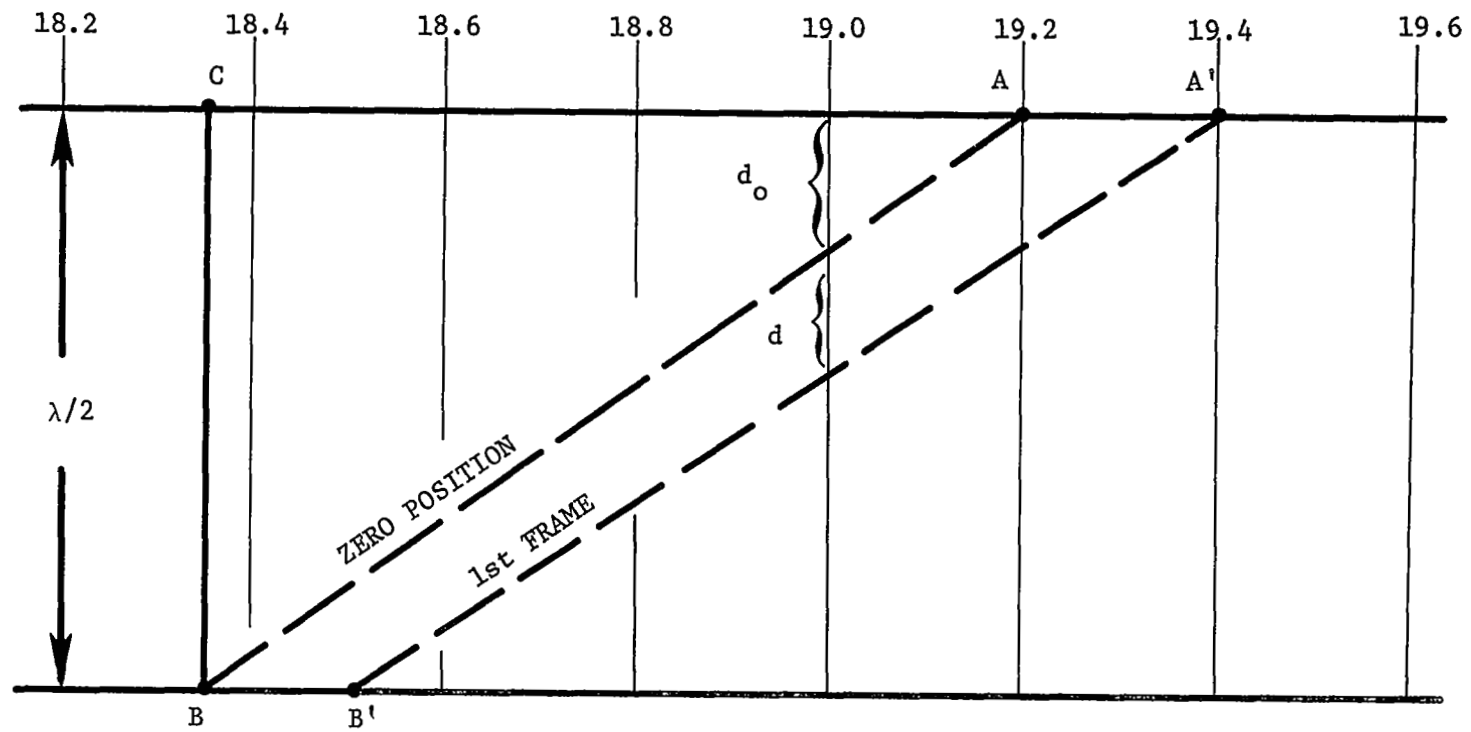
Figure 33 - Diagram for Interpolating Between Fringes

Additional calculations of a very straight-forward nature were necessary to determine the times corresponding to the individual movie frames. The frame just prior to impact was called "Frame 0" and was used to locate time t = 0. Timing marks were put on the edge of the film by a timing light in the high-speed camera. By counting the number of frames between timing marks and interpolating for intermediate frames, the time corresponding to each frame could be easily determined. The timing light had a nominal frequency of 1000 cps, and a time increment of 0.001 sec. was used in the initial data reduction. The frequency of the timing light was subsequently checked using a photocell and an electronic counter; this test gave a measured frequency of 1035 cps, which was then used in the final data reduction. Results of the film data are described in the next section.

Experimental Displacement – Time Histories and Comparison with Analysis

The data reduction procedure just outlined provided a detailed plot of the displacement-time history at the location x = 19.0 inches. The experimental results were compared with calculations of the transient response based upon elementary beam theory. These results are shown in Figure 34, which has three parts, (a), (b), and (c). In Figure 34, the vertical scale is in units of inches/lb-sec., i.e., the deflection has been normalized using the impulse of the applied loading. This normalization procedure was used to allow analysis and experiment to be directly compared; the impulse used to normalize the experimental data was 2.47×10^{-6} lb-sec., which was measured with the ballistic pendulum.

As Figure 34 shows, generally good agreement was obtained between the experimental data points and the calculated curves. The calculations were doen using the first ten modes of 20" cantilever, which were computed from Bernoulli-Euler beam theory. The theory used an idealized Dirac-delta function impulse, whereas the actual impulse had a time duration of approximately 5 micro-seconds. Slight errors in measuring the experimental impulse or in reading the film frames may account for the small discrepancies between theory and experiment shown in Figure 34.

Thus far, only the response at x = 19 inch (near the tip of the beam) has been discussed. An attempt was made to reduce the film data for the locations x = 10, 12, and 16 inches, but it was only partly successful. At these other locations, the illuminated portions of the beam were so short that only one fringe was visible at any one time. Since at least two fringes are required for the interpolation scheme to work, it was impossible to obtain data from each frame. Some data were provided each time a fringe fell directly upon the same position it had occupied at time t = 0; then it was known that the beam had moved an integral number of half-wavelengths ($\lambda/2$). By noting when the fringes changed direction in their motion (from right to left, etc.) it was possible to tell when a peak or a valley occurred in the response. Data obtained in this fashion are shown in Figure 35 for the x = 12 inch location. The experimental data
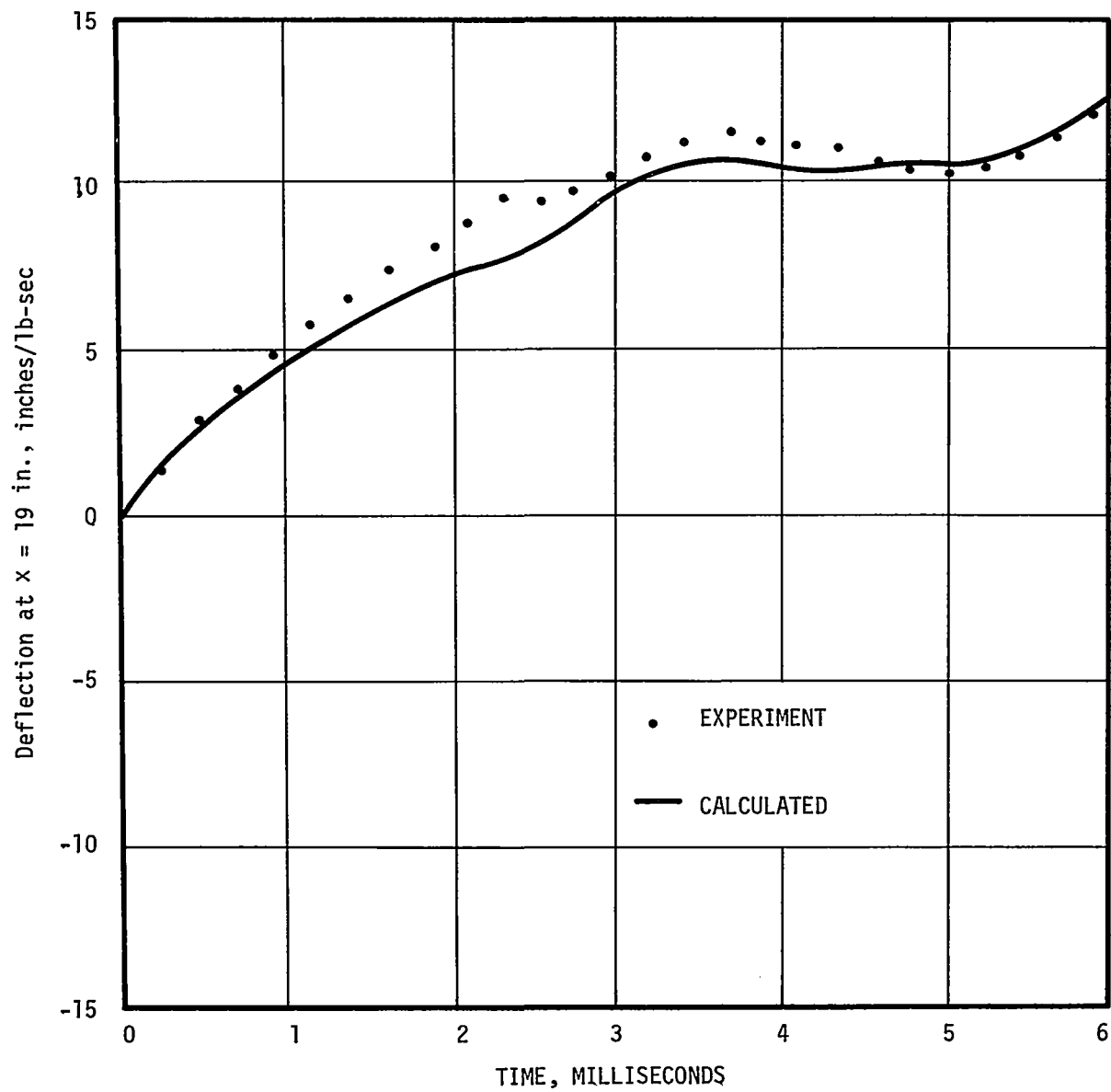
Figure 34(a) - Displacement-Time History at x = 19 Inches

61

TIME, MILLISECONDS
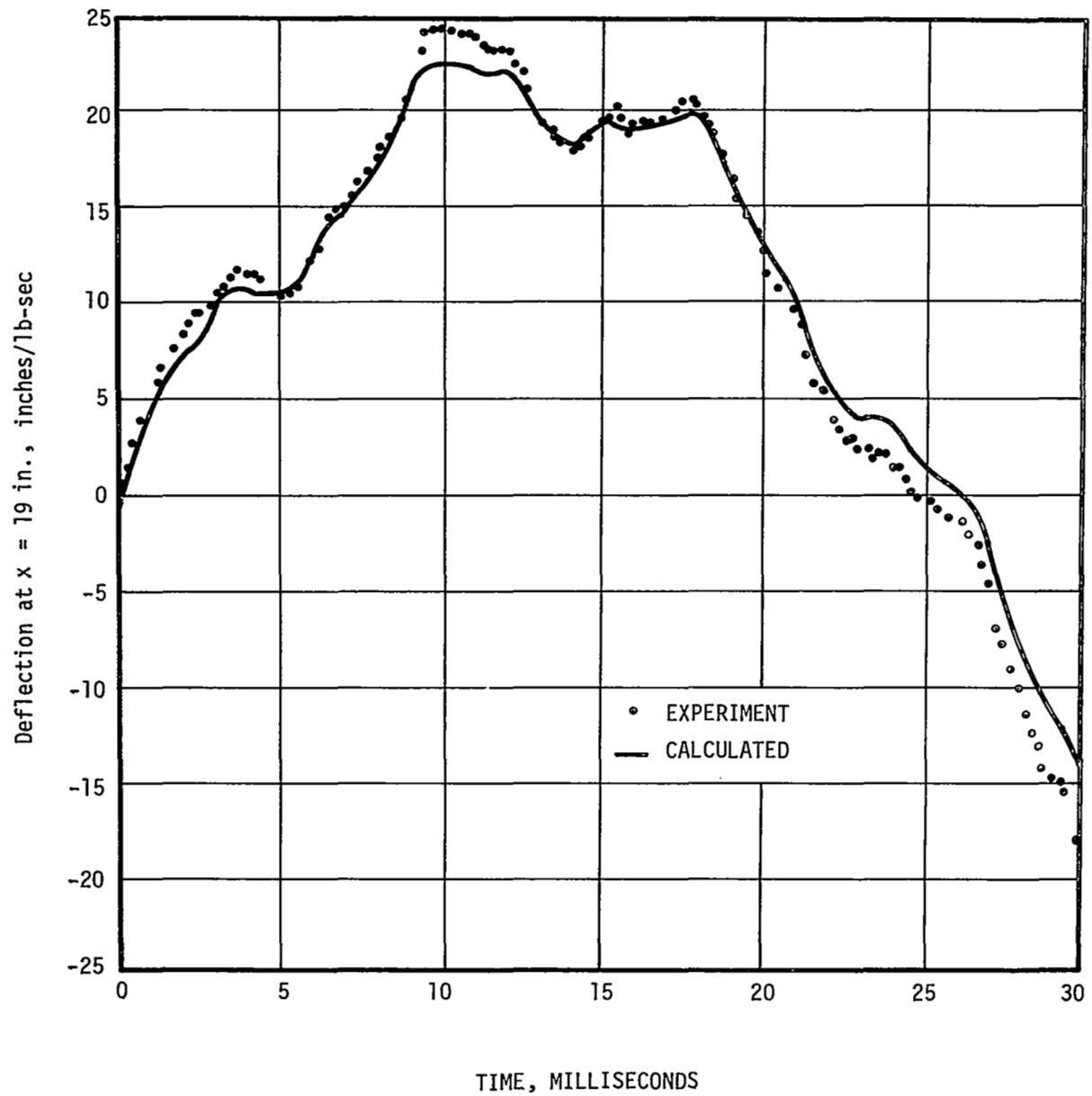
Figure 34(b) - Displacement-Time History at x = 19 Inches
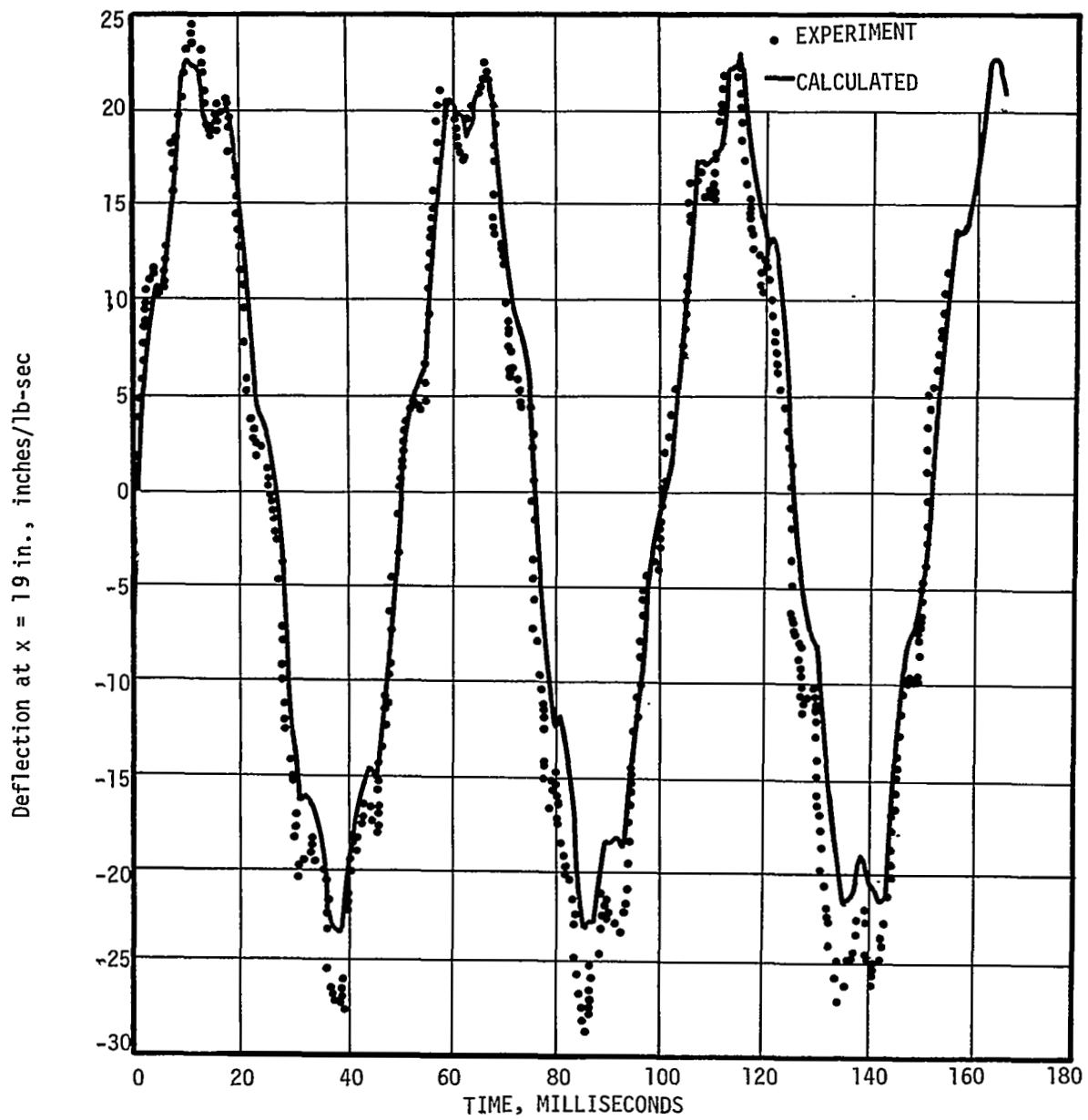
Figure 34(c) - Displacement-Time History at x = 19 Inches

points are scattered sporadically about the calculated curve, and qualitative agreement is seen. Because of the widely spaced data points, however, no detailed comparison of analysis and experiment was possible for the beam locations x = 10, 12, and 16 (inches).

This unfortunate development clearly points out that in future experiments of this type, the experimenter should capture two or more adjacent fringes and thereby have the ability to interpolate in obtaining displacement data.

Discussion of the Experimental Technique

The experimental method just presented has the advantage that no sensor or transducer need be attached to the structure. In addition, data can be recorded on movie film for a fairly large area of the structure and after the test it is possible to reduce the data at the points of greatest interest. This feature is in contrast with most currently available measurement techniques, which provide data at a point rather than over an area.

One characterization of conventional instrumentation is its "frequency response capability." By examining Figure 34, one can see that the present method will record motions of up to 500 cps. However, the recording capability depends on the amplitude of the motion, as well as its frequency. If the amplitude of the motion becomes too large, the back-and-forth motion of the interference fringes will occur too rapidly for the camera to record. An obvious solution is to use a higher speed camera, but then the duration of the data recorded will then be reduced. For a given camera speed, it seems possible to obtain a calibration curve of frequency vs. amplitude and establish a "capability envelope" for the system. Such a result would require several tests and was not attempted in this study.

Regarding the sensitivity of the technique, it should be mentioned that incremental displacements (from one frame to the next) on the order of 2×10^{-6} inches were readily determined. (See Equation 4-4, for example). Thus the method will record motions as small as 1/10th of a wavelength of the laser light. The resolution is limited only by ones' ability to detect lateral motion of the fringes in going from one frame to the next.

Lest the reader be misled, it should be noted that other recent investigators have made motion pictures of transient events using stored-beam interferometry. To the best of our knowledge however, they have not been successful in obtaining quantitative data from the movie film.

It should also be remarked that other methods of data reduction might have been used to obtain the displacement-time histories. The problem of finding the deflection (w) as a function of location (x) and time (t) can be regarded as the task of defining a surface in a three-dimensional w - x - t space. The movie film data provides the experimenter with discrete values of the function (w) at specific points x_i and t_i. The
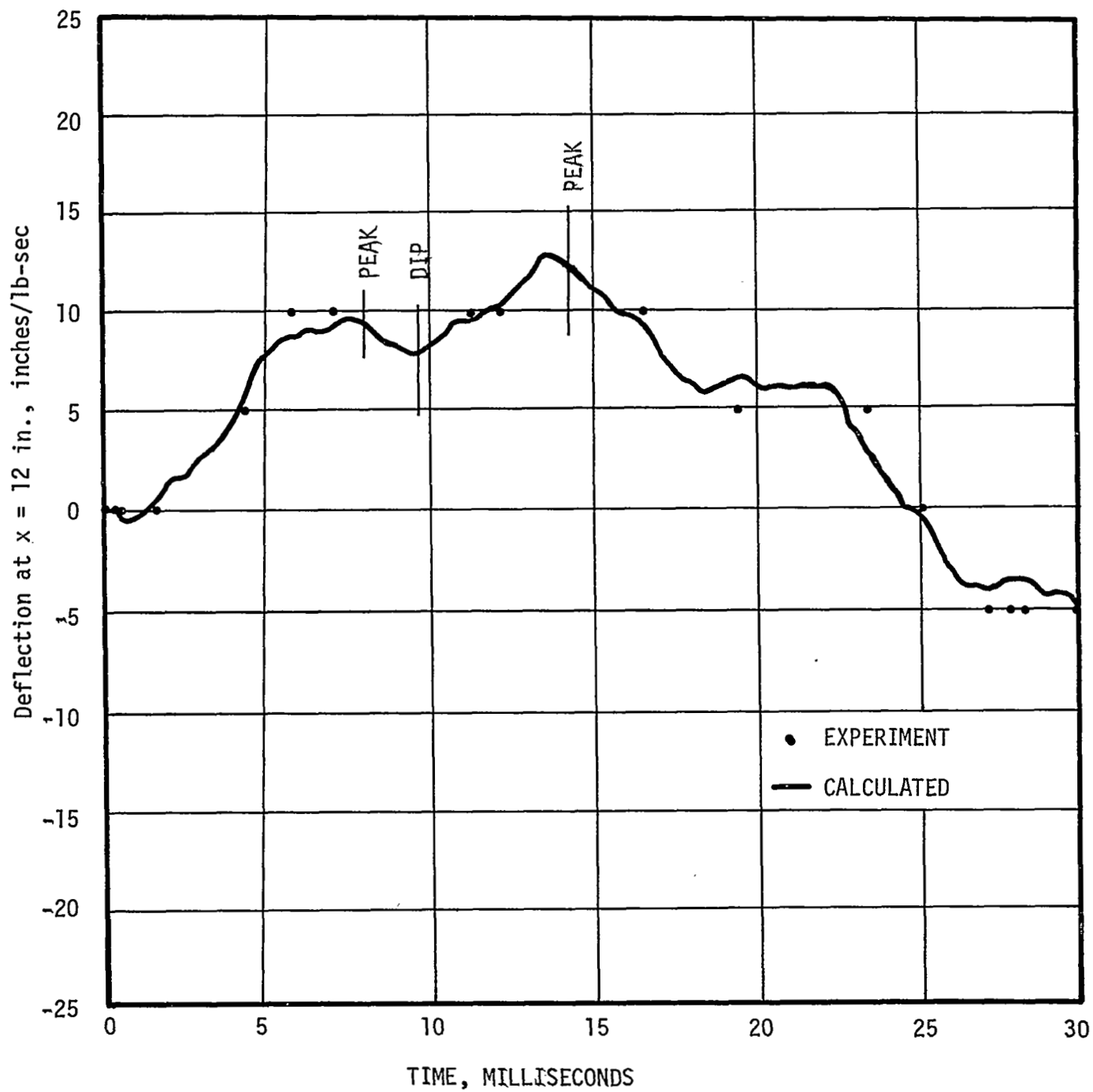
Figure 35 - Displacement-Time History at x = 12 Inches

points x_i correspond to locations of the fringes on the beam and the times t_i refer to the individual time of each movie frame. Using a two-dimensional interpolation routine (with a computer, say) one can fit a function (w) to the data points. Then by taking a "cut" through this surface at some x value, one would obtain the desired displacement-time history. This involved data-reduction process was not used herein, although it might provide more accurate data than the simple interpolation scheme which was used.

A distinct disadvantage of these methods is that each movie frame must be individually viewed and interpreted. It may be possible to automate this time-consuming process, and one such proposal is discussed in Section 6.

5.0 WAVE PROPAGATION STUDY

Summary

The objective of the wave propagation study was to demonstrate the use of holographic interferometry to measure transverse wave propagation in beams. Pulsed laser holography was used to record the bending wave created in a long beam by striking it in the center with a ballistic pendulum. Interferograms of the bending wave were obtained from three experiments, each one showing the deflected shape of the beam at a different time after impact. From the interferograms, plots of the transverse displacement vs. distance along the beam were obtained. The experimental data compared favorably with analytical results for the problem. A new experimental technique, called differential interferometry, was used to show how large amplitude motion can be recorded. Details of the experiment and the analysis are given in the sections which follow.

Experimental Set-Up

An aluminum beam (6061-T6) with a cross section one inch wide and 1/4 inch thick was used as the test specimen. The beam was clamped in a vise at each end, with a distance of 6 feet between supports. A liquid honing process was applied to the specimen to provide a diffuse optical surface well-suited for holography.

The optical arrangement used to make the holograms is shown schematically in Figure 36. Figure 37 is a photograph of the actual set-up. Referring to Figure 36, light is passed from the pulsed laser through a negative lens and thence to the front surface of the specimen. This light reflects from the specimen and forms the object beam for the hologram. Some of the light reflects from the first surface of the negative lens and is directed by mirrors to serve as the reference beam for the hologram. A continuous wave laser was used to align the lens and mirror arrangement and thereby insure uniform illumination of the specimen and the hologram. As things turned out, the arrangement of the optics was fairly straightforward and readily accomplished. A more difficult problem was to time the pulse of the laser to occur at a particular time delay after initiation of the wave. The details of the timing arrangement are discussed in the sections which follow.

The timing of the laser was accomplished electronically; in order to understand the electronics used, it is first desirable to discuss the characteristics of the pulsed ruby laser.

The basic components of the ruby laser which was used in this experiment are two mirrors, a ruby rod, a flash lamp, and a Pockels cell, arranged as shown in Figure 38. Referring to Figure 38, the two mirrors M_1 and M_2 serve to form the optical cavity. The ruby rod provides the optical energy (light) in a coherent, monochromatic form. The flash lamp
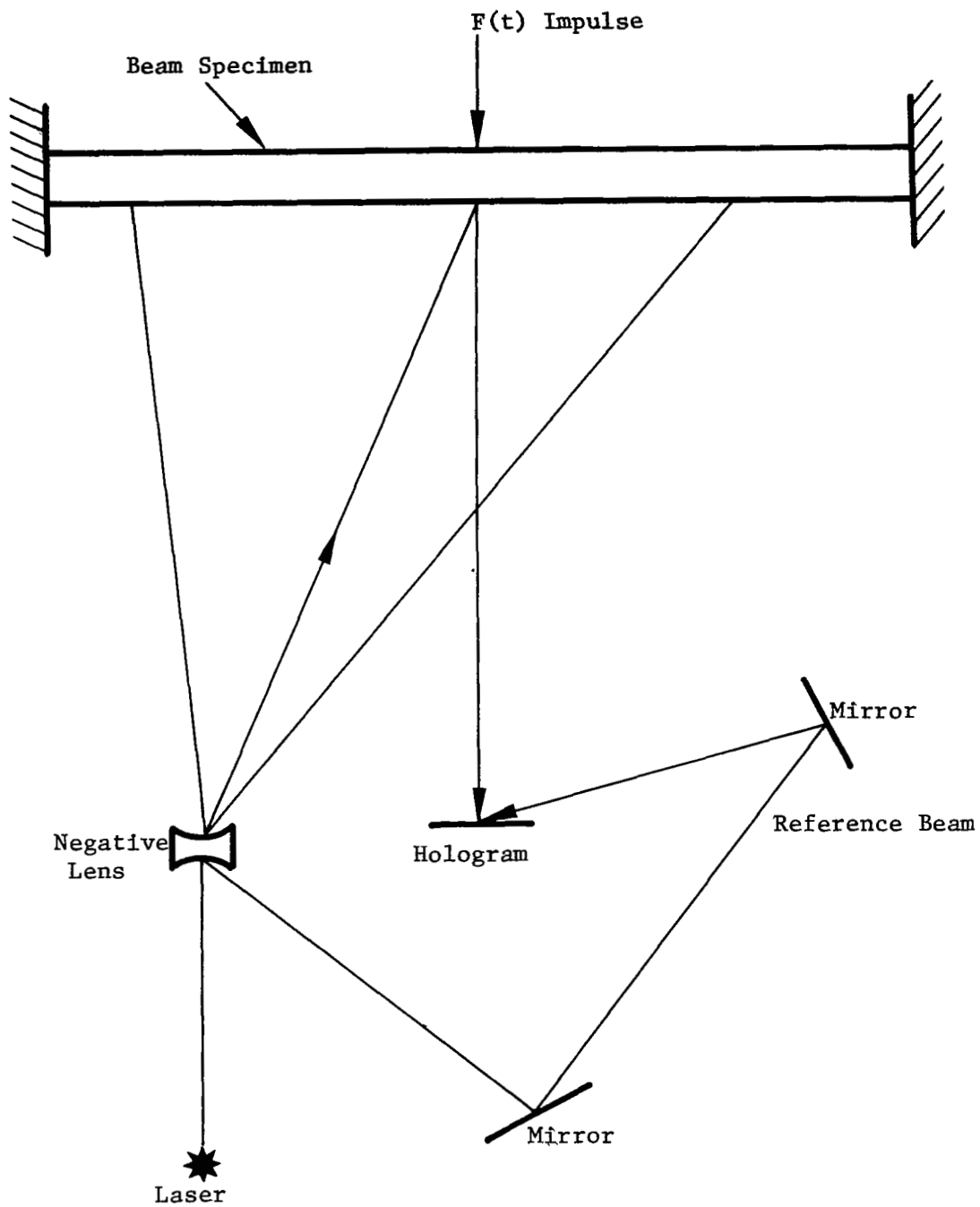
Figure 36 - Schematic of Apparatus for Transverse Wave Experiment
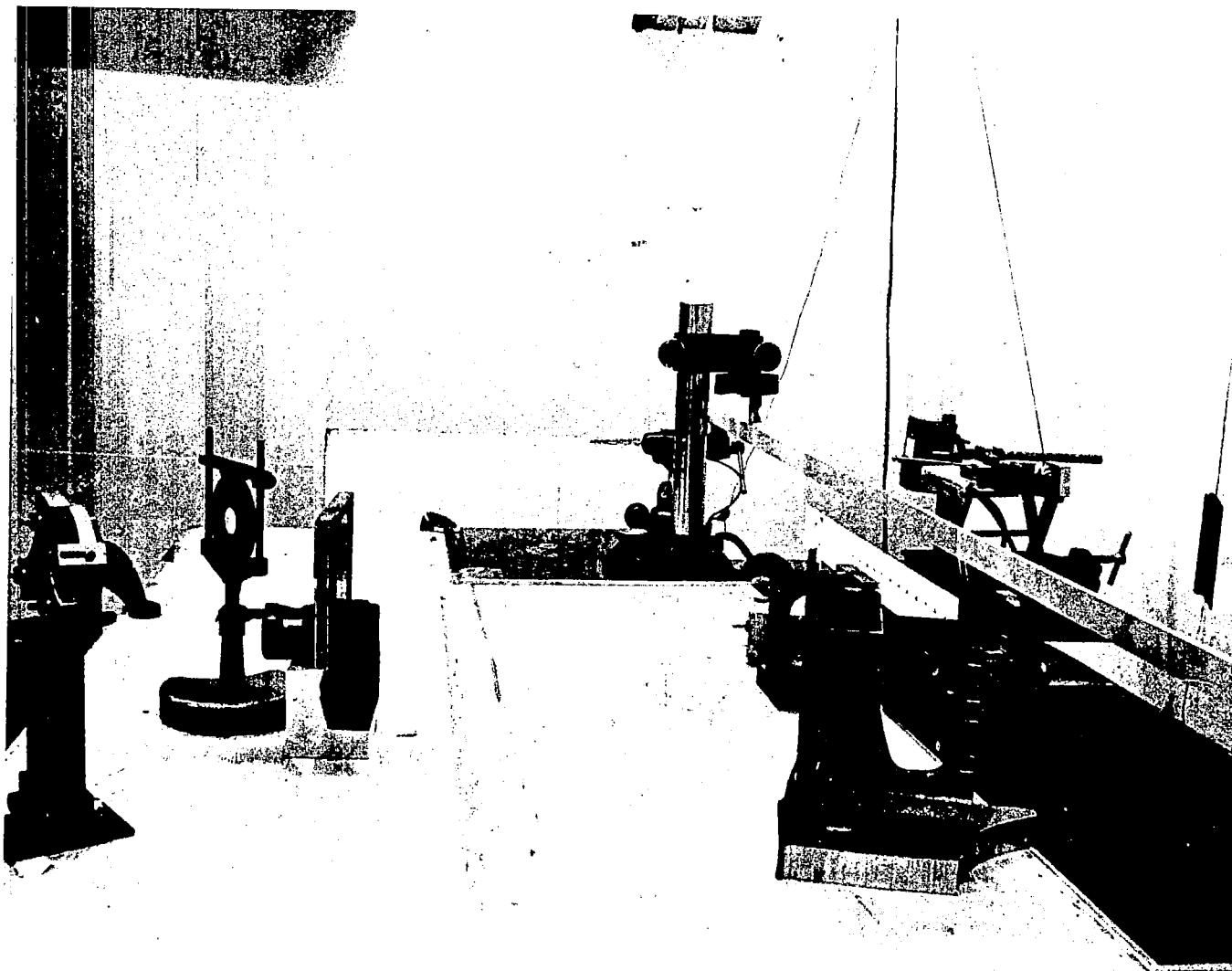
Figure 37 - Actual Set-Up Used for the Wave Propagation Study

FLASH LAMP

MIRROR M1

POCKELS
CELL

MIRROR M2
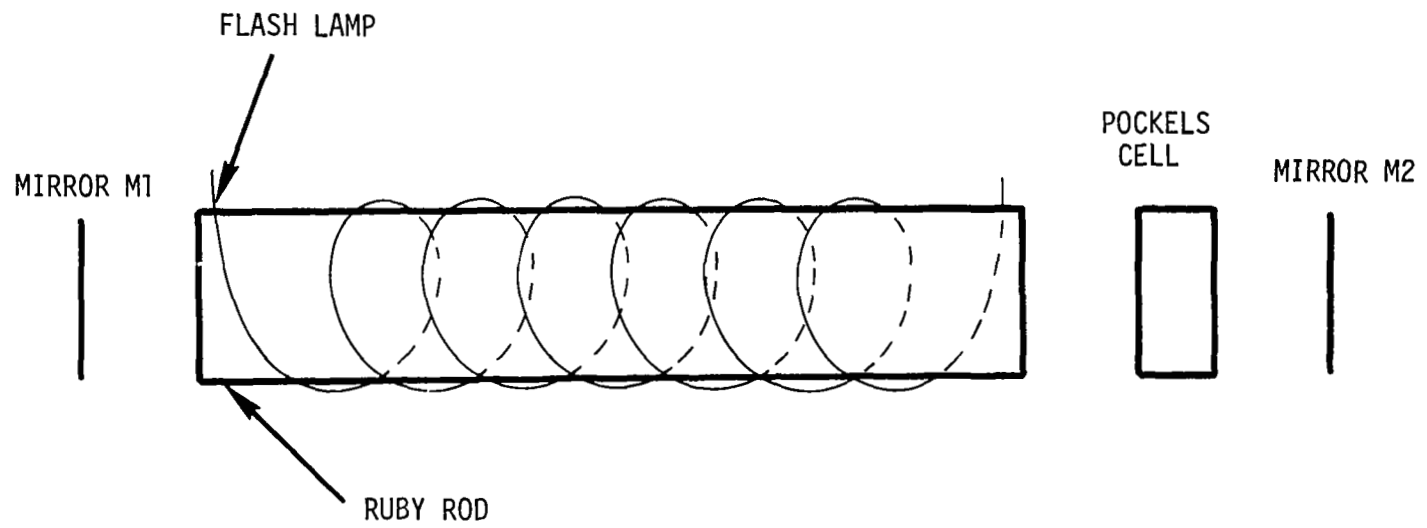
RUBY ROD

Figure 38 - Basic Components of the Ruby Laser

"pumps" the ruby rod, making it ready to lase. The Pockels cell acts as a shutter for the laser. When the proper voltage is applied to the Pockels cell, light is allowed to pass and the laser is permitted to lase. When there is no voltage, the Pockels Cell isolates the mirror M_2 from M_1 and the optical cavity is no longer complete.

Precise timing is required for successful operation of the laser. The voltage must be applied to the Pockels cell from 800 to 900 μsecs after the "pumping" of the ruby rod by the flashlamp. This requirement occurs because the flashlamp stays on for just 1000 μsecs and the ruby rod is sufficiently excited after 800 μsecs. After 900 μsecs the flashlamp begins to lose its intensity and consequently the rod loses its energy.

In summary, then, the laser requires that (1) the flashlamp be flashed about 800 μsecs before lasing, and (2) the Pockels cell must be activated 800 – 900 μsecs after flashing the flashlamp.

Timing Sequence for a Test

In performing the wave propagation experiment, electronic components were arranged to provide two electrical pulses – one to activate the flashlamp and the second to trigger the Pockels cell. A schematic of the electrical arrangement is shown in Figure 39. Referring to Figure 39, the sequence of events was as follows:

(1) The pendulum is released from its holder and starts on its way to impact the specimen.

(2) The ball of the pendulum interrupts the light from the CW laser. This breaking of the light beam causes a signal to be generated by the photocell. The signal enters the time delay circuit of oscilloscope 01 and, after a suitable time delay, the oscilloscope outputs a signal to flash the flashlamp.

(3) The pendulum continues to travel until it makes contact with the specimen. The impact causes a transverse wave to propagate away from the center of the beam. When the pendulum contacts the beam, it also completes an electrical circuit (pendulum, oscilloscope, battery pack, and beam). Closing this loop inputs a signal to the time-delay circuit of oscilloscope 02. After an appropriate time delay, Δ, the oscilloscope 02 generates a voltage which triggers the Pockels cell and allows the laser to lase.

The time delay used in Step 2 was chosen by carefully determining the travel time of the pendulum between points A and B (Figure 39). This travel time was found to be 8 millisec. Since 800 μsec was required by the flashlamp, the time delay for oscilloscope 01 was set at about 7.2 millisec.
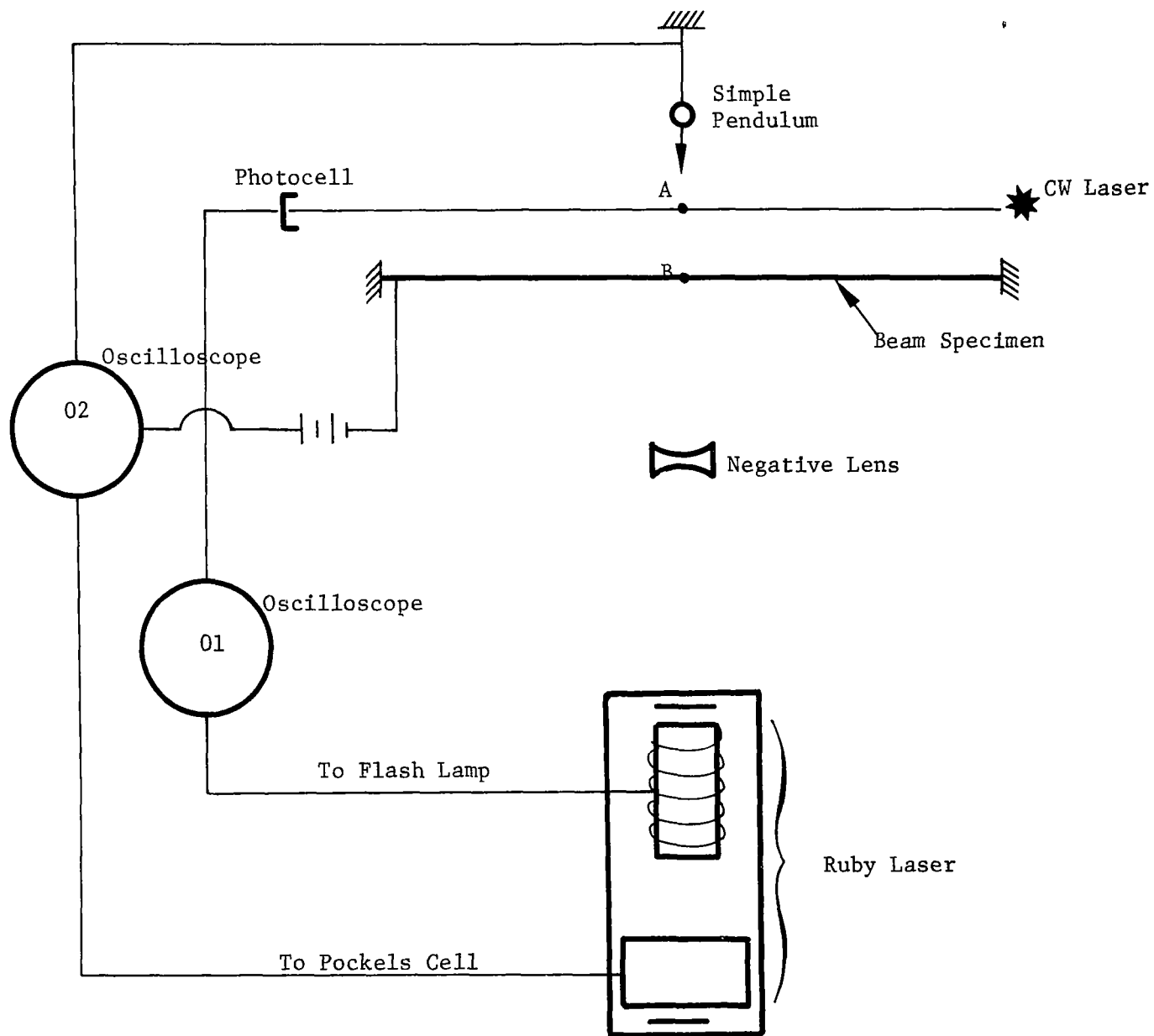
Figure 39 - Electrical Arrangement for Transverse Wave Experiments

The time delay, Δ, used in Step 3 was adjusted by the experimenter to allow the bending wave to travel various distances from the center of the beam before being photographed. The values used for Δ were 12.5, 25, and 50 μsec.

The test procedure was to first pulse the laser and make a hologram of the stationary beam, then release the pendulum and initiate the timing sequence to again expose the hologram when the bending wave was in the beam. This double exposure technique produced interferograms which were later reconstructed by a CW laser and then photographed. The resulting photos are discussed in the next section.

Experimental Results

Two sets of tests were made, using two different size pendulums. Results from the first tests (7/8 inch diameter pendulum ball) are shown in Figures 40 to 42. Figure 40 shows the central portion of the beam 12.5 μsec after impact (just opposite the point of impact); a ruler is shown in the lower half of the photo. The fringes in Figure 40 show that the beam "bulges out" in a nearly axisymmetric fashion in response to the impact. The leading fringe indicates that the front of the wave is about 1 inch from the center of the beam, but ahead of that, there may be a small amplitude precursor which has not caused any fringes.

Figure 41 is the result of a second test, which shows the wave 25 μsecs after impact. By this time the motion has started to change character from a two-dimensional surface (the bulging out) to a one-dimensional nature with the waves moving primarily to the right and left. The results of the third test are shown in Figure 42, which shows the bending wave 50 μsecs after impact. Figure 42 also contains a qualitative plot of the lateral deflection, y, vs. x, the distance along the beam.

Each fringe in Figure 40 to 42 is separated by a normal displacement of one-half a wavelength of the laser light, $\lambda/2 = 13.65 \times 10^{-6}$ in. Due to anticlastic behavior, the surface of the bent beam is doubly-curved; this curvature of the beam surface causes the interference fringes to be curved also. By comparison with the holograms made of beams in static bending (e.g., Refs. 3 and 9) it was evident that a hyperbola in the fringe pattern represents a relative maximum or a minimum in the displacement vs. x curve. Between one hyperbola and the next (adjacent) one, an inflection point occurs, which shows up as an interference fringe going straight across the beam. By counting the fringes (moving inward from the end of the beam) and noting where the hyperbolas occurred along the beam, it was possible to plot the lateral deflection, y, vs. position along the beam, x. Curves of this type are shown in Figure 43, which came from Figures 40-42 and show the deflection for the right half of the beam. Each data point on the curve labeled Δ = 50 μsec corresponds to a particular fringe in Figure 42; the x - location of the data point corresponds to the x - location of the fringe. Similarly, Figure 40 corresponds to the curve Δ = 12.5 μsec, and Figure 41 relates to Δ = 25 μsec. The
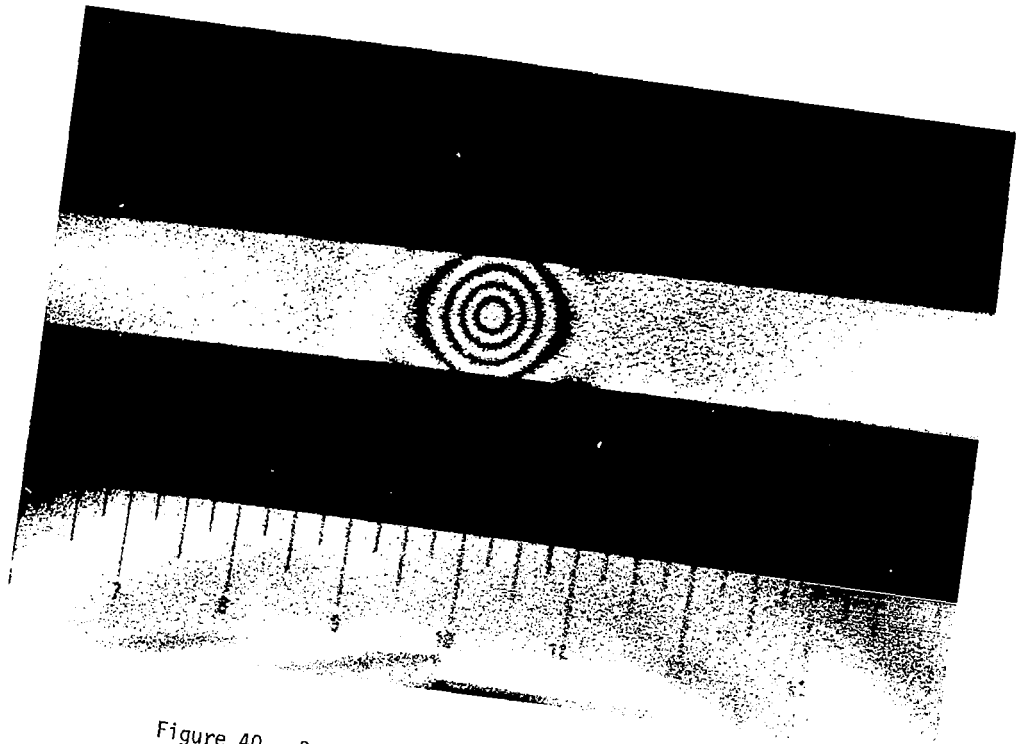
Figure 40 - Bending Wave 12.5 μsecs After Impact
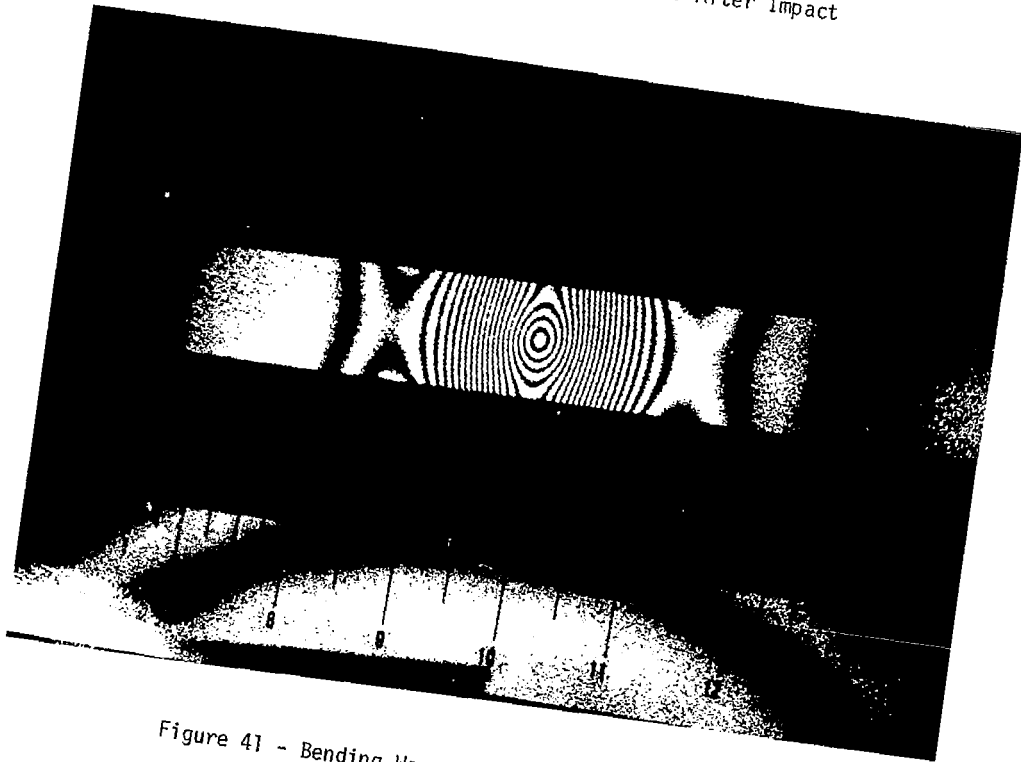
Figure 41 - Bending Wave 25 μsecs After Impact

74
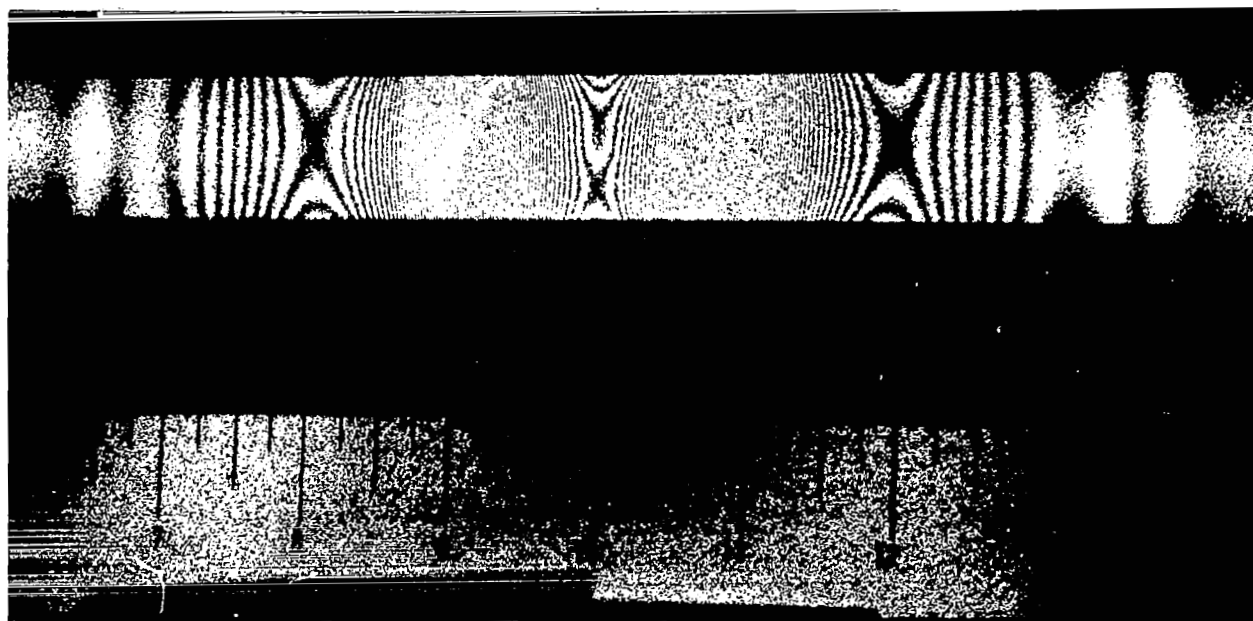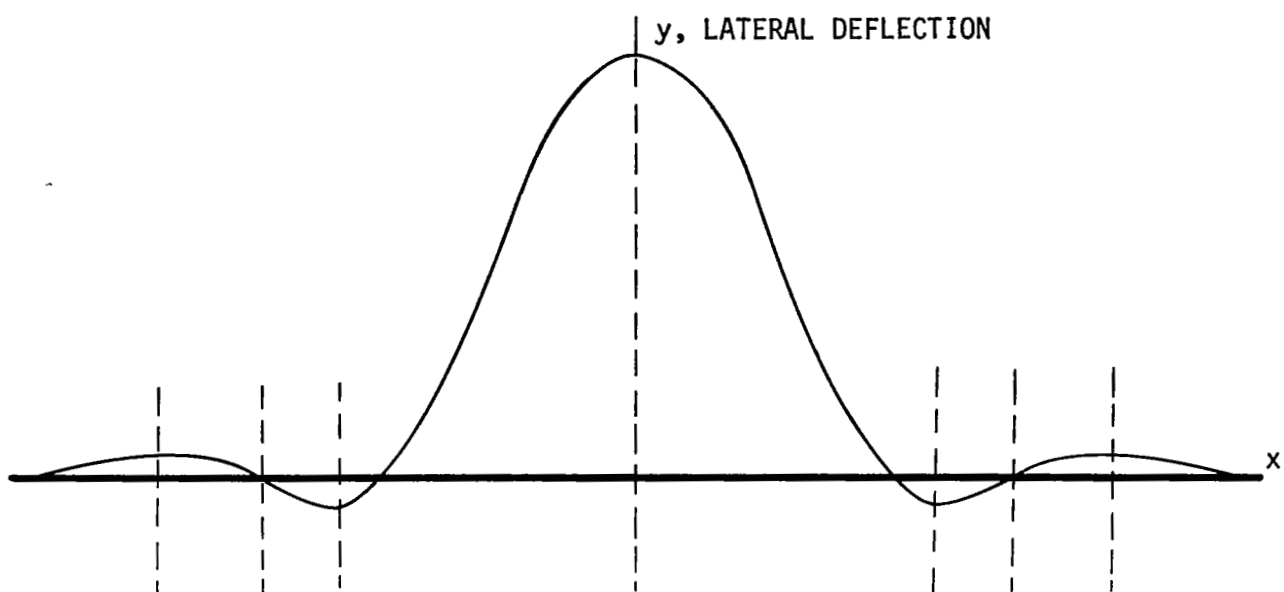
Figure 42 - Interferogram and Corresponding Displacement:
50 µsec After Impact

75
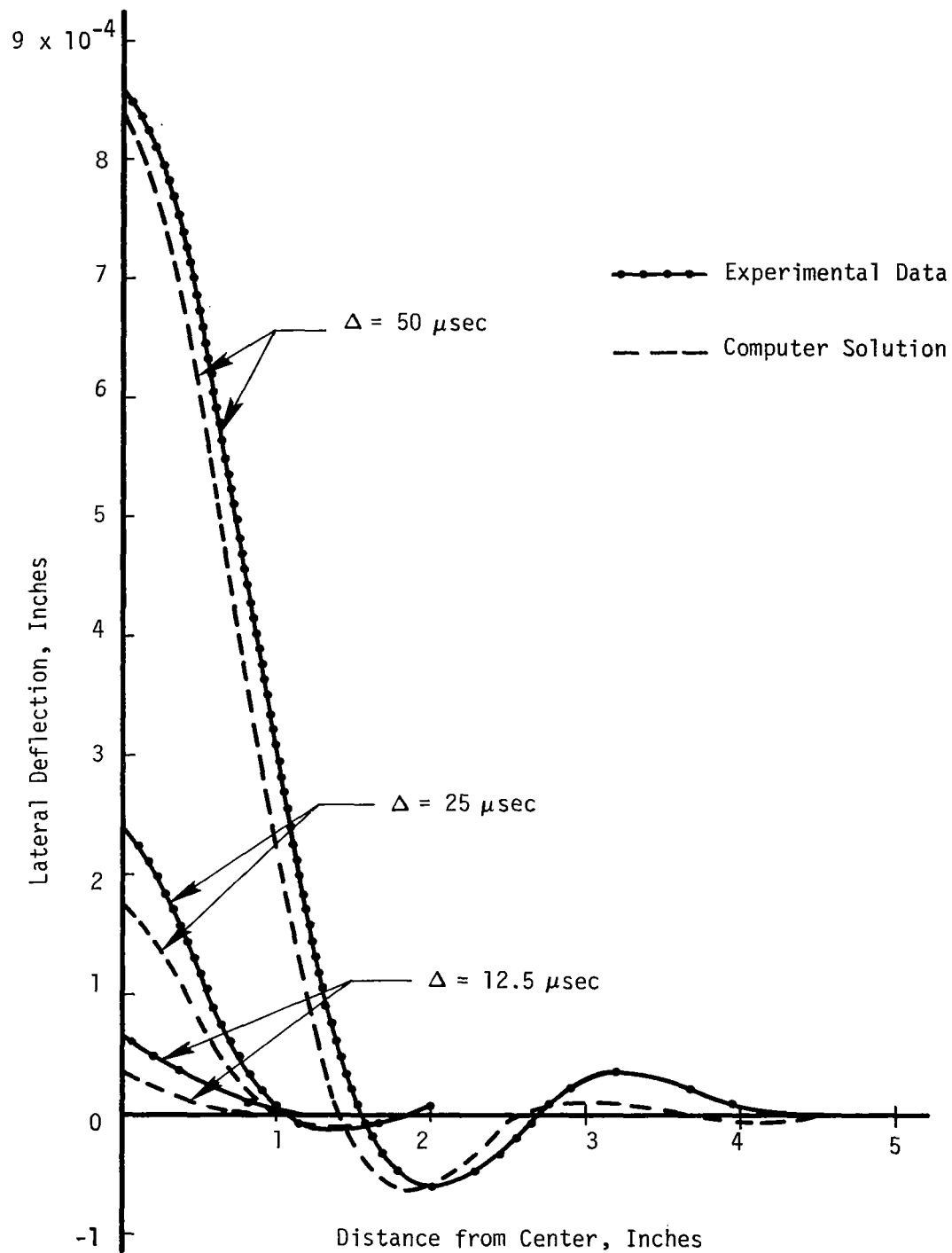
Figure 43 - Lateral Deflection (y) vs. Distance Along The Beam (x)

deflection pattern is nearly symmetrical with respect to the center of the beam. These experimental results are very similar to the calculated response of the beam which will be discussed shortly.

The first series of tests used a 7/8 inch diameter steel pendulum ball, and the duration of the impulse was measured electronically to be 100 μsecs. An oscilloscope measured the time the ball was in contact with the beam. The initial height of the pendulum was known, and the distance the ball rebounded after impact was measured. Using this data and the mass of the ball, it was possible to calculate the impulse applied to the beam. The impulse was not exactly the same in all tests, but a representative value was $I_o = 8.03 \times 10^{-3}$ lb-sec. A second series of tests were run using a smaller diameter ball (1/4") to shorten the duration of impact. In this case the impact duration was 30 μsec and the impulse was 2.92×10^{-4} lb-sec. These tests gave results very similar to Figures 40-42 and are presented in Appendix IV.

Differential Interferometry

In each of the double exposure interferograms discussed thus far, the stationary, undeformed specimen served as the reference image. Accordingly, the fringe patterns shown in Figures 40, 41 and 42 provide a measure of deflection referenced to the static undeformed beam. This approach would not have been practical if large displacements had been involved. For example, a large displacement between exposures would give rise to very many fringes so finely spaced that recognition would not be possible. An experimental procedure, termed "differential interferometry," was devised to overcome the difficulties involved with large displacements.

This differential procedure involves taking two exposures of the beam in rapid succession. The first laser pulse occurs at a time when the beam is deflected by the transverse wave; a second pulse of the laser occurs a short time later. The resulting interference fringe patterns can then be interpreted to provide the displacement of the beam between the two exposures. The procedure just described was used to obtain holographic interferograms of a transverse wave propagating in the beam specimen. The beam and loading conditions were the same as those described previously. The first exposure of the hologram was made 25 μsec after pendulum impact; this provided the reference scene for the interferogram. The second exposure of the hologram was made at t = 50 μsec after pendulum impact. The times of 25 and 50 μsec were chosen so that results can be compared directly with those of Figures 41, 42 and 43.

The differential fringe pattern which resulted is shown in Figure 44. By counting the individual fringes and knowing that the beam was at rest ahead of the wave, Figure 44 was interpreted to determine the differential displacement between the two exposures. This differential measurement is shown in Figure 45 by the solid data points. Also shown in Figure 45 is the differential displacement computed by subtracting the deflection at
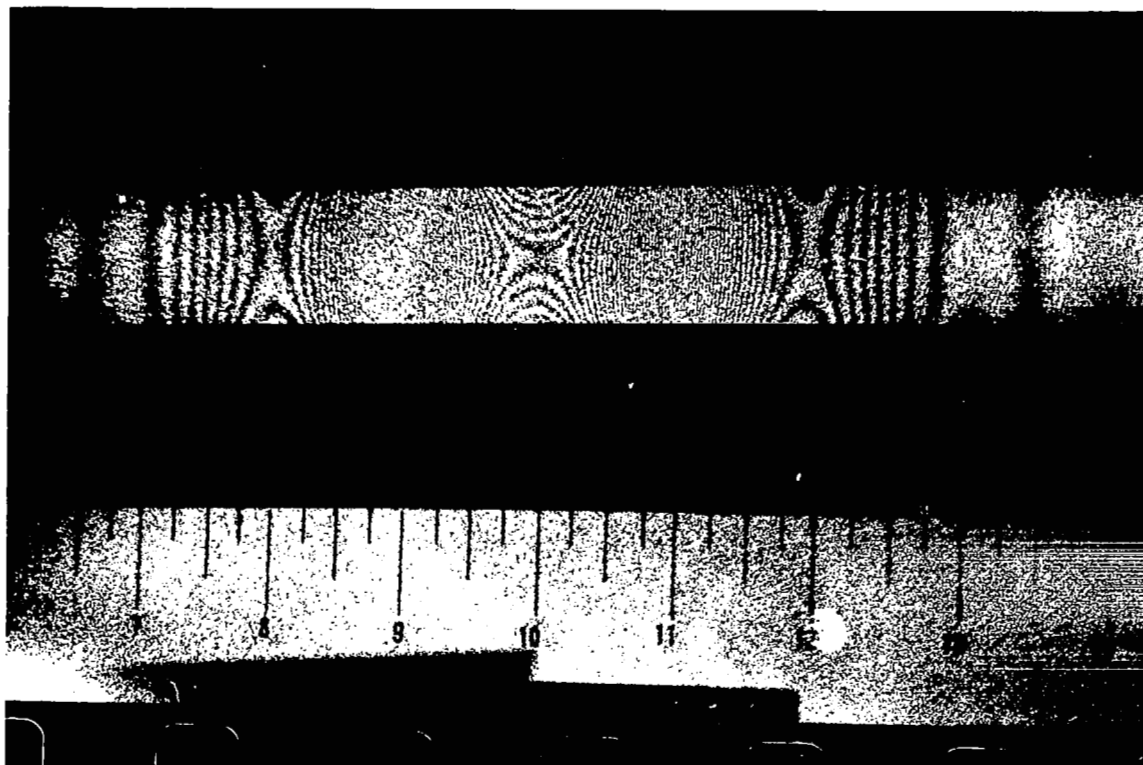
Figure 44 - Differential Fringe Pattern: Exposures at t = 25 and t = 50 μsec

78
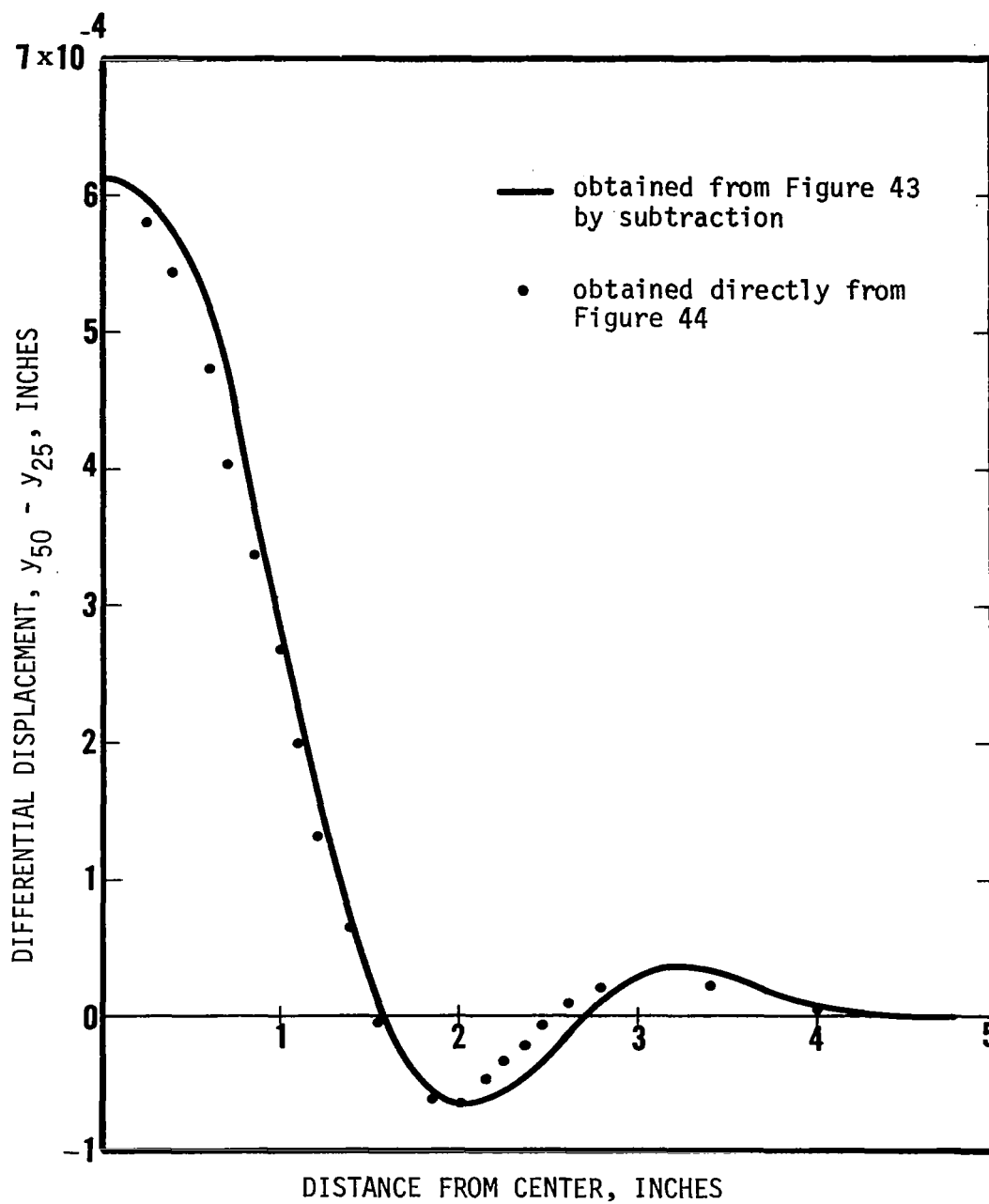
Figure 45 - Comparison of Differential Displacement
Obtained from Figures 43 and 44

t = 25 µsec from the deflection at t = 50 µsec given in Figure 43. This second set of data is shown by the solid line in Figure 45. Figure 45 shows that the differential displacements measured by the two techniques agree to within a few percent. Differences between the two curves in Figure 45 may be attributed to the non-repeatability of the impact. The results of this test were particularly gratifying; they showed that differential holographic interferograms can be used whenever structures undergoing large displacements need to be examined. This differential technique has also been used to obtain vibration modes of a plate at large amplitudes (.5 inches peak-to-peak); see Section 6.0.

Analytical Considerations

To set up the wave propagation experiment, an estimate was needed for the magnitude of the impulse to be applied to the beam. In order to answer these questions, a solution of the Timoshenko beam equations was obtained for a doubly-infinite beam subjected to an impulsive transverse load. The approach used parallels that of Dengler and Goland (29), who obtained the bending moment response for this problem. The Timoshenko Beam equations are given by

$$EI \frac{\partial^2 \psi}{\partial x^2} + k^2 AG \left(\frac{\partial y}{\partial x} - \psi \right) = \rho I \frac{\partial^2 \psi}{\partial t^2} \tag{5-1}$$

and

$$\rho A \frac{\partial^2 y}{\partial t^2} - W = k^2 AG \left(\frac{\partial^2 y}{\partial x^2} - \frac{\partial \psi}{\partial x} \right) \tag{5-2}$$

where y is the transverse deflection,
ψ is the bending slope,
EI is the bending stiffness,
$k^2 AG$ is the shear stiffness,
ρA is the mass per unit length,
ρI is the mass moment of inertia of the cross section,
W is the transverse load,
x is the coordinate along the length of the beam, and
t is the time

The initial and boundary condition associated with Equations (5-1) and (5-2) are

$$\left. \begin{array}{l} y(x,0) = 0 \\ \frac{\partial y}{\partial t}(x,0) = 0 \end{array} \right\} \quad -\infty < x < \infty$$

$$\left. \begin{array}{l} \psi(x,0) = 0 \\ \frac{\partial \psi}{\partial t}(x,0) = 0 \end{array} \right\} \quad -\infty < x < \infty \tag{5-3}$$

$$\lim_{\substack{|x|\to\infty \\ t \text{ finite}}} \left(y, \frac{\partial y}{\partial x}, \frac{\partial^2 y}{\partial x^2}, \psi, \frac{\partial \psi}{\partial x}, \frac{\partial^2 \psi}{\partial x^2} \right) = 0 \qquad (5\text{-}4)$$

for a doubly-infinite beam which is initially at rest.

An analytical solution to the Timoshenko Beam equations was obtained using Fourier and Laplace Transform Techniques. The analytical solution was for a loading W(x,t) taken as

$$W(x,t) = I_o \, \delta(x) \delta(t) \qquad (5\text{-}5)$$

where I_o is the applied impulse (lb-sec.) and $\delta(x)\delta(t)$ denotes Dirac-Delta functions for a point load in space and an idealized impulse in time. In order to readily invert the transforms involved, the preliminary analysis assumed that both wave speeds in the problem were equal $(k^2 G/\rho = E/\rho)$. Although this assumption is physically unrealistic, the resulting response calculations were accurate enough to design the experiment.

However, once the experiment had been performed, it was desired to compare the results with a more refined analysis. To accomplish this end, a computer program (Ref. 30) was used which solved Equations (5-1) and (5-2) by the method of characteristics. In this case, the applied load was taken in the form

$$W(x,t) = P(t)\delta(x) \qquad (5\text{-}6)$$

where the time-history of the form P(t) was assumed as

$$P(t) = \begin{cases} A_o \sin \frac{\pi t}{T} & 0 \leq t \leq T \\ 0 & T \leq t \leq \infty \end{cases}$$

The duration, T, of the applied load was set equal to 100 μsec, which was the measured value of the impact duration. The amplitude, A_o, was scaled in such a fashion that the impulse of the applied load was made equal to the measured impulse of 8.03×10^{-3} lb-sec. That is,

$$\int_o^T P(t)dt = I_o = 8.03 \times 10^{-3} \text{ lb-sec.}$$

The computer program used

$$\sqrt{E/\rho} = 1.967 \times 10^5 \text{ in/sec} = \text{bar velocity}$$

and

$$k\sqrt{G/\rho} = 1.0 \times 10^5 \text{ in/sec} = \text{shear velocity}$$

which are characteristic of a rectangular aluminum beam.

The computer program resulted in a plot of deflection, y, vs. x, the distance from the point of impact (the center of the beam). Computed results are shown in Figure 43, for the times t = 12.5, 25, and 50 μsec. As indicated previously, the impulse used in the analysis was set equal to the experimental value, and the experimental force-time history was idealized as a half-sine pulse.

Discussion and Conclusions

The primary results of this study are shown in Figure 43, which was derived from Figures 40 through 42 and the computer analysis. The best agreement between theory and experiment was obtained for t = Δ = 50 μsec after initiation of impact. In this case, the peak values of displacement differed by about 3%, which is good agreement, considering the approximations involved in the analysis and possible errors in measurement.

Theory and experiment agreed less well for Δ = 12.5 and 25 μsec. This lack of agreement at the early times is not surprising, when Figure 40 and 41 are considered. These figures show that initially the beam behaved much like a plate when impacted by the pendulum. For the early times, the response was two-dimensional in nature, rather than one-dimensional as assumed by Timoshenko Beam Theory.

The results demonstrate that pulsed laser holography can be used to obtain reliable quantitative measurements for problems involving transverse wave propagation. Holographic interferograms of the type presented here can be interpreted to yield displacement (y) vs. space (x) at individual discrete times (t_i). These full-field results are in contrast with the usual point measurements (such as strain gages) which give time histories of the event at discrete locations.

The holographic method used herein is limited in that the displacement must be at least $\lambda/4 = 6.83 \times 10^{-6}$ inches for the first interference fringe to form. Also, since the pulse duration of our laser is approximately 10×10^{-9} seconds, the wave motion to be recorded must have a

characteristic time longer than 10 nanoseconds. For many problems involving transverse wave propagation in structures, the pulse duration of the laser is short enough to effectively "freeze" the motion of the structure. These features of pulsed laser holographic interferometry make it attractive for problems involving wave propagation in rods, beams, plates, and shells. Some exploratory studies have been made by the authors on transverse axisymmetric waves in a plate, and more work is planned on flexural waves in cylindrical and conical shells.

The technique of differential holographic interferometry allows the extension of conventional pulsed laser methods to include measurement of large displacements. By making a series of differential holograms, the experimenter can study large displacement phenomena which previously exceeded the capabilities of conventional holographic interferometry.

It is expected that these experimental methods will receive wider application as more investigators come to appreciate the capabilities of pulsed laser holography.

6.0 SUGGESTIONS FOR FUTURE EXPERIMENTS

Introduction

This section of the report departs from the scientific description of details and results presented in Sections 1.0 through 5.0. Instead, this section describes exploratory studies in search for improvements and new applications of holography; consequently, it contains the authors' judgments and speculations concerning holographic techniques. Since the ideas presented in this section are still under development, their outcome is not yet certain.

Vibrations of Plates and Shells

Holography is particularly adapted to the study of vibrations which are two-dimensional in nature, such as the flexural vibrations of plates, membranes, and shells. Most of the early work using holography for vibration analysis made use of such two-dimensional structures (See Ref. 9-12). Holography will work on curved surfaces as well as flat ones, and it has been applied to turbine blades (Ref. 13) and cylindrical shells (Figure 46). Figure 46 shows the result of a time-average hologram for a cylindrical shell vibrating in one of its flexural modes. The shell was excited using a piezoelectric transducer, just as in the beam and plate experiments.

When curved surfaces are used, care must be exercised in interpreting the fringe patterns to obtain mode shape data. The formation of fringes is affected by the $\cos\theta$ terms in equation (3-2), and for curved surfaces this angular term can be quite significant. For plate vibration work, it is customary to make the angles θ_1 and θ_2 nearly zero and then forget about them. In shell vibrations (e.g., cylinders or cones) the fact that θ changes around the circumference must be included.

Accounting for this change in angle is not a major problem, and future investigators can be expected to apply holography to the vibrations of shells and curved panels. Stiffened plates, sandwich panels, and stiffened shell structures also represent potential areas for holographic vibration analysis. Structures with cut-outs or discrete masses can readily be analyzed by means of holography. The ability to give rapid, area-type measurements means that holography will be used increasingly for vibration studies of two-dimensional structures.

One particular experiment of considerable theoretical interest would be the high-frequency vibrations of a cylindrical shell. Based upon the results given herein for plates (Section 3.0), it appears possible to detect shell modes on the order of $m = 15$, $n = 20$ (or even higher). These high modes could be compared with a Mindlin-type theory for shells, which would include rotary inertia and shear effects. (See Ref. 27). Such high shell modes have not been observed previously and might show unusual effects.

84
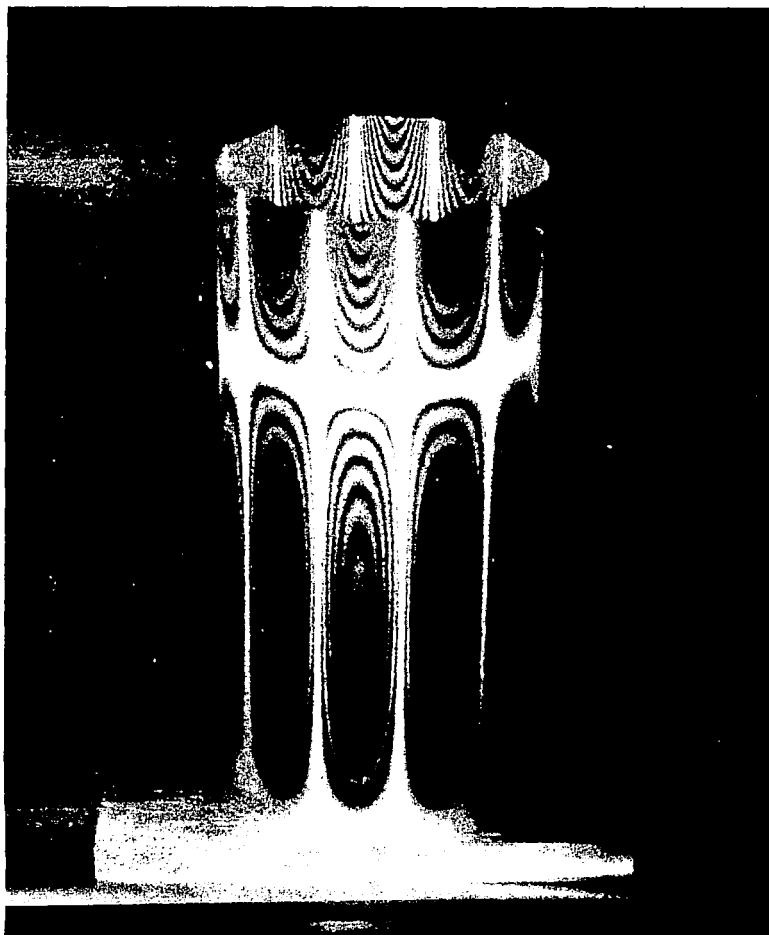
Figure 46 – Time-Average Hologram of a Cylindrical Shell
Vibrating in a Flexural Mode

Another area of application for holography appears to be in the vibration analysis of plates and shells at high temperature. When the surface temperature of the structure exceeds 500°F or so, conventional vibration pick-ups (such as capacitance or inductance probes) tend to run into difficulties. Preliminary results indicate that holography can be used for vibration studies of plates at temperatures as high as 1500 - 2000°F. In fact, it appears that holography may be the only technique which is practical at such temperatures.

Pulsed Laser Experiments on the Vibration of Large, Noisy Subjects*

Time-average holography and stored-beam interferometry are limited in application to small amplitude vibrations. If large vibration amplitudes are used with these holographic techniques, the interference fringes crowd closely together in regions of high slopes and cannot be readily distinguished from one another. For example, a slope of 6×10^{-4} radians corresponds to a fringe spacing of 0.01 inches when light of 6328 Angstroms is used. Larger slopes result in even closer fringe spacing. This limitation on allowable vibration amplitudes is a fundamental drawback to applying holography with large-scale, flexible structures.

Another limitation of the holographic techniques used to date for vibration analysis is the fact that the entire system must be isolated from background vibrations and noise. This isolation requirement presents a problem when large-scale structures are involved.

To overcome these limitations of present techniques for holographic vibration analysis, the use of pulsed laser holography appears very promising. Consider what happens if a structure is vibrating, sinusoidally in a normal mode, and a double exposure hologram is made by pulsing the laser once at time t_1 and again at time t_2. From the first pulse, we have the displacement

where

$$w_1(\vec{x},t) = A \; \Phi(\vec{x}) \; \sin \omega t_1$$

    A is the amplitude,
    $\Phi(x)$ represents the mode shape,
    ω is the vibration frequency
and t_1 is the time of the first exposure

The second pulse at time t_2 gives the displacement

$$w_2(\vec{x},t) = A \; \Phi(\vec{x}) \; \sin \omega t_2$$

The interference patterns which forms is a measure of the difference in displacements at time t_1 and t_2. Thus, the interference pattern is proportional to

$$w_1 - w_2 = A \, \Phi(x) \, [\sin\omega t_1 - \sin\omega t_2]$$

$$= K\Phi(x)$$

where K is a constant representing the product $A[\sin\omega t_1 - \sin\omega t_2]$. By adjusting the times t_1 and t_2 to be close together, only a few interference fringes will be formed, regardless of the amplitude of vibration. From this fringe pattern, the mode shape $\Phi(\vec{x})$ can be found. This technique of double-pulsing thus eliminates the restriction of small amplitude vibrations.

In addition, since the duration of each pulse is on the order of 10^{-8} seconds, the recording of the hologram is not influenced by seismic disturbances and other background noise. An example of a hologram of a vibrating object made by this double-pulse method is shown in Figure 47. The vibrating specimen was a piece of aluminum sheet, 6 inches wide and 36 inches long, supported at the center on the armature of a shaker. (See schematic, Figure 48.) Only the right half of the specimen is shown in Figure 47. The laser was pulsed at times t_1 and t_2 with a 50 μsec delay between pulses. Notice that the number of fringes formed was not unduly large, although the plate was vibrating with a peak-to-peak displacement of 1/2 inch at the tip.

The vibration shape indicated by the hologram is compared with data obtained by direct measurement and shown in Figure 49. The circled data points in Figure 49 were obtained using a hand-held ruler and measuring the peak-to-peak displacement at locations along the beam at one-inch intervals. The solid line was obtained by counting the fringes in Figure 47, choosing as zero a point 14 inches from the tip of the beam. The data have been scaled such that 115 fringes is equivalent to .55 inches, making the first and last points of the two data sets coincide. In general, the agreement between the two measurement schemes is quite good, inches with the differences being less than 1/20 of an inch. This is within the tolerance achieveable with the hand-held ruler.

Figures 47 through 49 demonstrate that pulsed laser holograms can be made and analyzed in the manner just described. These results are particularly significant for future applications of holography to vibrations, since they demonstrate that we are no longer limited to small amplitude motions. From the experiment described here, the way to future holographic vibration analysis of aircraft flutter models or large-scale structures seems fairly clear.

6"
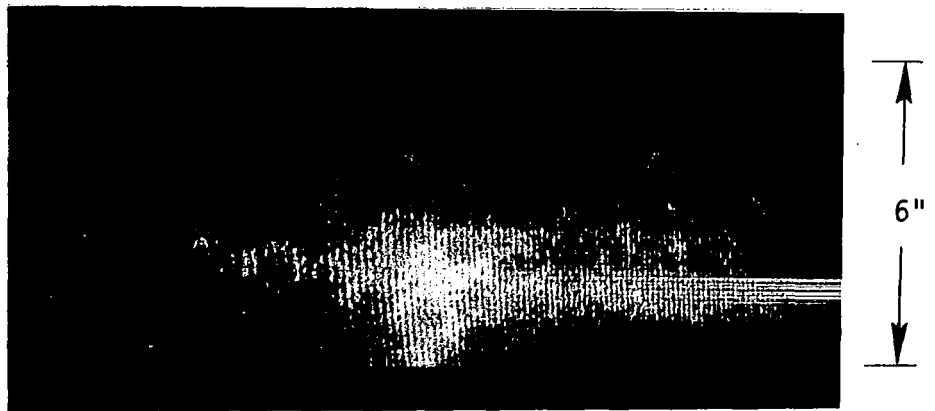
Figure 47 - Fringe Pattern from a Vibrating Plate
Using Double-Pulse Holography

Shaker

18"

.5 in

Hologram   Pulsed Laser
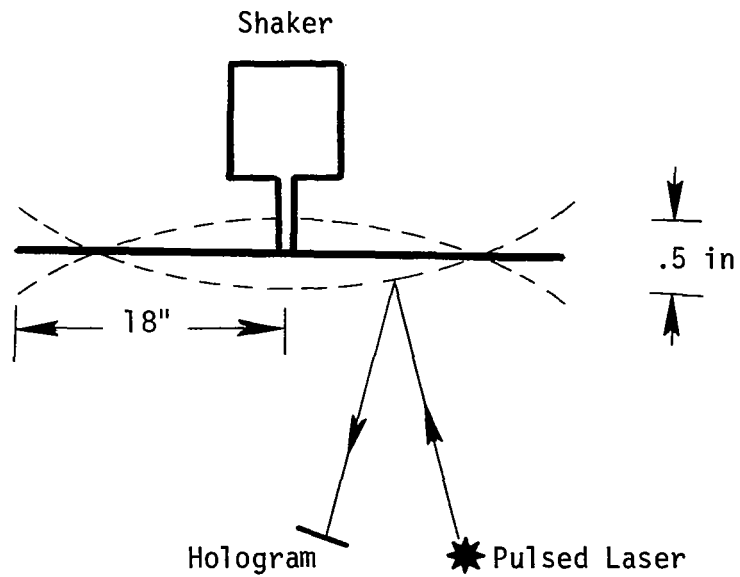
Figure 48 - Pulsed Laser and Vibrating
Beam Schematic Arrangement
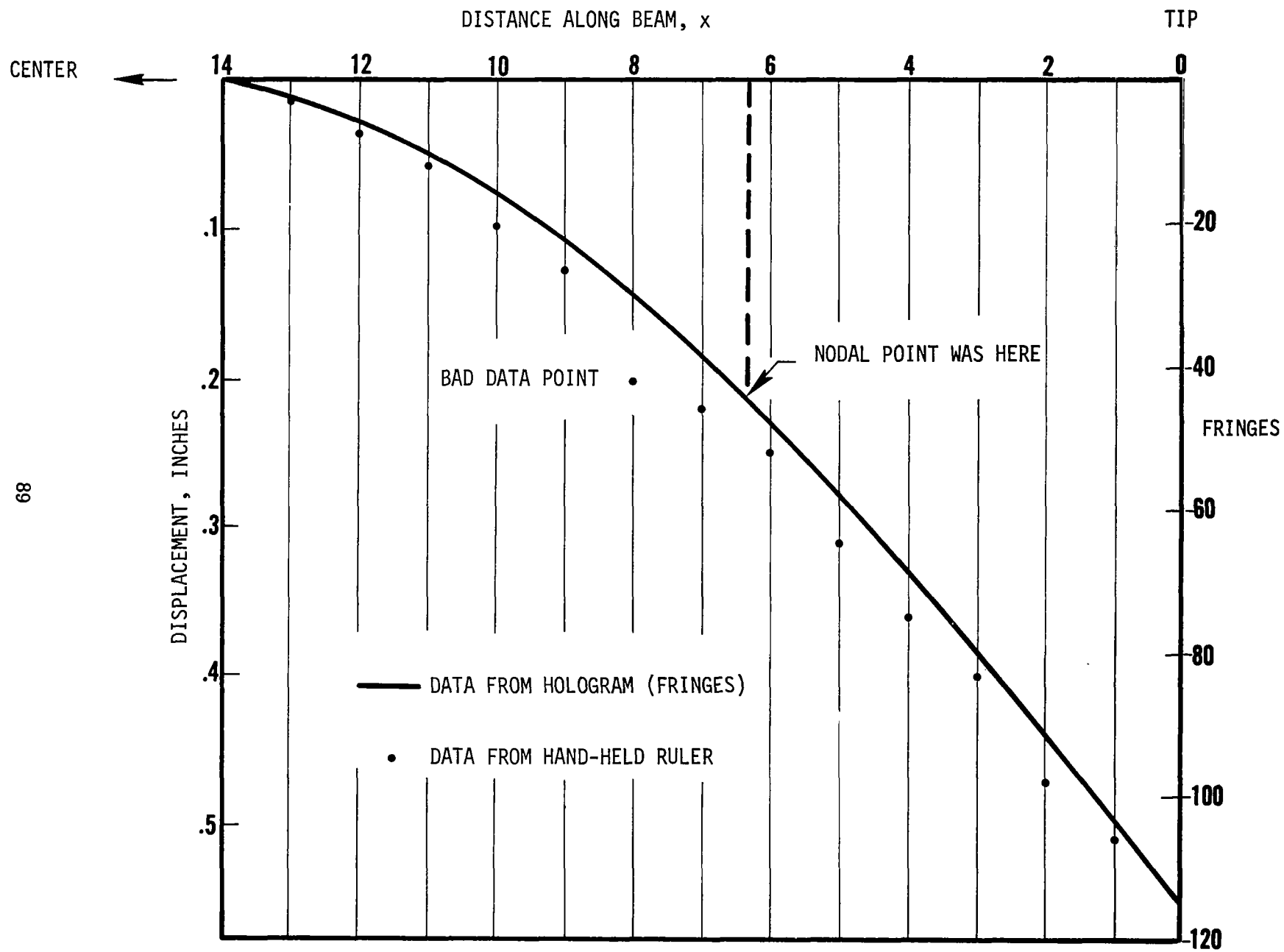
Figure 49 - Measured Vibration Shape for Large Aluminum Plate

DISTANCE ALONG BEAM, x

CENTER

TIP

DISPLACEMENT, INCHES

FRINGES

BAD DATA POINT

NODAL POINT WAS HERE

DATA FROM HOLOGRAM (FRINGES)

DATA FROM HAND-HELD RULER

68

The reader will notice that this double-pulse technique does not show up the nodal lines of the vibration mode. It may be advisable to use a combination of time-average holography (to find nodal lines) and pulsed holography (to determine mode shapes) in actual practice.

Transient Measurements Using a Photocell-Counter Technique*

Section 4.0 of this report discusses transient response measurements using high-speed movies to record the fringe motion. As indicated therein, considerable time was required to read the individual movie frames and to reduce the data from them. This data reduction procedure involves counting fringes and determining the direction in which the fringes are moving.

One means of automating the data reduction procedure is to use a photocell (a photomultiplier tube) to "count" the fringes directly as they move. To understand the use of the photocell, consider Figure 50. A stored-beam hologram is made of the stationary object, and subsequent motion of the object results in live interference fringes which can be used to trigger the photocell. For example, as the object (e.g., a cantilever beam) moves toward the hologram, fringes will form on the surface and they will move up or down the beam (Figure 50), depending upon its slope. If the beam is vibrating in its fundamental mode, the fringes will move toward the root of the beam when the beam moves toward the hologram. As each fringe passes the point where the photocell is focused, the voltage output of the photocell will drop. Between fringes, the light reflected from the cantilever illuminates the photocell and the voltage output reaches a maximum. Thus as several fringes move rapidly along the beam, the output voltage from the photocell will be a series of peaks and valleys, with each valley corresponding to the passage of a fringe. Since the distance between fringes (in a direction normal to the cantilever) corresponds to a displacement of one-half a wavelength ($\lambda/2$), the photocell output recorded on the oscilloscope can be directly converted into a displacement-time history.

A photocell arrangement of this type has been used at TRW to obtain the displacement-time history of the free end of an aluminum rod which was impacted by a ballistic pendulum. The results are shown in Figures 51 and 52, which show the photocell output and the displacement-time history, respectively. Note that the time scale is in microseconds which gives an indication of the high frequency-response capability of the photocell technique.

The method can be further improved by using the photocell output to trigger an electronic counter, which would count the fringes. The counter could be connected to a digital-to-analog converter, and the analog signal sent to an oscilloscope to give a displacement-time history directly. Additional development work is needed for such an automatic system. The end result would be a holographic displacement measuring device having high sensitivity and good high frequency capability. Further work along these lines is planned at TRW, and all indications are that the proposed technique is feasible.

---

*This work was not performed on contract NAS 1-8361.

90

FILTER

MIRROR

MIRROR

PHOTOCELL

OBJECT

STORED BEAM HOLOGRAM
(OF THE STATIONARY OBJECT)
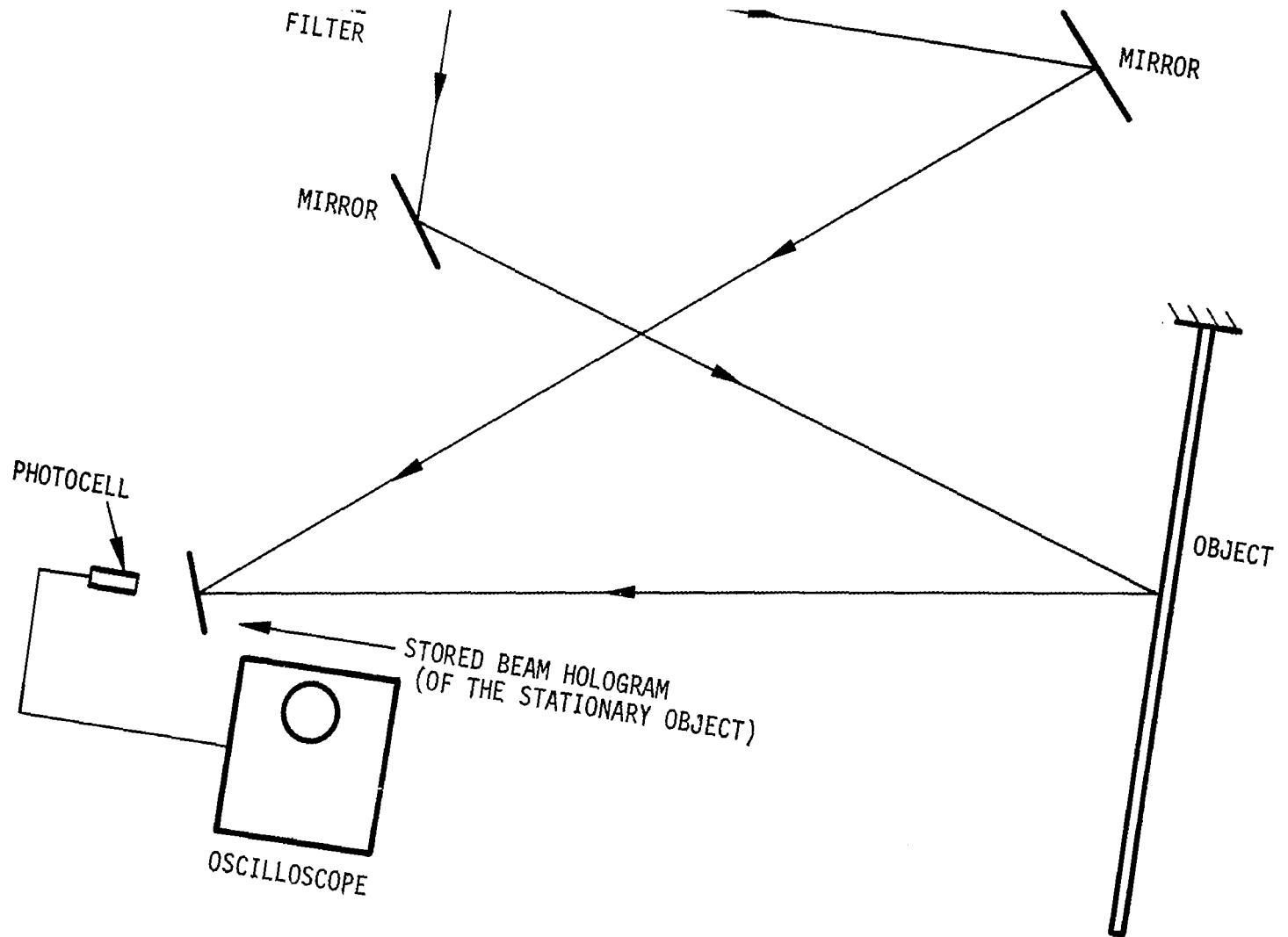
OSCILLOSCOPE

Figure 50 - Photocell Arrangement for Counting Fringes
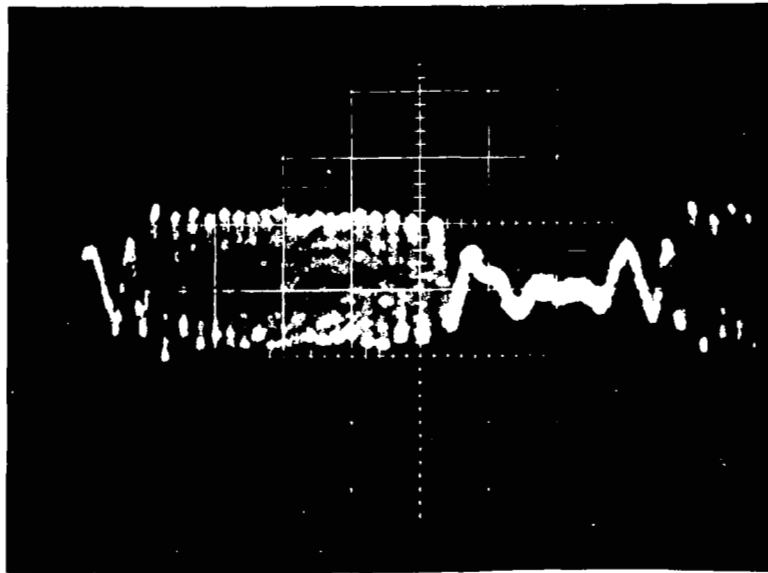
Figure 51 - Oscilloscope Trace of the Photocell Output;
Aluminum Cylinder Subjected to Longitudinal Impact
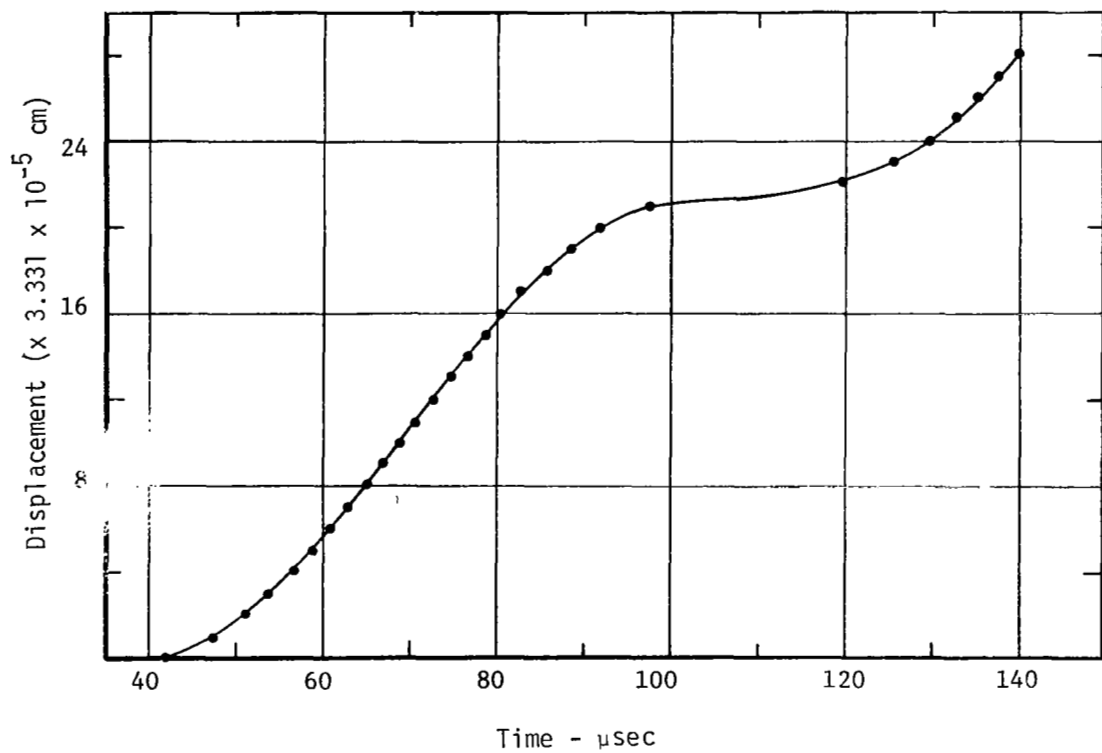
Figure 52 - **Displacement-Time History of Free End of Cylinder**

It should be noted that the photocell technique provides displacement-time histories at a <u>point,</u> rather than over an area. In this respect, the photocell technique is similar to methods of point measurement presented in References 31 and 32.

Applications to Static Problems

The work reported herein has dealt primarily with the application of holography to dynamic <u>problems.</u> As one might imagine, holography has also been applied to <u>static</u> problems in applied mechanics. The purpose of this section is to mention some of these applications to statics and to suggest future work along these lines.

Holography can be used to good advantage in the field of <u>photoelasticity,</u> as discussed by Fourney in Ref. (33). Regarding such applications, Ref. (33) states, "the holographic method holds much more potential than has thus far been demonstrated, and it is felt that an efficient utilization of this potential will yield significant advances in the area of photoelasticity in the future." Since Fourney's paper appeared (in 1968), photoelasticians have begun to use holography more and more, and advances continue to be made.

While some researchers have been improving photoelasticity, others have been applying holography directly for the measurement of in-plane strains. Such results are reported in Ref. (34), which points out that holographic interferometry forms a useful addition to conventional methods of stress analysis. With holographic interferometry, no model of the structure need be made, the method is very sensitive and no contact with the surface is required, and the whole surface can be investigated at the same time, rather than point-by-point. Very little work has appeared in this area since the publication of Ennos' paper (34), and it seems that static stress analysis represents a fruitful topic for future holographic studies. An exploratory paper along these lines is Ref. (35) which discusses strains near a crack tip and permanent deformation recorded by holographic interferometry.

Another natural application of holographic interferometry might be in the static buckling of thin shells. For years experimenters have tried to record the deformation pattern of the shell just prior to buckling, but they have achieved only limited success. These small prebuckling deformation could be recorded using holographic interferometry as the shell was being loaded. In addition, it might be possible to record the dynamic deformation of the shell (as buckling initiated) by means of stored-beam holography and a high-speed movie camera (see Section 4.0).

The examples of static problems where holography could be applied have just been briefly illustrated herein. It is felt that the use of holography for statics problems will grow rapidly as researchers recognize this new area just waiting to be explored.

7.0 REFERENCES

1. D. Gabor, "Microscopy by Reconstructed Wavefronts," Proc. Roy. Soc. (London) Series A, Vol. 197, 1949, pp. 457-484.

2. E. N. Leith and J. Upatnieks, "Wavefront Reconstruction with Diffuse Illumination and Three-Dimensional Objects," Journal Opt. Soc. Am., Vol. 54, No. 11, November 1964, pp. 1295-1301.

3. L. O. Heflinger, R. F. Wuerker and R. E. Brooks, "Holographic Interferometry," Journal of Applied Physics, Vol. 37, February 1966, pp. 642-649.

4. K. A. Haines and B. P. Hildebrand, "Surface Deformation Measurement Using the Wavefront Reconstruction Technique," Applied Optics, Vol. 5, No. 4, April 1966, pp. 595-602.

5. W. G. Gottenberg, "Some Applications of Holographic Interferometry," Experimental Mechanics, Proc. Soc. for Experimental Stress Analysis, September, 1968. Also published as TRW Report No. EM 17-13, August 1967.

6. R. Aprahamian, "Holographic Techniques Applied to Strain Measurements and Microcrack Detection," TRW Report No. EM 17-25, December, 1967.

7. A. B. Witte and R. F. Wuerker, "Laser Holographic Interferometry Study of High-Speed Flow Fields," AIAA 4th Aerodynamic Testing Conf., Cincinnati, April 28-30, 1969.

8. J. K. Beamish, D. M. Gibson, R. H. Sumner, S. M. Zivi, and G. H. Humberstone, "Wind-Tunnel Diagnostics by Holographic Interferometry," AIAA Journal, Vol. 7, No. 10, October, 1969, pp. 2041-2043.

9. R. L. Powell and K. A. Stetson, "Interferometric Vibration Analysis by Wavefront Reconstruction," Journal Opt. Soc. Am., Vol. 55, No. 12, December 1965, pp. 1593-1598.

10. B. M. Watrasiewiez and P. Spicer, "Vibration Analysis by Stroboscopic Holography," Nature, Vol. 217, No. 5134, March 23, 1968, pp. 1142-1143.

11. M. A. Monahan and K. Bromley, "Vibration Analysis by Holographic Interferometry," J. Acous. Soc. Amer., Vol. 44, No. 5, November, 1968, pp. 1225-1231.

12. C. D. Johnson and G. M. Mayer, "Hologram Interferometry as a Practical Vibration Measurement Technique," Shock and Vibration Bulletin, No. 39, Part 2, February 1969, pp. 41-49.

13. A. F. Peter, "Practical Holographic Mode Shapes on Turbine Blades," ASME Paper 69-VIBR-32, presented at the Vibrations Conference, Philadelphia, Pa., March 30 - April 2, 1969.

14. R. Aprahamian and D. A. Evensen, "Applications of Holography to Dynamics: I. High-Frequency Vibrations of Beams," accepted for publication by the Journal of Applied Mechanics. Also published as TRW Applied Mechanics Laboratory Report AM 69-10.

15. R. Aprahamian, and D. A. Evensen, "Applications of Holography to Dynamics: II. High-Frequency Vibrations of Plates," accepted for publication by the Journal of Applied Mechanics. Also available as TRW Applied Mechanics Laboratory Report AM 69-11.

16. R. Aprahamian and D. A. Evensen, "Applications of Holography to High-Frequency Vibrations and Transient Response," presented at the 40th Shock and Vibration Symposium, Hampton, Va., Oct. 21-23, 1969.

17. J. B. Develis and G. O. Reynolds, Theory and Applications of Holography, Addison-Wesley Publ., Reading, Mass., 1967.

18. J. W. Goodman, Introduction to Fourier Optics, McGraw-Hill, 1968, pp. 209-268.

19. H. Smith, Principles of Holography, John Wiley & Sons, 1969.

20. G. M. Brown, R. M. Grant, and G. W. Stroke, "Theory of Holographic Interferometry," J. Acous. Soc. Amer., Vol. 45, No. 5, May 1969, pp. 1166-1179.

21. R. A. Stetson and R. L. Powell, "Interferometric Hologram Evaluation and Real-Time Vibration Analysis of Diffuse Objects," J. Opt. Soc. Amer., Vol. 55, No. 12, 1965, 1694-1695.

22. R. E. Brooks, L. O. Heflinger, and R. F. Wuerker, "Interferometry with a Holographically Reconstructed Comparison Beam," Applied Physics Letters, Vol. 7, No. 9, 1965pp. 248-249.

23. P. Shajenko and C. D. Johnson, "Stroboscopic Holographic Interferometry," Applied Physics Letters, Vol. 13, No. 1, July 1, 1968, pp. 44-46.

24. E. Archbold and A. E. Ennos, "Observation of Surface Vibration Modes by Stroboscopic Hologram Interferometry," Nature, Vol. 217, No. 5132, March 9, 1968, pp. 942-943.

25. H. L. Gamage, "Digital Bending Mode Program for Timoshenko Beams," TRW Systems Report EM 13-17, July 1963.

26. H. Kolsky, Stress Waves in Solids, Dover, 1963, pp. 96-98.

27. R. D. Mindlin, "Influence of Rotatory Inertia and Shear on Flexural Motions of Isotropic Elastic Plates," Jour. Appl. Mech. Vol. 18, March, 1951, pp. 31-38.

28. N. E. Molin and K. A. Stetson, "Measuring Combination Mode Vibration Patterns by Hologram Interferometry," Jour. Sci. Instr. Series 2, Vol. 2, 1969, pp. 609-612.

29. M. A. Dengler and M. Goland, "Transverse Impact of Long Beams, Including Rotatory Inertia and Shear Effects," Proc. 1st U.S. Nat'l. Cong. of Applied Mech., ASME, 1951, pp. 179-186.

30. R. W. Mortimer and J. L. Hoburg, "MCDIT 21 - A Computer Code for One-Dimensional Elastic Wave Problems," NASA CR-1306, April, 1969.

31. H. A. Deferrari, R. A. Darby, and F. A. Andrews, "Vibrational Displacement and Mode Shape Measurement by a Laser Interferometer," J. Acous. Soc. Am. Vol. 42, No. 5, November, 1967, pp. 982-990.

32. G. A. Massey, "Study of Vibration Measurement by Laser Methods," NASA CR-985, January, 1968.

33. M. E. Fourney, "Application of Holography to Photoelasticity," Experimental Mechanics, Proc. of the SESA, Vol. 8, No. 1, January, 1968, pp. 33-38.

34. A. E. Ennos, "Measurement of In-Plane Surface Strain by Hologram Interferometry," J. Sci. Instr. Vol. 1, Series 2, 1968, pp. 731-734.

35. T. D. Dudderar, "Applications of Holography to Fracture Mechanics," Experimental Mechanics, Proc. of the SESA, Vol. 9, No. 6, June, 1969, pp. 281-285.

APPENDIX A

SOME USEFUL EQUATIONS USED
IN THE FIELD OF HOLOGRAPHY

Introduction

Many papers have been written describing the phenomenon of holography and holographic interferometry. Some of these papers on interferometry present equations which serve to aid in interpreting the fringes which result from double-exposure, time-average and stored-beam interferometry. Generally, only results of analysis are given with little or no regard to presenting the step-by-step derivation.

To provide a review and a concise documentation of the equations used in engineering applications of holography, this appendix has been prepared. No claims as to the originality are made. The list of originators is large, and no attempt has been made to assign specific credits. The reader who is interested in the original works can consult references given in the body of the report.

HOLOGRAPHY

Image Recording

Holograms are made using coherent, monochromatic light sources, such as lasers. The light from the laser serves to illuminate the object whose image is to be recorded and to provide a reference beam. Figure A1 shows a typical set-up used to obtain reflected light holograms.
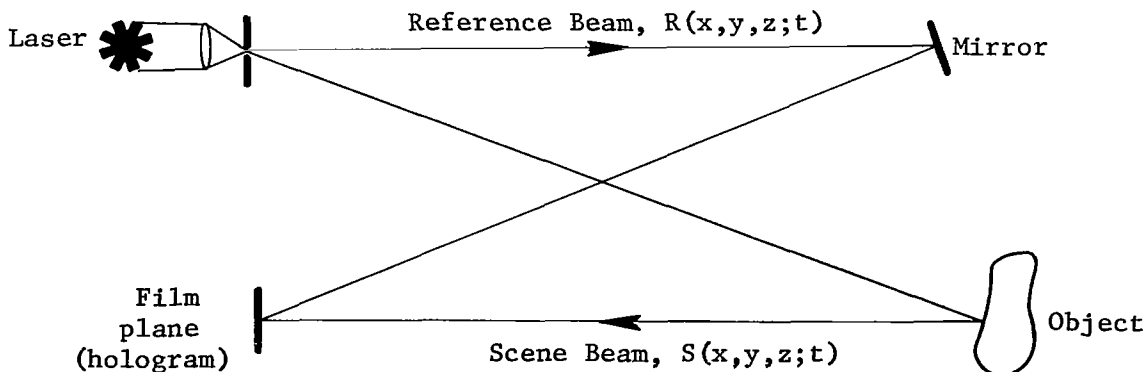
Figure A1: Typical experimental setup to
make reflected light holograms

The amplitude of the reference, R, and scene beam, S, are given by

$$R(x,y,z;t) = r(x,y,z)e^{i\omega t}$$

$$S(x,y,z;t) = s(x,y,z)e^{i\omega t}$$

respectively, where ω is the frequency of the laser light.

During the recording process, the film responds to the intensity, I, of light reaching it. The intensity is in turn given by the square of the light amplitude, i.e.,

$$I = \left|A\right|^2 = \left|R + S\right|^2 \tag{A-1}$$

where $|A|$ denotes the absolute magnitude of A.
Since the film is exposed to the light for a finite time, E_t, its exposure, E, is given by

$$E = \int_0^{E_t} I\,dt$$

$$= \int_0^{E_t} \left|R + S\right|^2 dt$$

$$= \int_0^{E_t} (RR^* + SS^* + RS^* + R^*S)dt$$

$$= \int_0^{E_t} (\underbrace{rr^* + ss^* + rs^* + r^*s}_{\text{Time independent; Standing Waves}})dt$$

$$E = (rr^* + ss^* + rs^* + r^*s)E_t \tag{A-2}$$

98

Image Retrieval Process (Reconstruction)

The image is retrieved by illuminating the developed film (termed the hologram) with light from a laser at approximately the same angle the reference beam made with the hologram during the recording phase as shown in Figure A2.
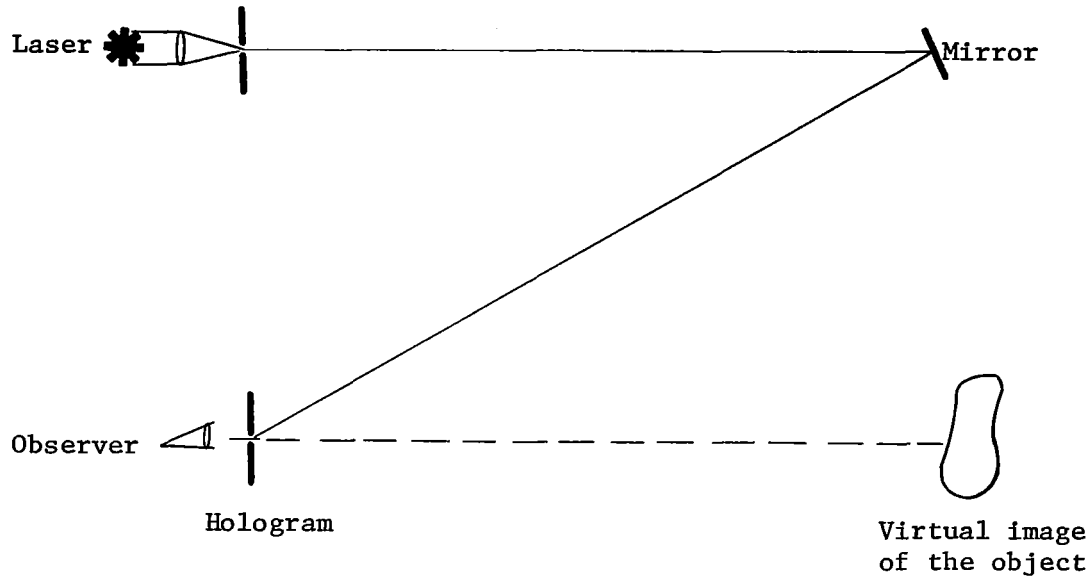
Figure A2:   Image Retrieval Process

The fraction of light transmitted through the hologram is given by

$$T = (1 - kE) \qquad k = \text{constant}$$

Illuminating the hologram with a reference beam identical to the recording reference beam yields

$$RT = R(1 - kE)$$
$$= R - kRE$$

for unit exposure time, i.e., $E_t = 1$, we obtain

$$RT = R - k \left[(rr* + ss*)R + rs*R + Rr*s \right]$$

$$= \left[1 - k(rr* + ss*) \right] R - krs*R - krr*S \qquad (A-3)$$

since $Rr*s = rr*se^{i\omega t} = rr*S$. For our discussion only the last term, $-krr*S$ is meaningful. Careful inspection of this term shows that it represents the <u>original</u> amplitude of the scene beam, S, altered in amplitude and phase by the multiplicative factor $-krr*$. This suggests that the 3-dimensionality of the image is preserved. The intensity of this reconstructed image is then given by

$$I_o = k^2 \left| r \right|^4 \left| s \right|^2$$

HOLOGRAPHIC INTERFEROMETRY

Double-Exposure

Suppose a hologram was made of an object having a scene beam amplitude, S_1. If the object is strained and a second exposure made corresponding to scene beam amplitude, S_2, on the same hologram, then upon reconstruction, two virtual images will be seen when viewing through the hologram. Their composite amplitude is given by

$$A = - krr* (S_1 + S_2) \qquad (A-4)$$

These two scene beams will interfere with one another constructively or destructively, depending on their relative phase. Areas of destructive interference will cause fringes (absence of light). The intensity of the composite image, I_r, is given by $\left| A \right|^2$ or

$$I_r = \left| A \right|^2 = (krr*)^2 (S_1 + S_2)(S_1{}^* + S_2{}^*) \qquad (A-5)$$

The two scene beam amplitudes, S_1 and S_2, can be related by simple geometry. Let $\ell_1 + \ell_2$ be the path of light taken by the scene beam when exposing the film to the unstrained object. Similarly, $\ell'_1 + \ell'_2$ is the path length of the scene beam when the second exposure is made. Then, referring to the following Figure A3 we have

$$\ell'^2_1 = \ell^2_1 + m^2 - 2m\ell_1 \cos \theta_1$$

$$\ell'^2_2 = \ell^2_2 + m^2 - 2m\ell_2 \cos \theta_2$$

Solving for ℓ'_1 and ℓ'_2,

$$\ell'_1 = \ell_1 \left(1 + \left(\frac{m}{\ell_1}\right)^2 - \frac{2m}{\ell_1} \cos \theta_1\right)^{1/2} \simeq \ell_1\left(1 - \frac{m}{\ell_1} \cos \theta_1\right) \text{ for } \frac{m}{\ell_1} \ll 1$$

$$\ell'_2 = \ell_2 \left(1 + \left(\frac{m}{\ell_2}\right)^2 - \frac{2m}{\ell_2} \cos \theta_2\right)^{1/2} \simeq \ell_2\left(1 - \frac{m}{\ell_2} \cos \theta_2\right) \text{ for } \frac{m}{\ell_2} \ll 1$$
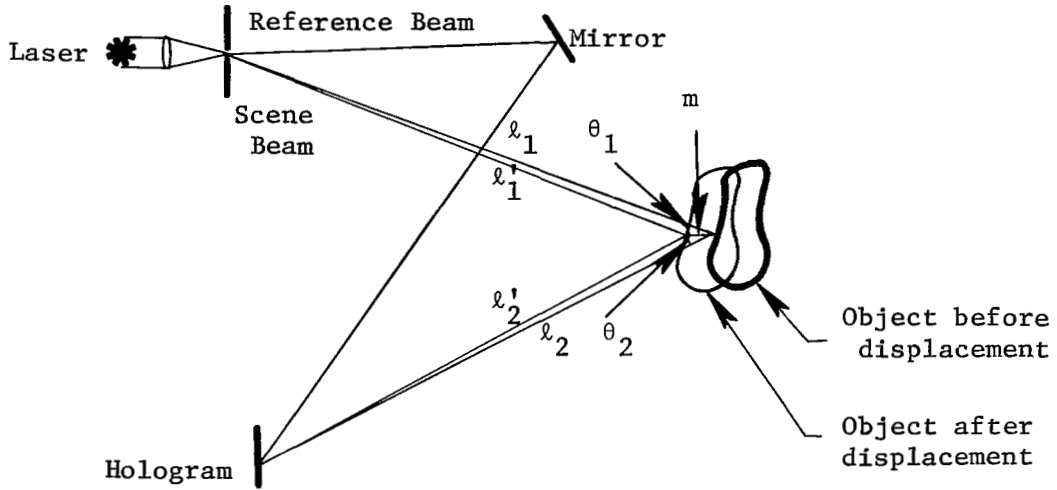
Figure A3: Phase change of light due to the motion of the object

Therefore,

$$\left.\begin{array}{l} \ell'_1 - \ell_1 = -m \cos \theta_1 \\[2ex] \ell'_2 - \ell_2 = -m \cos \theta_2 \end{array}\right\} \quad \text{or} \quad \left\{\begin{array}{l} \ell_1 - \ell'_1 = m \cos \theta_1 \\[2ex] \ell_2 - \ell'_2 = m \cos \theta_2 \end{array}\right.$$

Total pathlength change $\Delta L = (\ell_1 + \ell_2) - (\ell'_1 + \ell'_2)$

$$= m(\cos \theta_1 + \cos \theta_2)$$

The difference in phase is given by

$$\Delta \emptyset = \frac{2\pi}{\lambda} \Delta L = \frac{2\pi}{\lambda} m(\cos \theta_1 + \cos \theta_2) \qquad (A-6)$$

If the scene beam, S_1, during the first exposure is given by

$$S_1 = s \, e^{i\emptyset_o}$$

then the scene beam, S_2, during the second exposure is given by

$$S_2 = s \, e^{i\emptyset_o + \frac{2\pi i}{\lambda} m(\cos \theta_1 + \cos \theta_2)} \qquad (A-7)$$

$$S_2 = S_1 \, e^{\frac{2\pi i}{\lambda} m(\cos \theta_1 + \cos \theta_2)} \qquad (A-8)$$

Equation (A-5) becomes

$$I_r = (krr^*)^2 \, S_1 S_1^* \, \left| 1 + e^{\frac{2\pi i}{\lambda} m(\cos \theta_1 + \cos \theta_2)} \right|^2$$

$$= (krr^*)^2 \, |s|^2 \left[2 + 2 \cos \left(\frac{2\pi}{\lambda} m(\cos \theta_1 + \cos \theta_2) \right) \right]$$

$$= 2k^2 \, |r|^4 |s|^2 \left[1 + \cos \left(\frac{2\pi}{\lambda} m(\cos \theta_1 + \cos \theta_2) \right) \right] \qquad (A-9)$$

Note that the intensity given by Equation (A-9) has zeros indicating the presence of fringes, namely, when

$$1 + \cos \left(\frac{2\pi}{\lambda} m(\cos \theta_1 + \cos \theta_2) \right) = 0 \qquad (A-10)$$

102

or

$$\frac{2\pi}{\lambda} (\cos \theta_1 + \cos \theta_2)m = (2n - 1)\pi \quad n = 1,2,3,\ldots$$

or

$$m = \frac{2n - 1}{2(\cos \theta_1 + \cos \theta_2)} \lambda \qquad (A-11)$$

If $\theta_1 = \theta_2 = 0$, that is, normal incidence and reflection of the illuminating light and normal displacement, then

$$m = \frac{2n - 1}{4} \lambda \qquad (A-12)$$

This says that a fringe will be formed whenever the body moves an odd number of quarter wavelengths between exposures. Figures 40-42 in the body of this report show examples of double exposure interferometry. The subject is a rectangular prismatic beam which experienced a ballistic impact at its center.

Time-Average Holography

When making a hologram of an object which moves during the exposure time, say of a vibrating body, the film gets exposed to light from the object in each position the object assumes during the exposure. Hence, the film is exposed according to (analogous to the derivation of Equation A-2)).

$$E = \int_o^{E_t} (RR* + SS* + RS* + R*S)dt$$

Considering only the last term, since it alone contributes to the holographic virtual image, we get

$$E = r*s \int_o^{E_t} e^{-i\omega t + i\omega t + i\emptyset}dt$$

$$= r*s \int_o^{E_t} e^{i\emptyset}dt \qquad (A-13)$$

103

where $\emptyset$ is the change in phase due to the motion. If the motion is sinusoidal of the form $m \sin(\Omega t + \emptyset_o)$, then

$$E = r*s \int_o^{E_t} e^{\frac{2\pi i}{\lambda} m(\cos \theta_1 + \cos \theta_2) \sin(\Omega t + \emptyset_o)} dt$$

$$= r*s \, E_t \, J_o\left(\frac{2\pi}{\lambda} m(\cos \theta_1 + \cos \theta_2)\right), \text{ where } E_t > \frac{2\pi}{\Omega}. \tag{A-14}$$

The amplitude, A, of the reconstructed image is given by (analogous to last term of Equation A-3))

$$A = - kRE = - kr*rSE_t \, J_o\left(\frac{2\pi}{\lambda} m(\cos \theta_1 + \cos \theta_2)\right)$$

The intensity, I_r, of the reconstructed image is

$$I_r = I_o \, J_o^2\left[\frac{2\pi}{\lambda} m(\cos \theta_1 + \cos \theta_2)\right] \tag{A-15}$$

where I_o corresponds to the intensity if the object did not move during the exposure time. The intensity, I_r, versus amplitude, m, is shown schematically in Figure A4. Examination of Equation (A-15) suggests that fringes will appear on the reconstructed image wherever the amplitude of motion satisfies the condition

$$m = \frac{\lambda \alpha_i}{2\pi (\cos \theta_1 + \cos \theta_2)}$$

where α_i are roots of the zeroth-order Bessel function, i.e.

$$J_o(\alpha_i) = 0$$

$$J_o^{\;2}\left(\frac{2\pi}{\lambda}\, m(\cos\,\theta_1 + \cos\,\theta_2)\right)$$

$\dfrac{I_r}{I_o}$

Fringes

$$\frac{2\pi}{\lambda}\, m(\cos\,\theta_1 + \cos\,\theta_2)$$
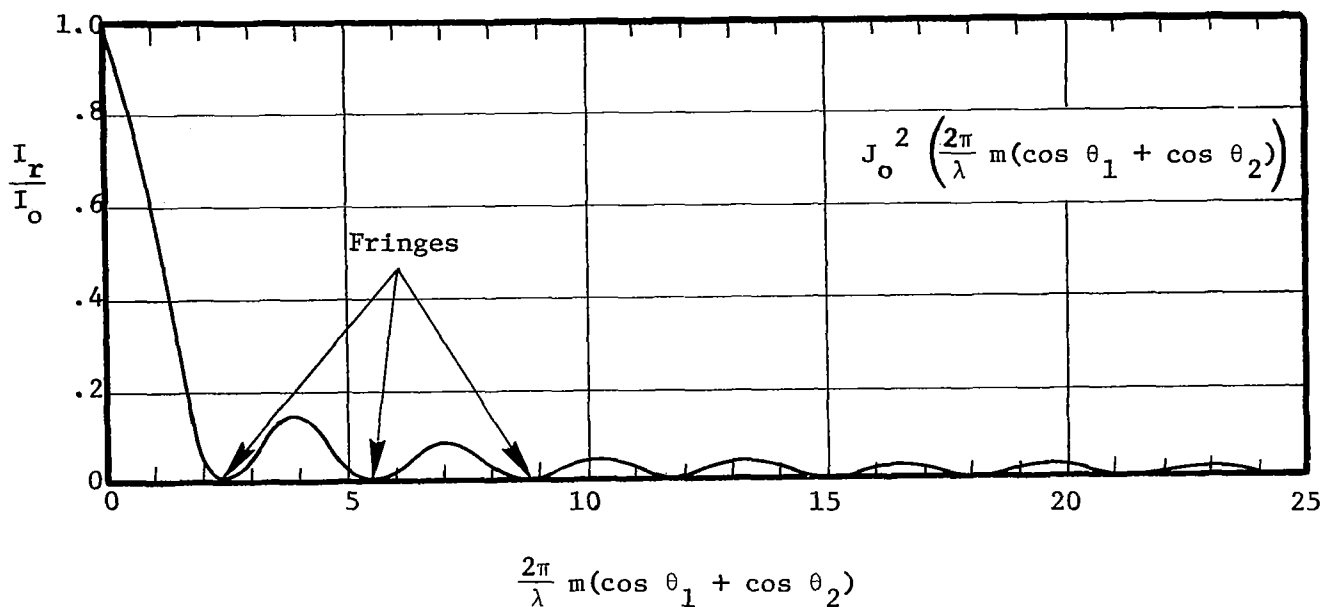
Figure A4:   Intensity vs. amplitude for time-average holography

Figure A-5 shows the holographic reconstruction of a time average hologram made of a vibrating plate. Also shown is the mode shape as determined by interpreting the fringes.

A second example of time-average holography is that of making a hologram of an object moving at a constant velocity. Suppose the velocity of the surface is given by v; then proceeding in a manner similar to the sinusoidal case discussed above, one finds the intensity of the recon-structed image is given by
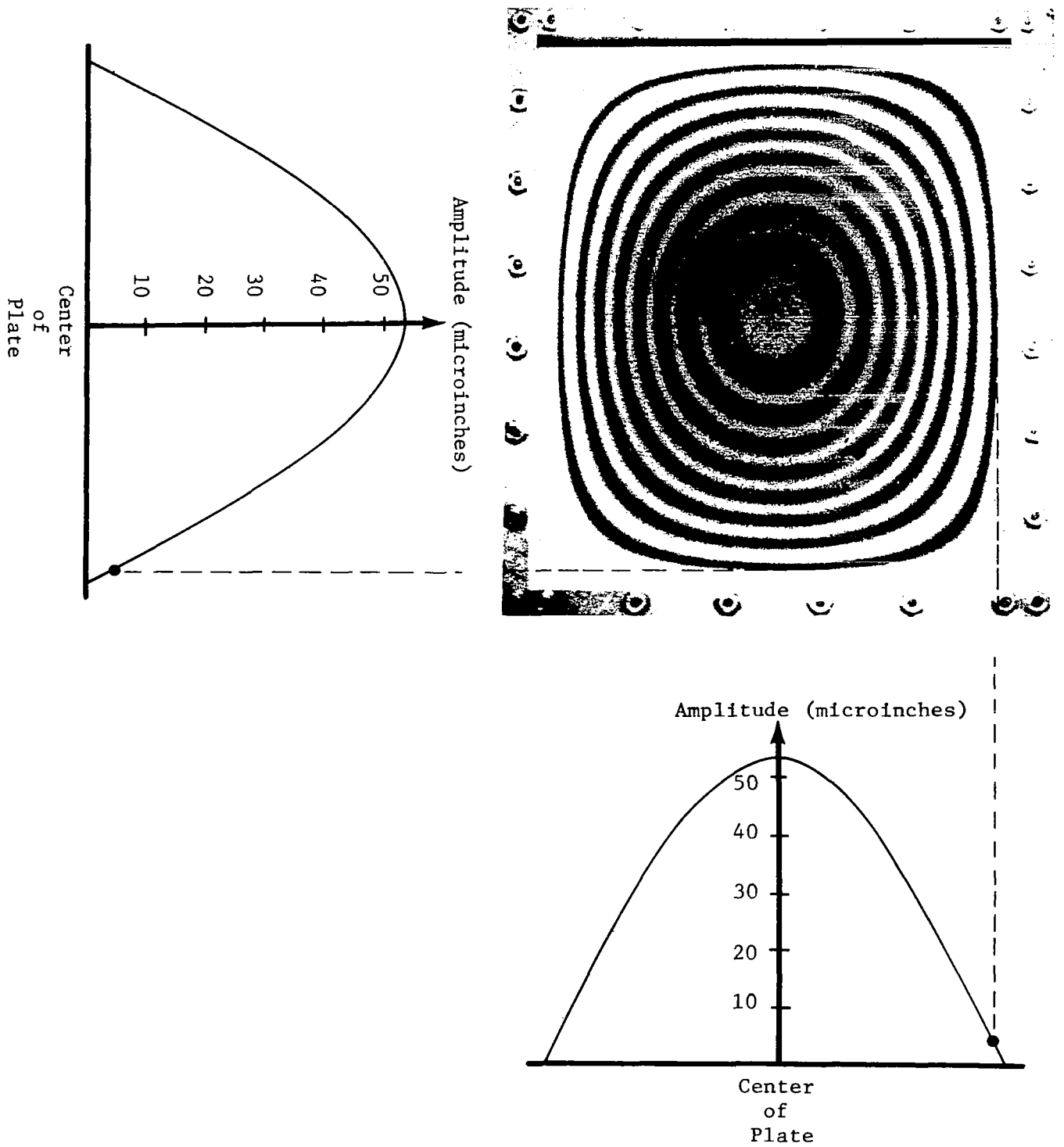
Figure A5 – Mode shape of the fundamental mode of
an 8" x 10" simply supported plate using
time-average holographic interferometry

$$I \sim \left| \int_0^{E_t} e^{i\frac{2\pi}{\lambda}(\cos\theta_1 + \cos\theta_2)vt} \, dt \right|^2$$

$$= \left| \frac{\lambda e^{i\frac{2\pi}{\lambda}(\cos\theta_1 + \cos\theta_2)vt}}{2\pi i(\cos\theta_1 + \cos\theta_2)v} \right|_0^{E_t} \Bigg|^2$$

$$= \left| \frac{\lambda}{2\pi i(\cos\theta_1 + \cos\theta_2)v} \right|^2 \left| e^{\frac{i2\pi}{\lambda}(\cos\theta_1 + \cos\theta_2)vE_t} - 1 \right|^2$$

$$= 2 \left| \frac{\lambda}{2\pi i(\cos\theta_1 + \cos\theta_2)v} \right|^2 \left[1 - \cos\left(\frac{2\pi}{\lambda}(\cos\theta_1 + \cos\theta_2)vE_t \right) \right]$$

$$= \left(\frac{\lambda}{\pi(\cos\theta_1 + \cos\theta_2)v} \right)^2 \sin^2\left(\frac{\pi}{\lambda}(\cos\theta_1 + \cos\theta_2)vE_t \right)$$

Note that this function has zeros whenever

$$\frac{\pi}{\lambda}(\cos\theta_1 + \cos\theta_2)vE_t = n\pi, \quad n = 1,2,\ldots$$

This suggests that areas of the object which move with a velocity

$$v = \frac{n\lambda}{(\cos\theta_1 + \cos\theta_2)E_t}$$

will be covered with a fringe.₀ To get a feeling for the velocities, assume a ruby laser (λ = 6943A) is used to expose the subject for 50 nanoseconds, and $\theta_1 \simeq \theta_2 \simeq 0$.

Then

$$v = \frac{n \ 6943 \times 10^{-8}}{2 \times 50 \times 10^{-9}} = 694.3 \ n \ \frac{cm}{sec}$$

$$v \simeq .0007 \ n \ cm/\mu s$$

A more convenient way of expressing this condition may be in terms of displacement during the exposure, (ie vE_t) resulting in

$$vE_t = \frac{n\lambda}{\cos \theta_1 + \cos \theta_2}$$

$$= \frac{n\lambda}{2} \text{ for } \theta_1 \simeq \theta_2 \simeq 0.$$

This equation says that if a particle moves at constant velocity an integral number of half-wavelengths during an exposure, it will be covered by a fringe.

Stored-Beam Interferometry

Stored-beam interferometry uses a hologram to store an image of an object which can be later compared to the actual object. This is accomplished by making a hologram of the object and carefully replacing it into the same position it assumed during the exposure. When looking through the hologram at the object, an observer will see two images. One is due to the interaction of the reference beam with the hologram (reconstructed image) and the second being the object itself. The amplitude of light formed by the hologram is $-krr* S_o$ (Equation A-3). The object scatters light denoted by S. The amplitudes sum resulting in an amplitude

$$A = S - krr* S_o$$

The eye of the observer integrates the intensity resulting in

$$I_r = \int \left| S - krr* S_o \right|^2 dt$$

If the object is sinusoidally vibrating, then S can be related to the stationary amplitude, S_o, to yield $S = S_o e^{i\emptyset}$. The above integral then becomes

$$I_r = \int \left| S_o e^{i\emptyset} - krr* S_o \right|^2 dt$$

108

where

$$\emptyset = \frac{2\pi}{\lambda} m(\cos \theta_1 + \cos \theta_2) \sin(\Omega t + \emptyset_o)$$

Then

$$I_r = \int |s|^2 (e^{i\emptyset} - krr^*)(e^{-i\emptyset} - krr^*)dt$$

$$= |s|^2 \int \left(1 - krr^* e^{i\emptyset} - krr^* e^{-i\emptyset} + k^2 (rr^*)^2\right) dt$$

If we assume the two images are of equal intensity, ie, $(krr^*)^2 = 1$, then

$$I = I_o \int 2 - (e^{i\emptyset} + e^{-i\emptyset})dt$$

where I_o is the intensity of the scene beam.

Then

$$I_r = \frac{I_o \omega}{2\pi} \int_o^{\frac{2\pi}{\omega}} 2 - 2 \cos\left(\frac{2\pi}{\lambda} m(\cos \theta_1 + \cos \theta_2)\sin(\Omega t + \emptyset_o)\right) dt$$

$$= \frac{2\omega I_o}{2\pi} \left[\frac{\pi}{\omega} - \frac{\pi}{\omega} J_o\left(\frac{2\pi}{\lambda} m(\cos \theta_1 + \cos \theta_2)\right)\right]$$

$$= I_o \left[1 - J_o\left(\frac{2\pi}{\lambda} m(\cos \theta_1 + \cos \theta_2)\right)\right]$$

This equation suggests that when the hologram has been precisely reposi-tioned and there has not yet been any motion (ie m=o) the intensity, I, is zero. That is, the observer sees the object as black. It is interesting to note that this is the only condition that results in I = 0. The fringes seen when viewing the vibrating object through the stored beam interferogram are shades of gray as shown by Figure A6.

$$\frac{2\pi}{\lambda} m(\cos \theta_1 + \cos \theta_2)$$
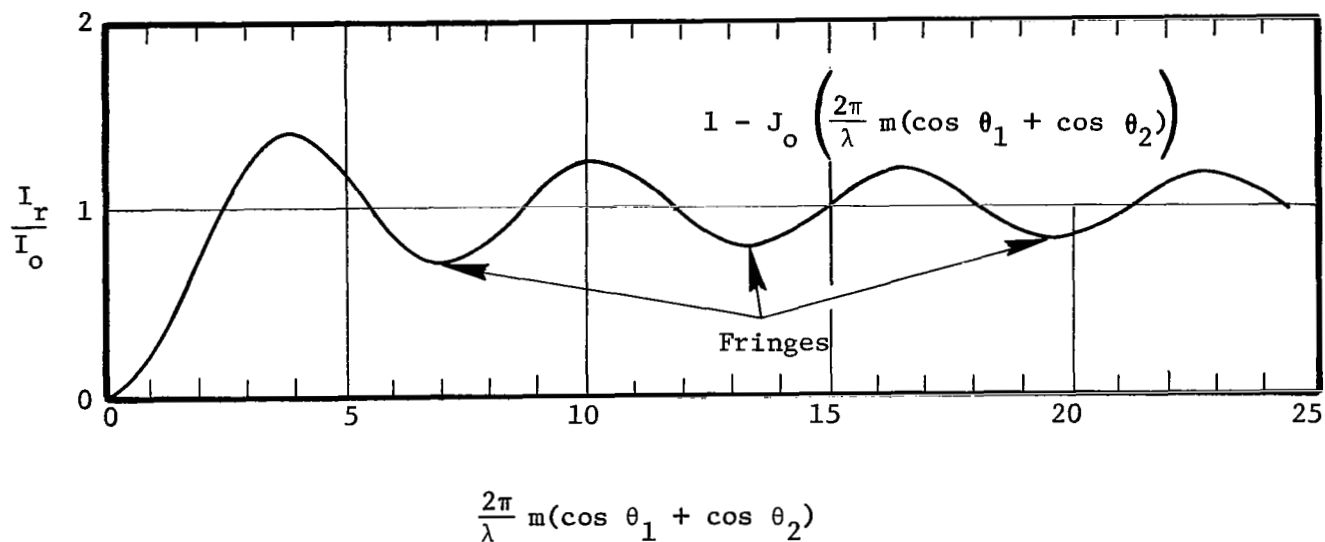
Figure A6: Intensity vs. amplitude for
stored-beam holography

Figure A7 shows one mode of a 8" x 10" vibrating plate as seen through
a stored beam hologram. This plate was oscillating at exactly the same
amplitude as in Figure A5. It is seen that the data reduction process
to obtain the amplitude gives equal results.
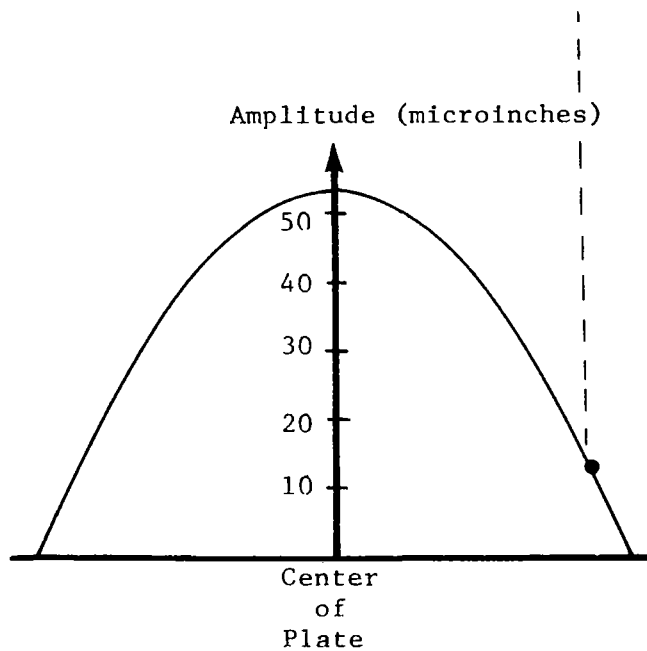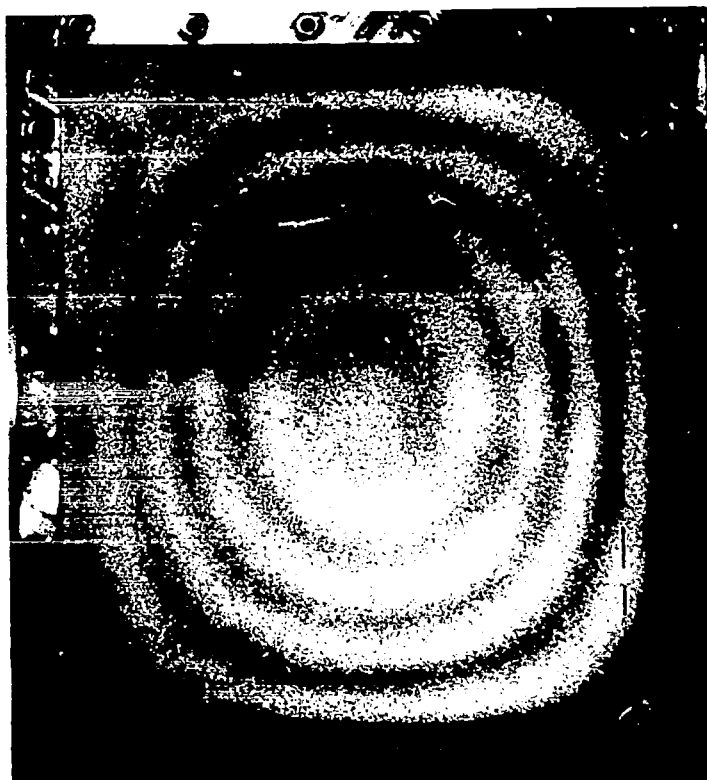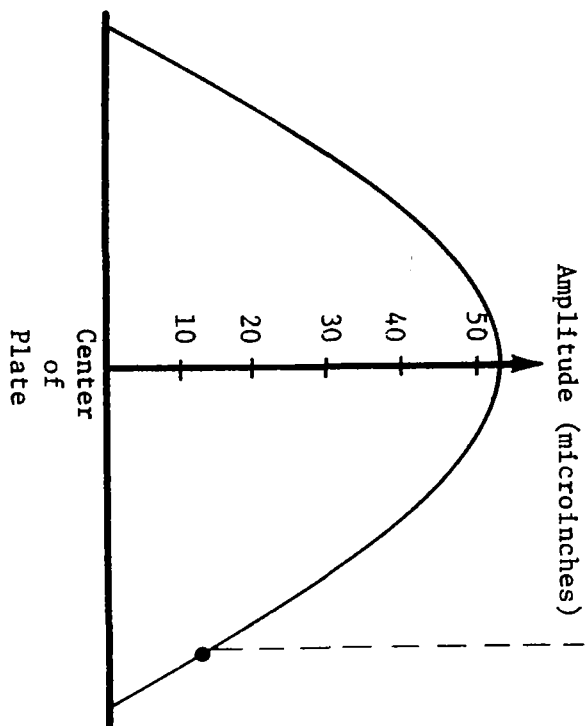
Figure A7 - Mode shape of the fundamental mode of an
8" x 10" simply supported plate using
stored-beam holographic interferometry

111

APPENDIX B

ADDITIONAL BEAM VIBRATION MODES

This appendix is intended as a supplement to Figures 6, 9, and 10, which are discussed in the body of the report. The figures presented here are from time-average holograms of the cantilever beam vibrating in various resonant modes. The mode number, m, and the experimental resonant frequency, f, are given in the figure captions.
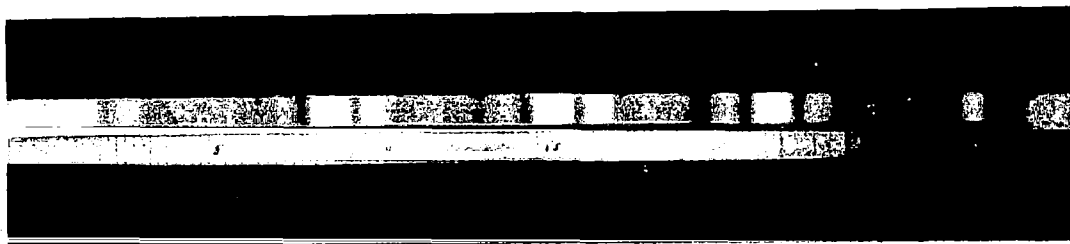
(a) m = 5, f = 500 cps
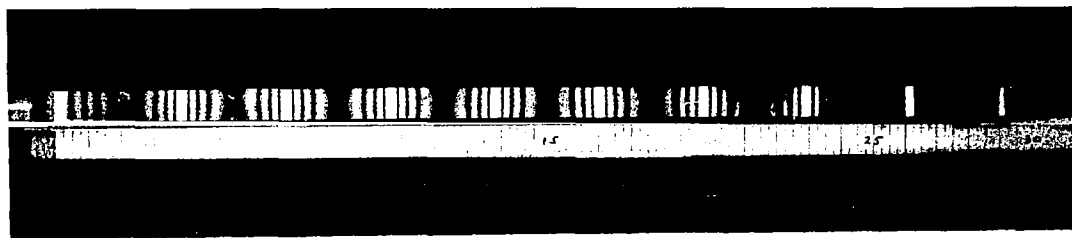
(b) m = 10, f = 2214 cps

(c) m = 12, f = 3262 cps
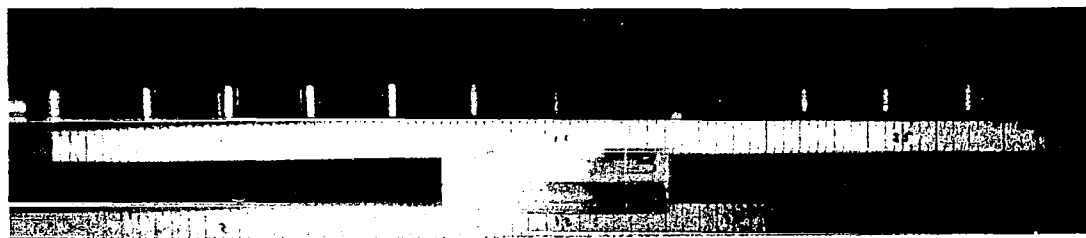
(d) m = 13, f = 3843 cps

Figure B1 - Beam Vibration Modes

113

(a) m = 14,   f = 4477 cps
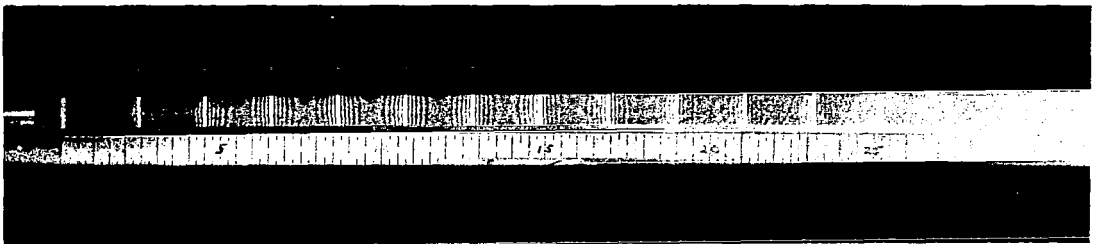
(b) m = 15,   f = 5155 cps
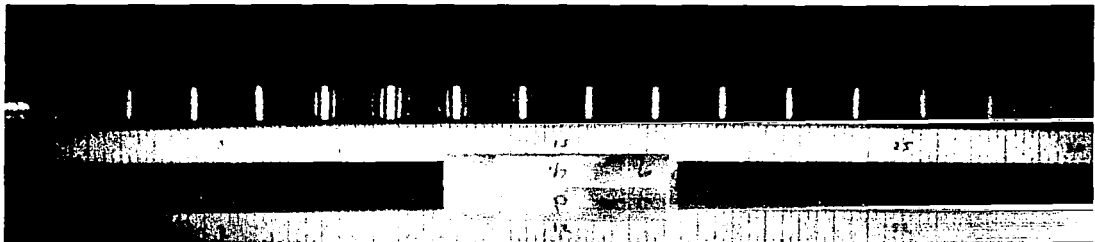
(c) m = 16,   f = 5870 cps
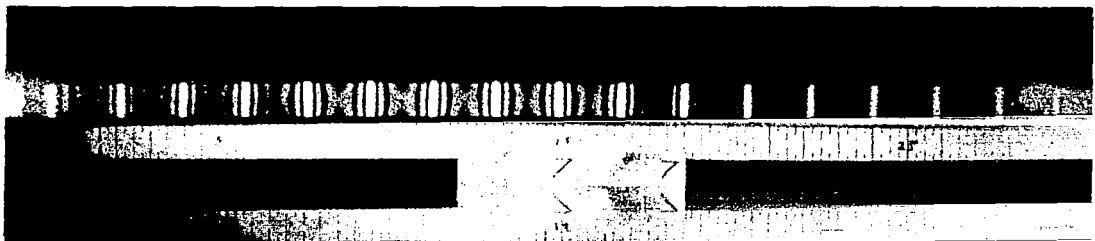
(d) m = 17,   f = 6640 cps

Figure B2 - Beam Vibration Modes

114

(a) m = 18,   f = 7454 cps
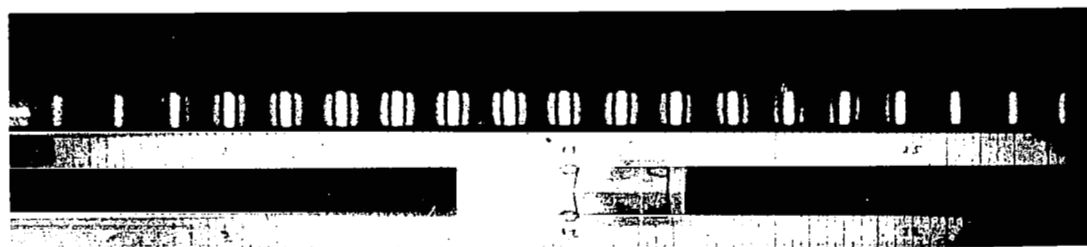
(b) m = 19,   .f = 8308 cps
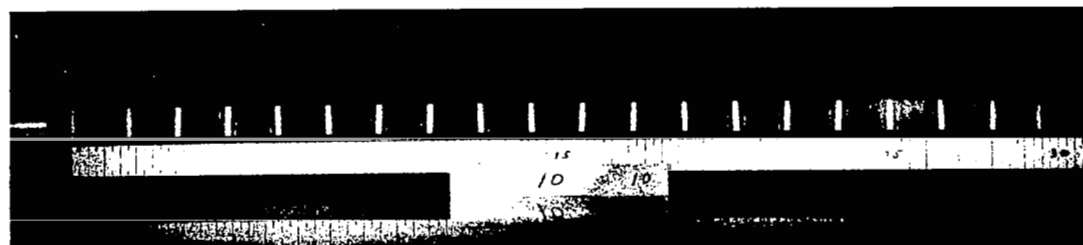
(c) m = 20,   f = 9204 cps
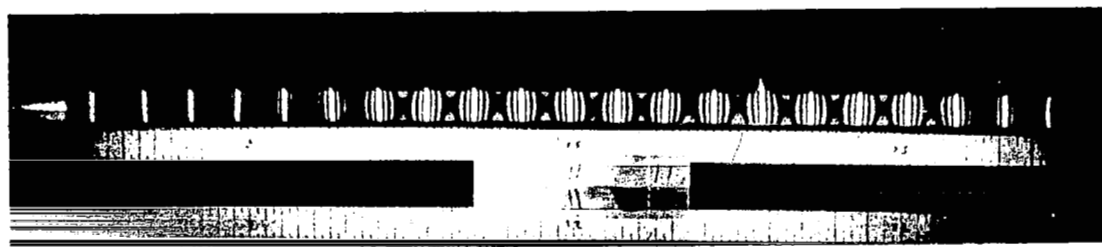
(d) m = 21,   f = 10121 cps

Figure B3 - Beam Vibration Modes

115
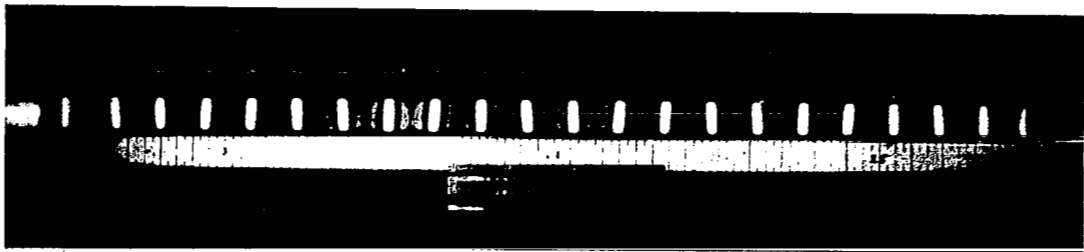
(a) m = 22,   f = 11,106 cps
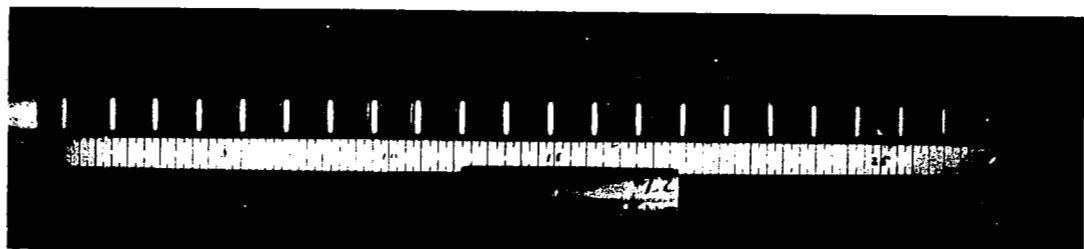
(b) m = 23,   f = 12,111 cps
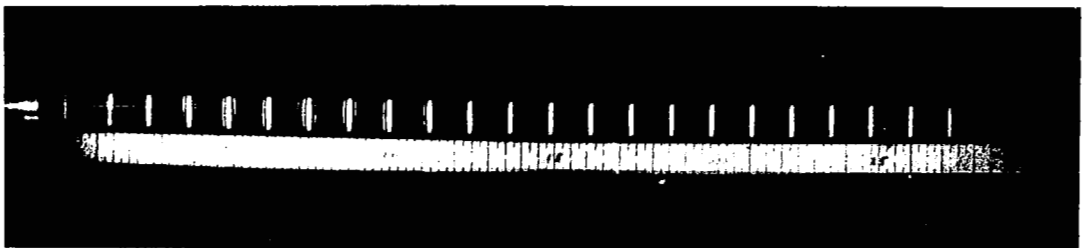
(c) m = 25,   f = 14,200 cps
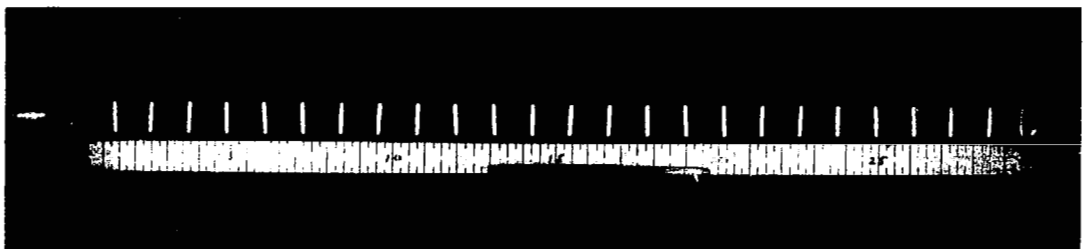
(d) m = 26,   f = 15,365 cps

Figure B4 - Beam Vibration Modes

116
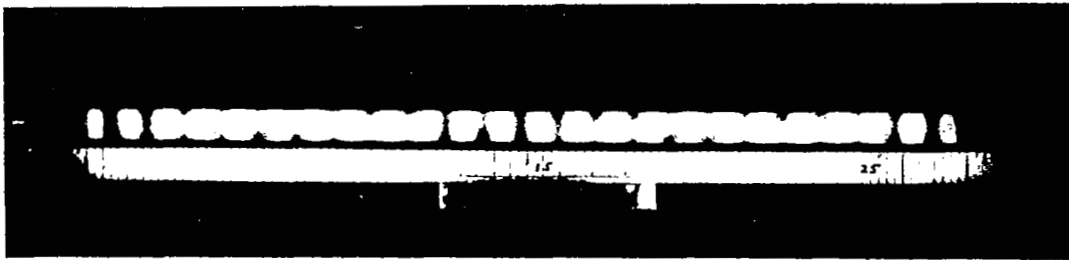
(a) m = 27,   f = 16,401 cps

(b) m = 28,   f = 17,550 cps

(c) m = 29,   f = 19,085 cps
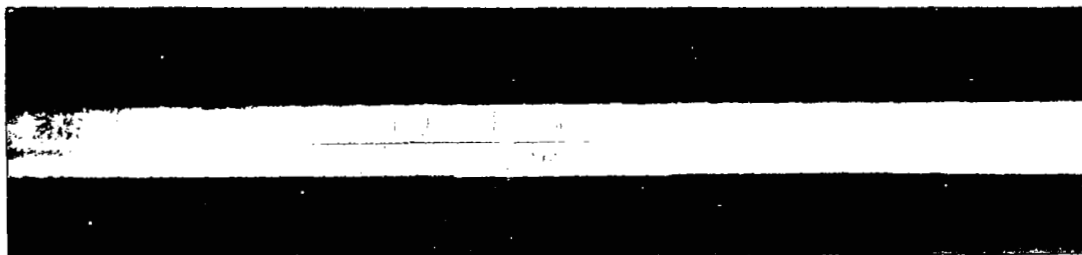
(d) m = 30,   f = 20,336 cps

Figure B5 - Beam Vibration Modes

117
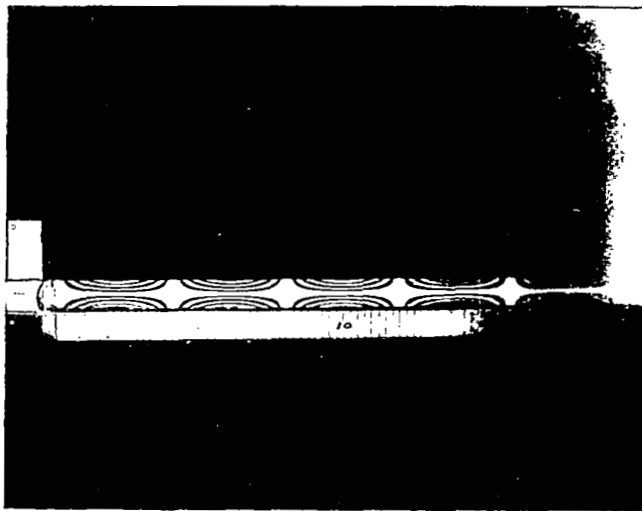
(a) Torsional Mode   f = 6,010 cps
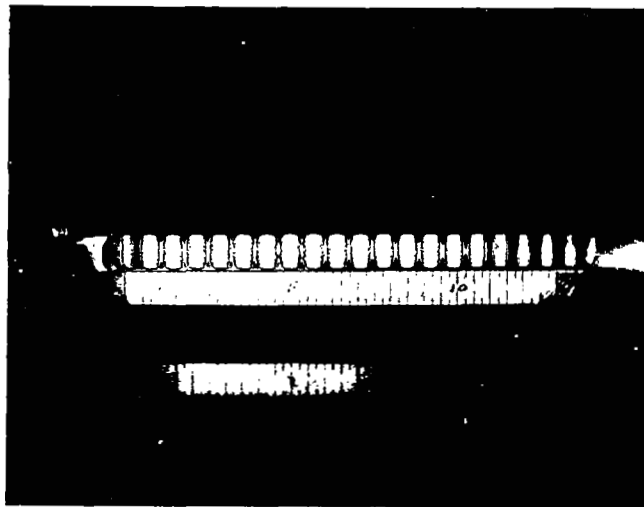
(b) Transverse Mode   f = 39,230 cps

Figure B6 - Beam Vibration Modes

118

APPENDIX C

ADDITIONAL PLATE VIBRATION MODES

This appendix is intended to supplement Figures 18, 19, 20 and 27, which are discussed in the body of the report. The figures presented here are from time-average holograms of the simply-supported plate vibrating in various resonant modes. The modal numbers, m and n, are given in the figure captions together with the experimental resonant frequency, f.
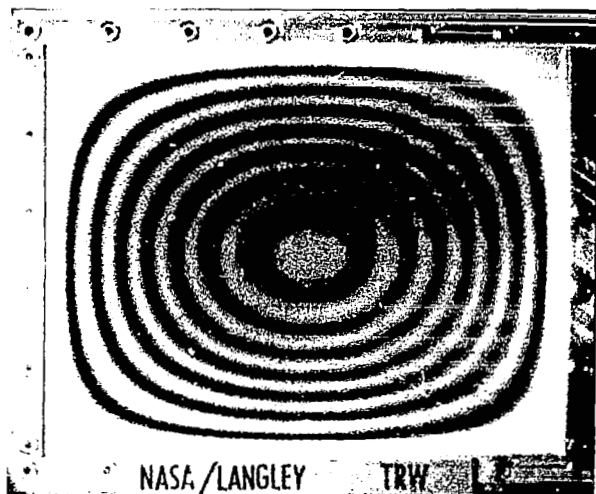
(a) m = 1, n = 1, f = 162 cps
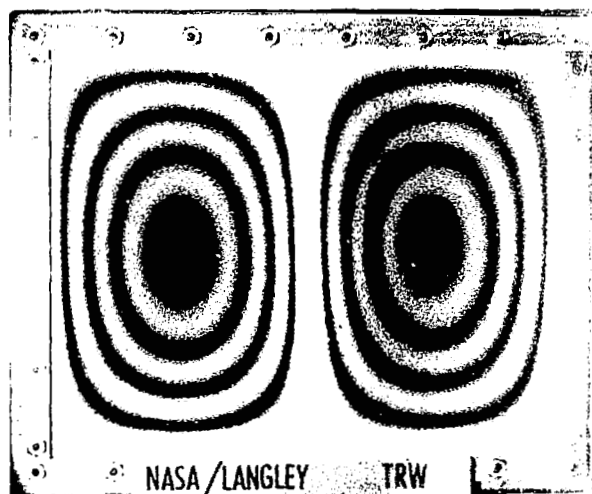
(b) m = 1, n = 2, f = 357 cps

(c) m = 2, n = 1, f = 425 cps
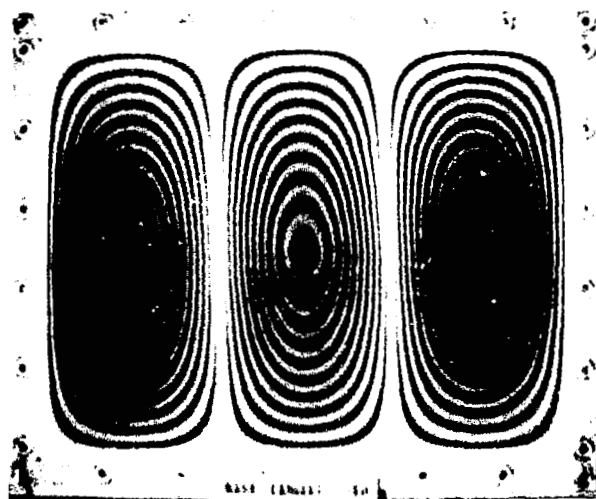
(d) m = 1, n = 3, f = 665 cps

Figure C1 - Plate Vibration Modes
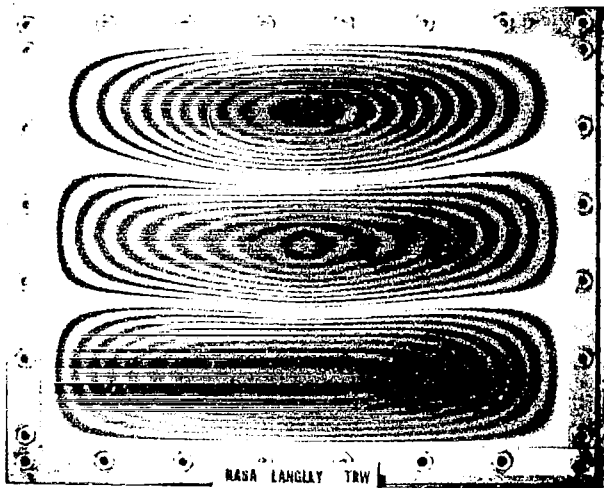
(a) m = 3, n = 1, f = 950 cps
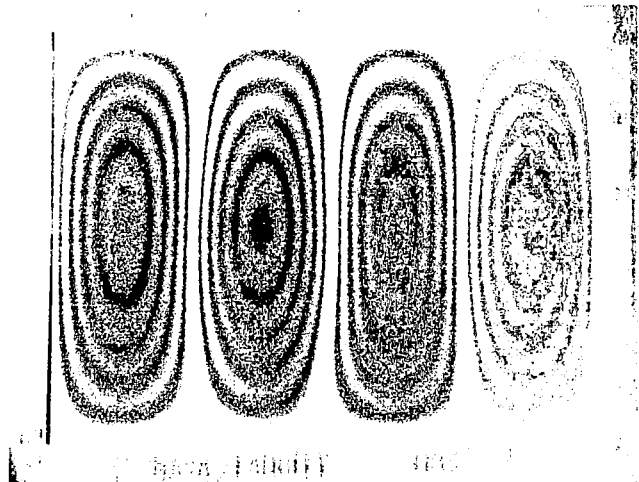
(b) m = 1, n = 4, f = 1,071 cps
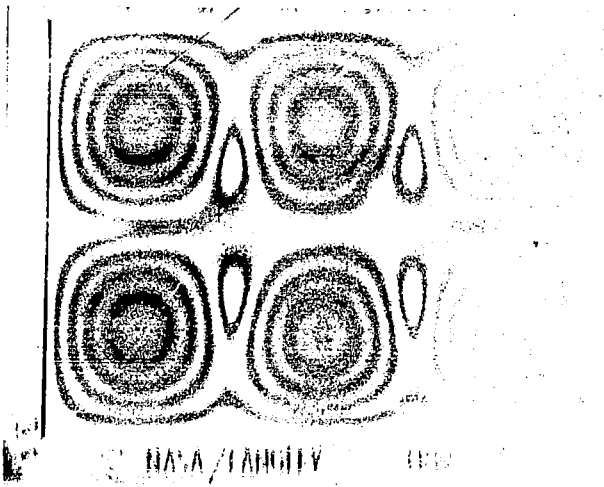
(c) m = 2, n = 3, f = 1,135cps
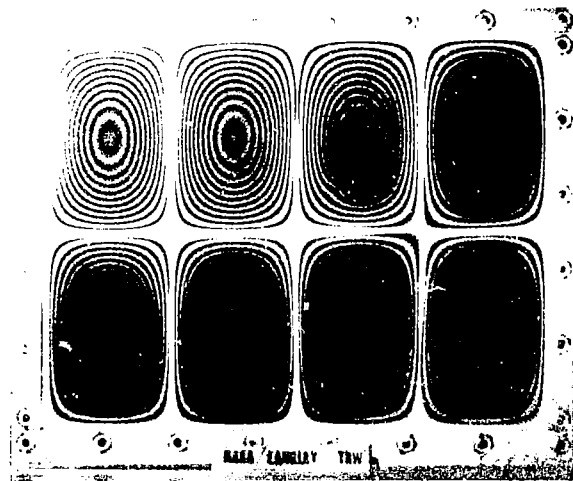
(d) m = 2, n = 4, f = 1,360 cps

Figure C2 - Plate Vibration Modes
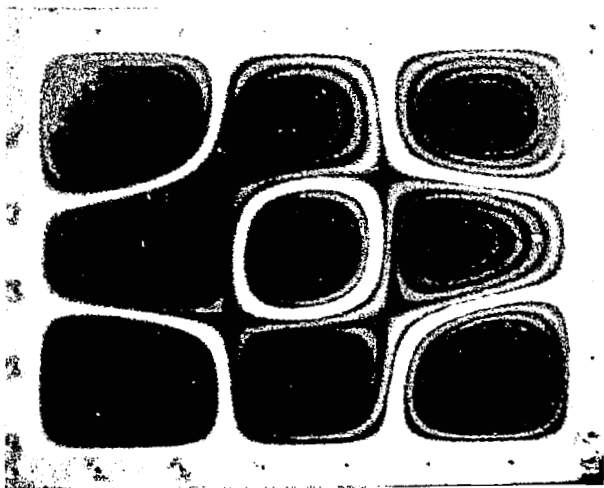
(a) m = 3, n = 3, f = 1,421 cps
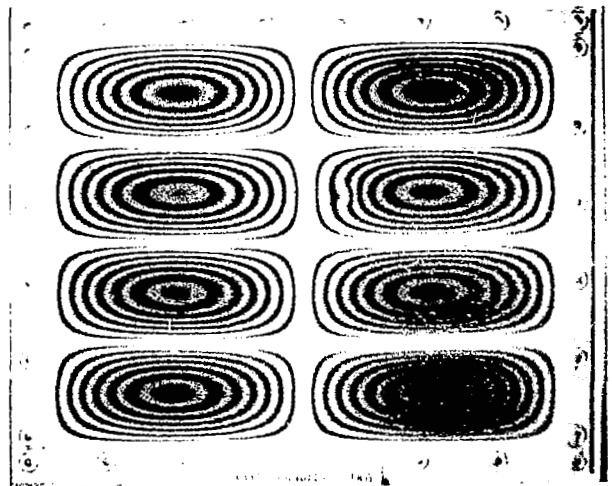
(b) m = 4, n = 2, f = 1,790 cps.
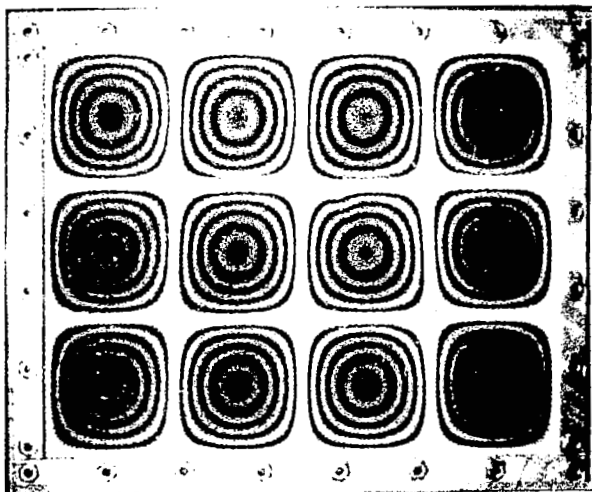
(c) m = 4, n = 4, f = 1,831 cps
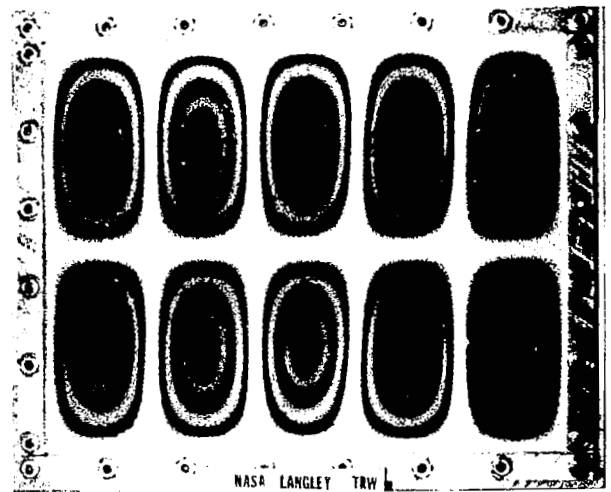
(d) m = 2, n = 5, f = 1,892 cps

Figure C3 - Plate Vibration Modes
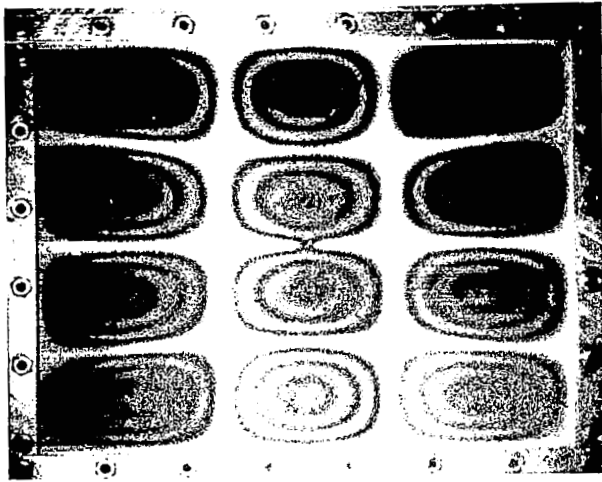
(a) m = 4, n = 3, f = 2,074 cps
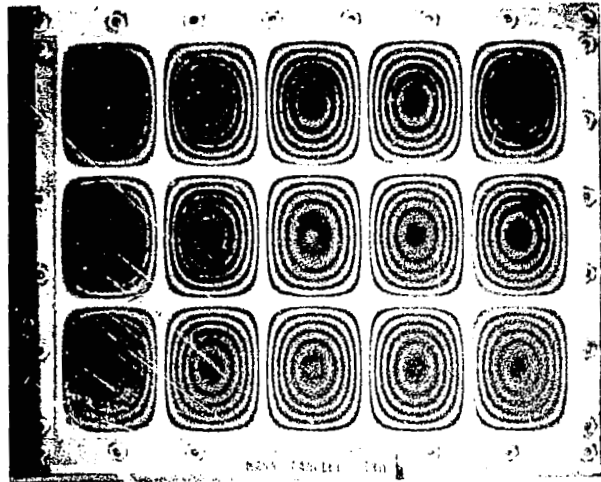
(b) m = 3, n = 5, f = 2,368 cps
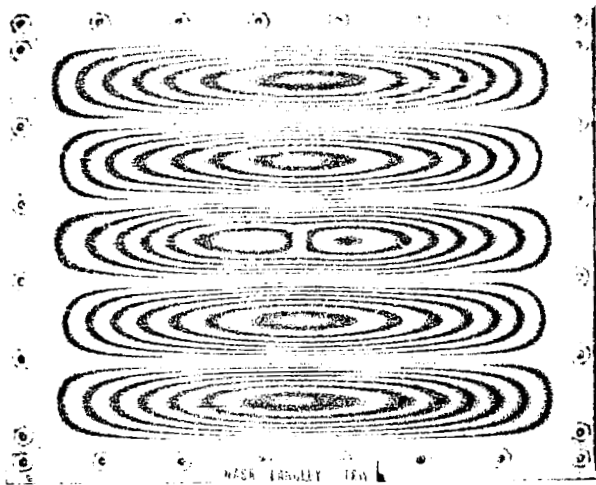
(c) m = 5, n = 1, f = 2,465 cps
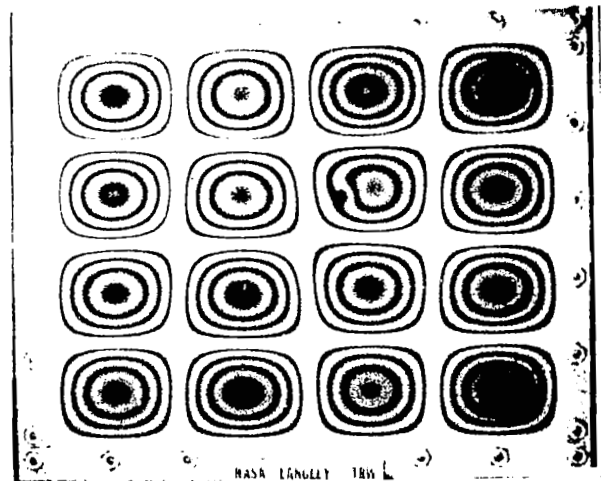
(d) m = 4, n = 4, f = 2,481 cps

Figure C4 - Plate Vibration Modes

123
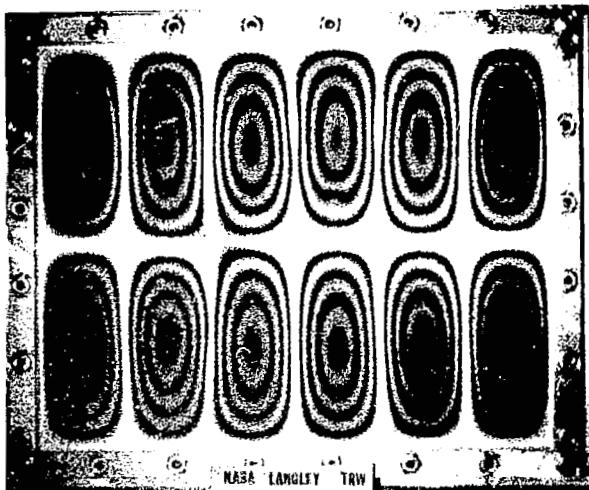
(a) m = 2, n = 6, f = 2,546 cps
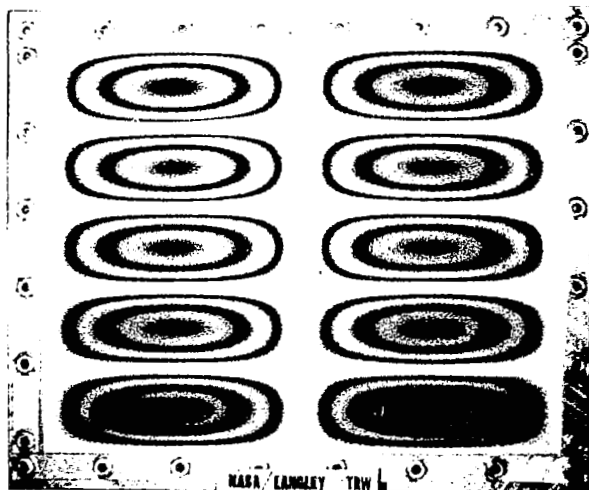
(b) m = 5, n = 2, f = 2625 cps
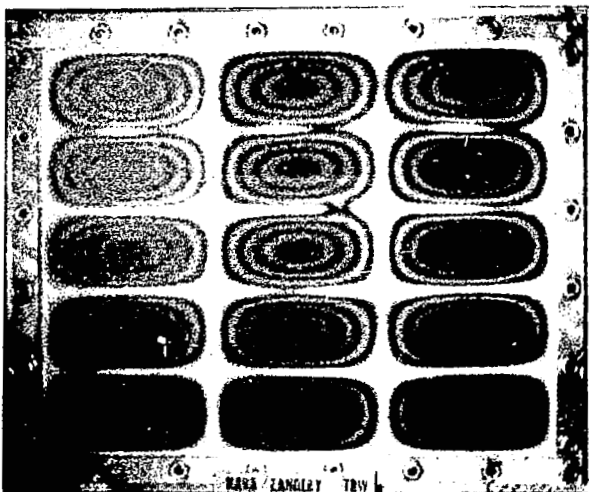
(c) m = 5, n - 3, f = 2,915 cps
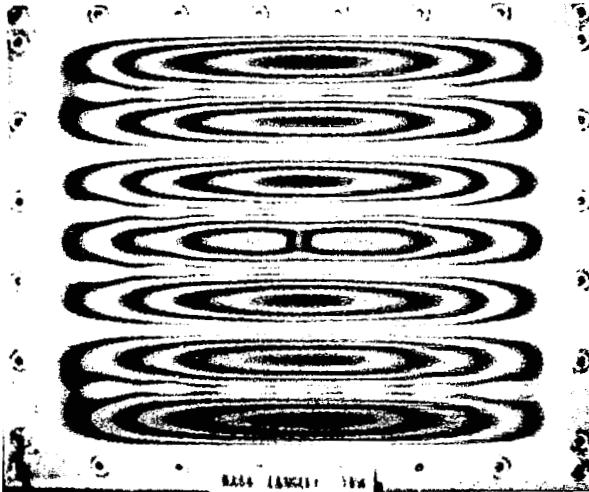
(d) m - 7, n = 1, f = 3,058 cps

Figure C5 - Plate Vibration Modes
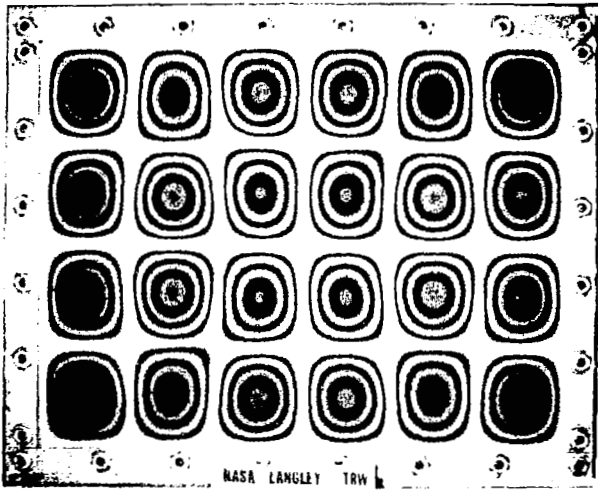
(a) m = 4, n = 6, f = 3,668 cps
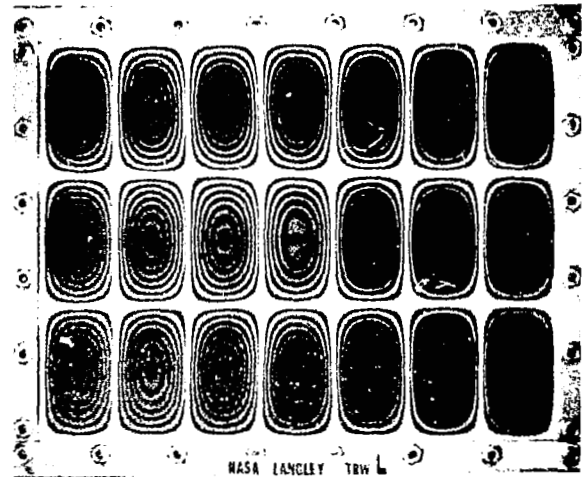
(b) m = 3, n = 7, f = 3780 cps
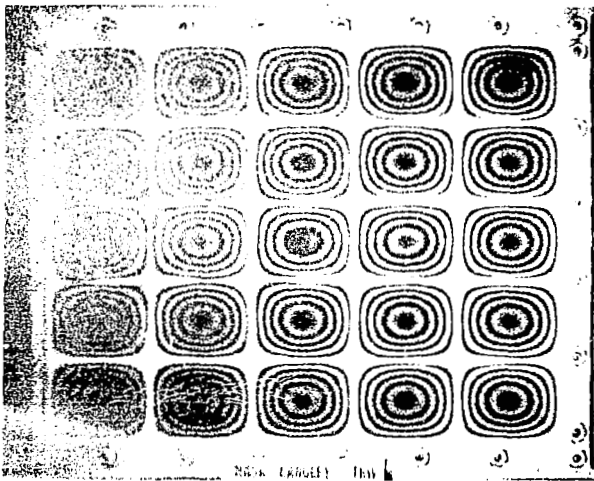
(c) m = 5, n = 5, f = 3,845 cps
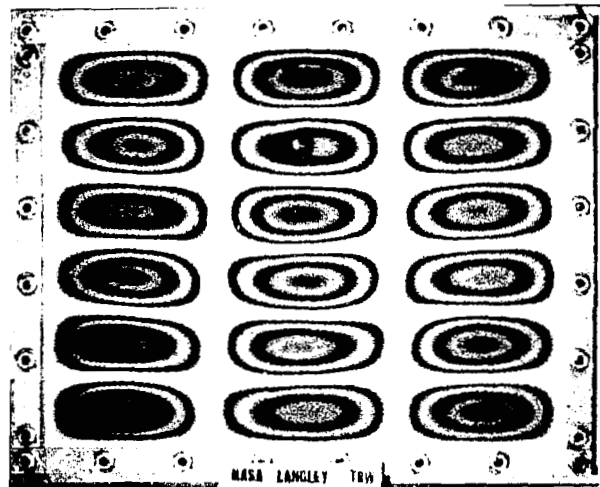
(d) m = 6, n = 3, f = 3,948 cps

Figure C6 - Plate Vibration Modes

125
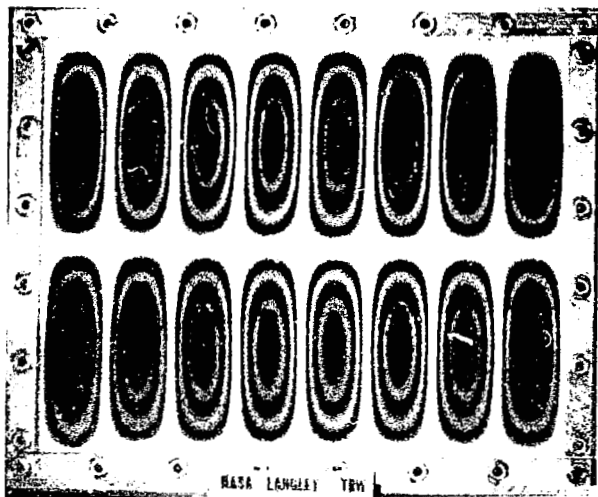
(a) m = 2, n = 8, f = 4198 cps
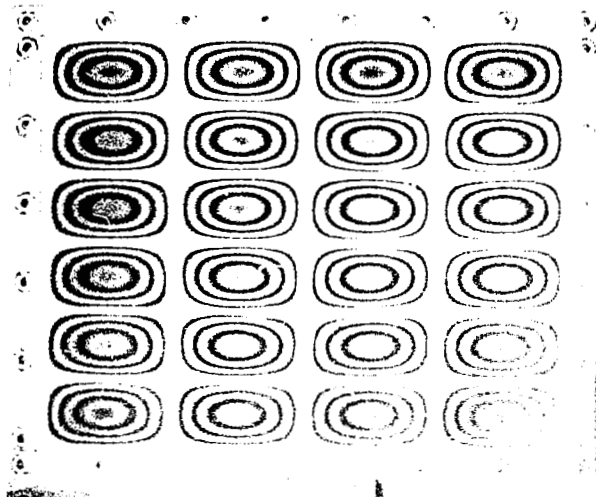
(b) m = 6, n = 4, f = 4,333 cps
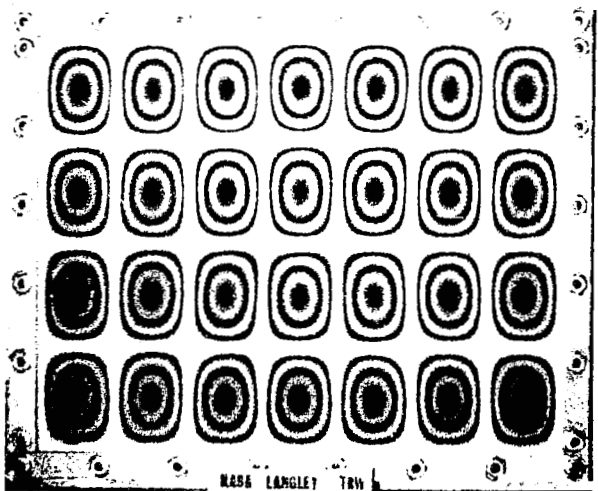
(c) m = 4, n = 7, f = 4,489 cps
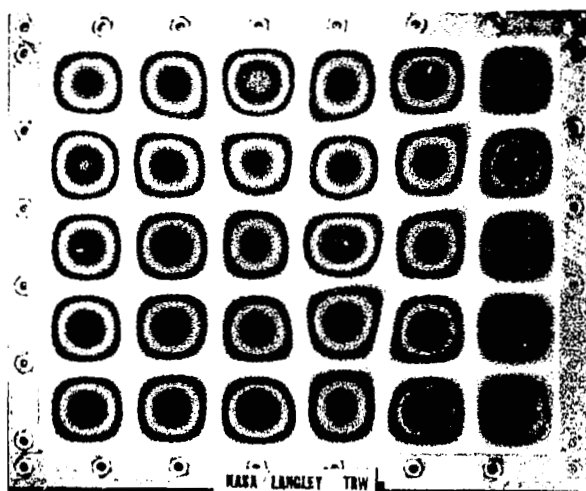
(d) m = 5, n = 6, f = 4,489 cps

Figure C7 - Plate Vibration Modes
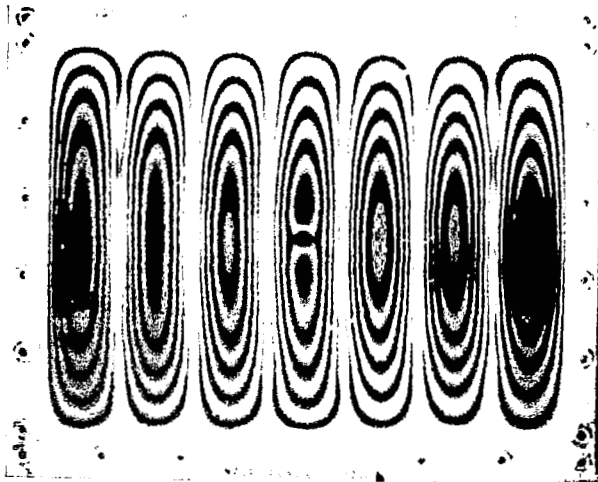
(a)   m = 1, n = 7,   f = 4,682 cps

(b)   m = 6, n = 5,   f = 4,868 cps
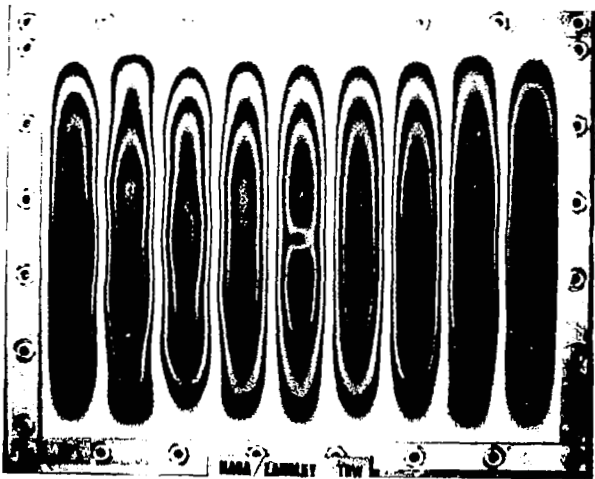
(c)   m = 1, n = 9,   f = 4,949 cps
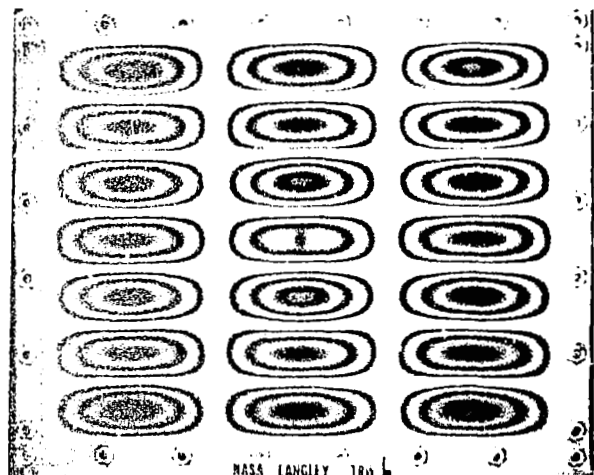
(d)   m = 7, n = 3,   f = 5,132 cps

Figure C8 - Plate Vibration Modes

127
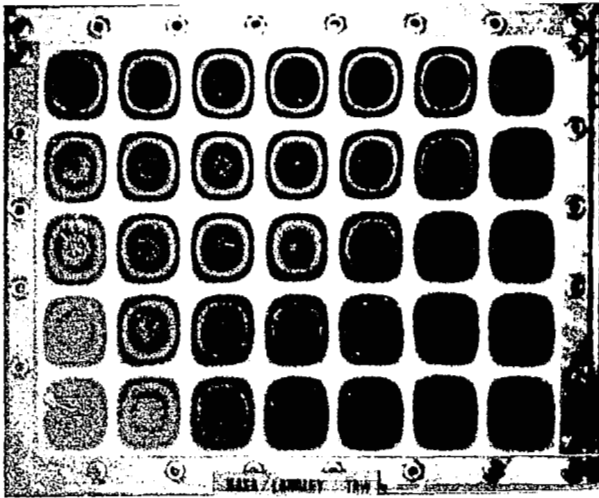
(a) m = 5, n = 7, f = 5,256 cps
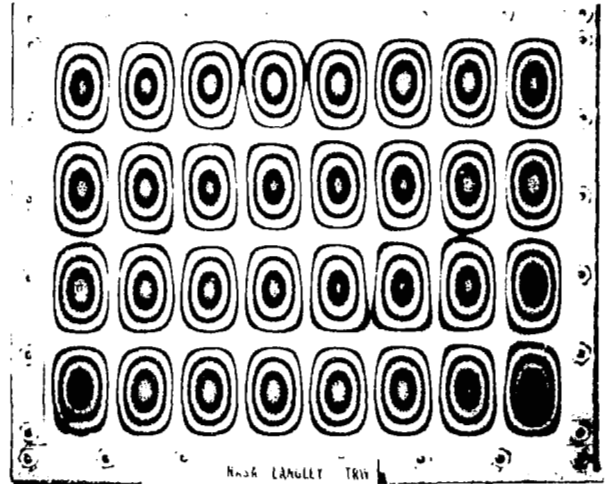
(b) m = 4, n = 8, f = 5306 cps
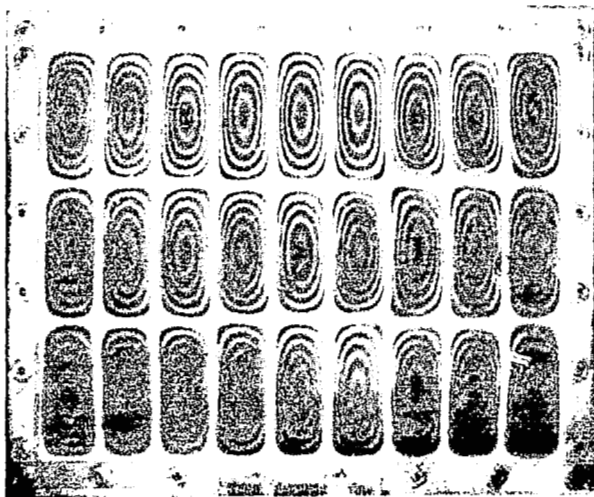
(c) m = 3, n = 9, f = 5,648 cps
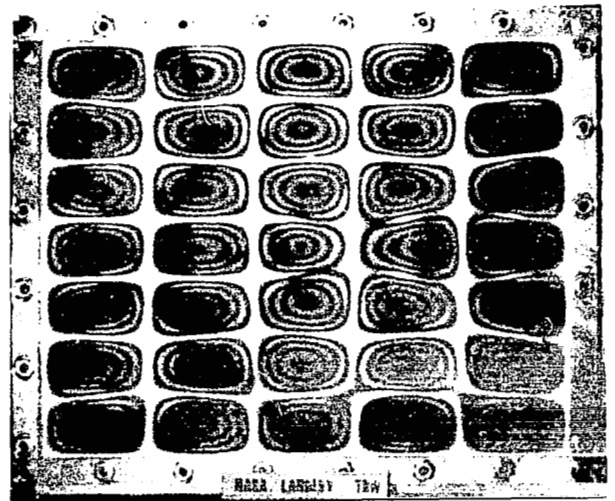
(d) m = 7, n = 5, f = 6,019 cps

Figure C9 - Plate Vibration Modes

128
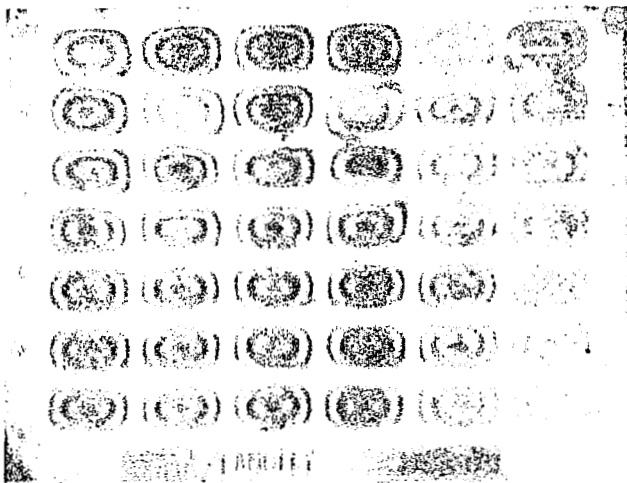
(a) m = 7, n = 6, f = 6,712 cps
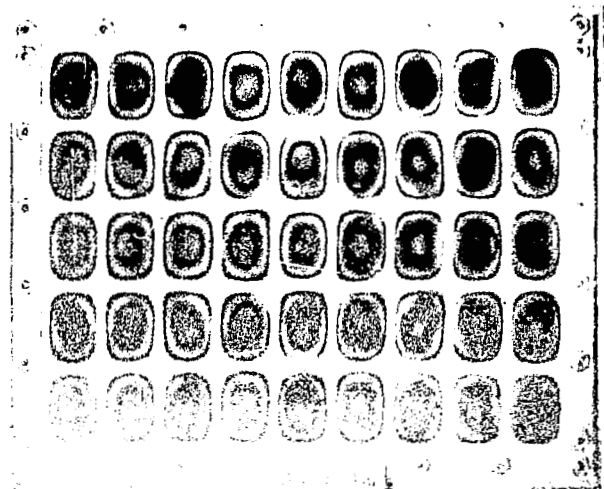
(b) m = 5, n = 9, f = 7147 cps
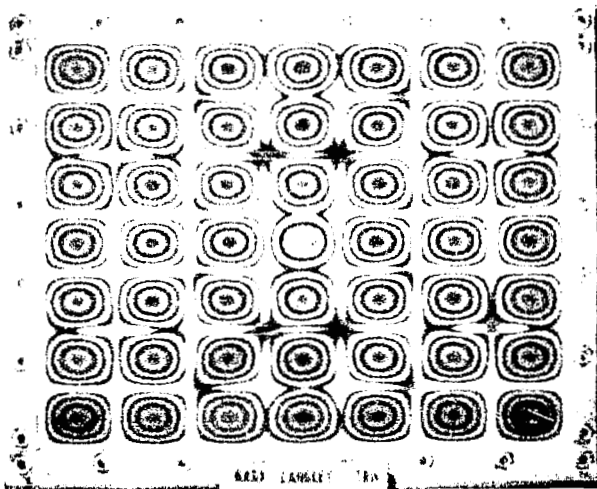
(c) m = 7, n = 7, f = 7470 cps
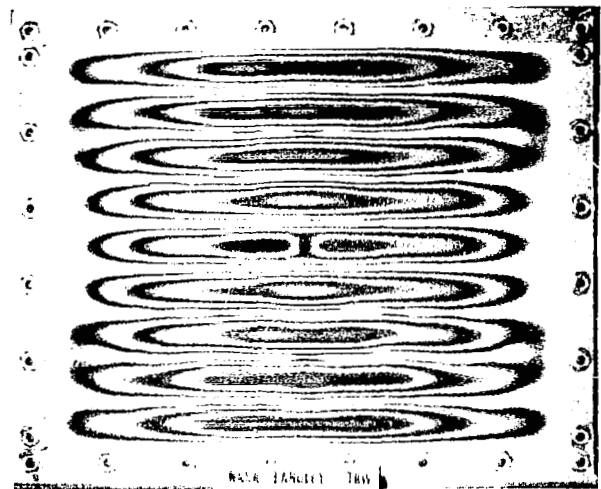
(d) m = 9, n = 1, f = 7,647 cps

Figure C10 - Plate Vibration Modes

129
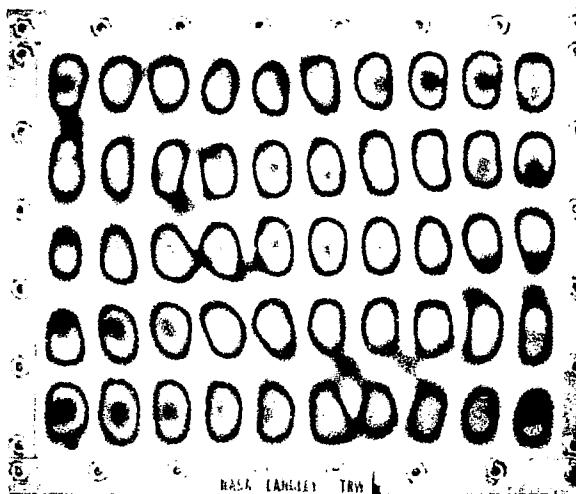
(a) m = 5, n = 10, f = 8,255 cps
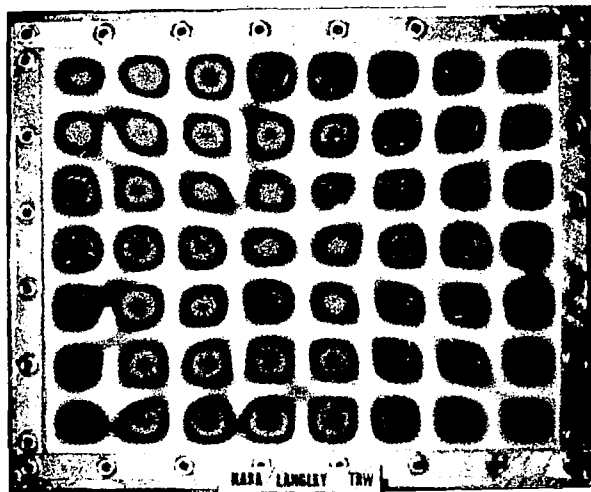
(b) m = 7, n = 8, f = 8,353 cps
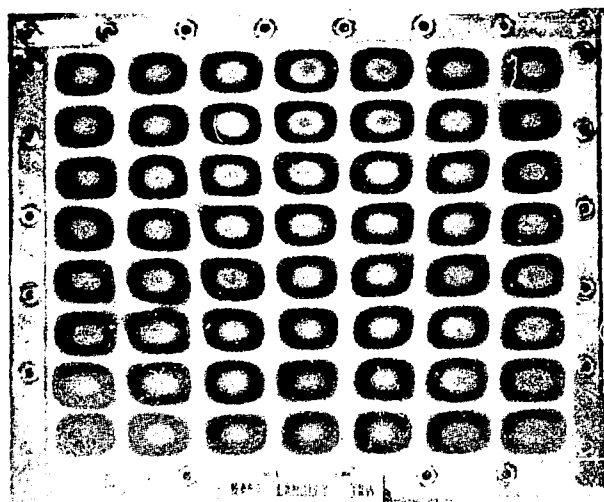
(c) m = 8, n = 7, f = 8,839 cps
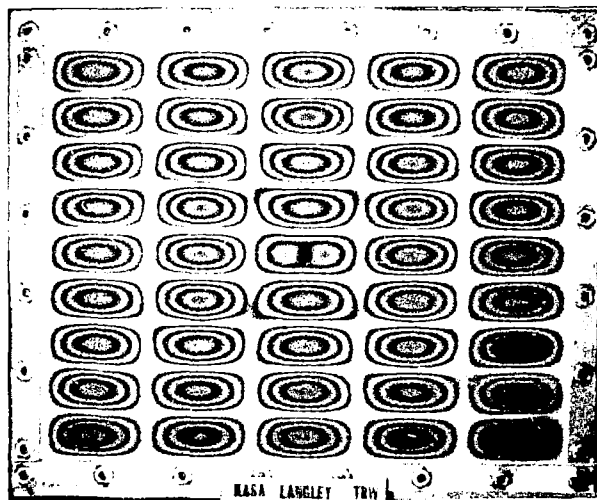
(d) m = 9, n = 5, f = 9,026 cps

Figure C11 - Plate Vibration Modes
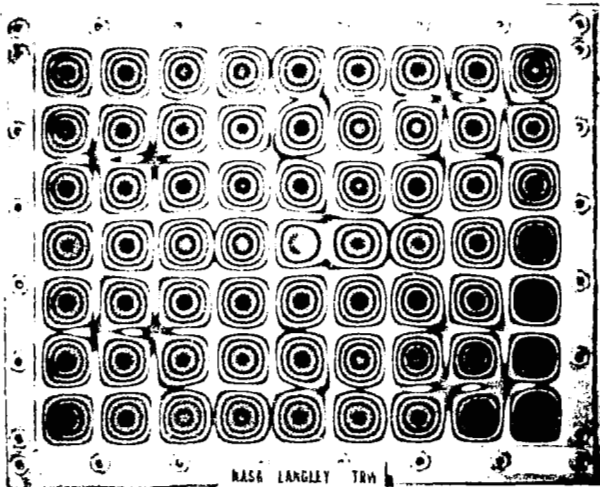
(a) $m = 7, n = 9,$ $f = 9,353$ cps
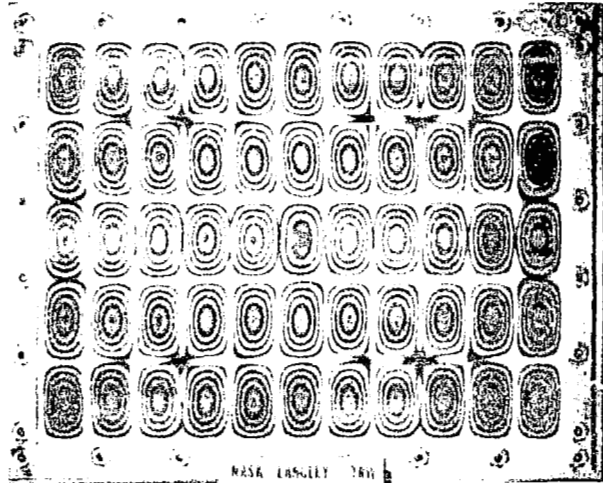
(b) $m = 5, n = 11,$ $f = 9,493$ cps
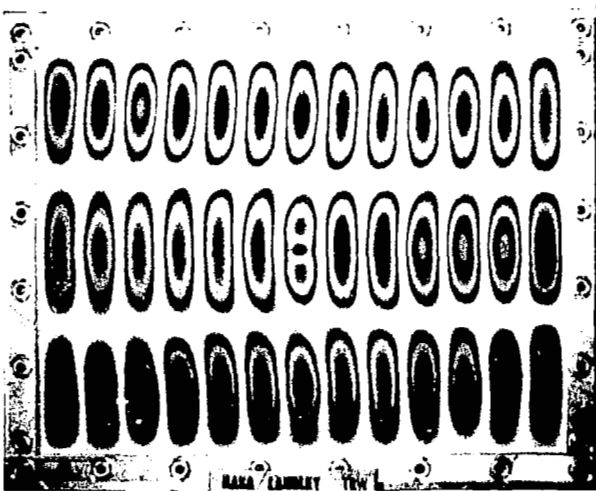
(c) $m = 9, n = 7,$ $f = 10,414$ cps
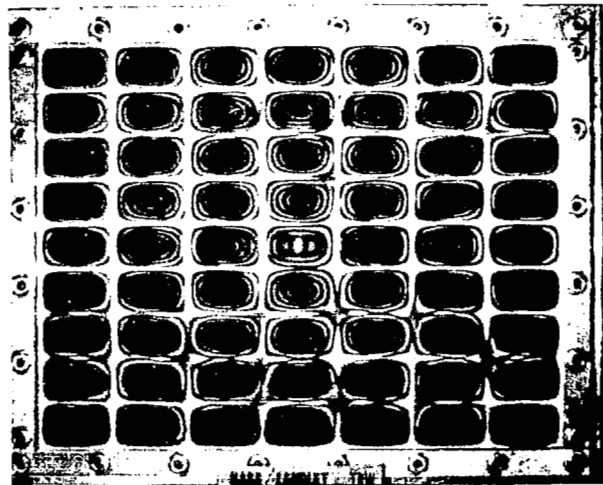
(d) $m = 3, n = 13,$ $f = 10,886$ cps

Figure C12 - Plate Vibration Modes

131
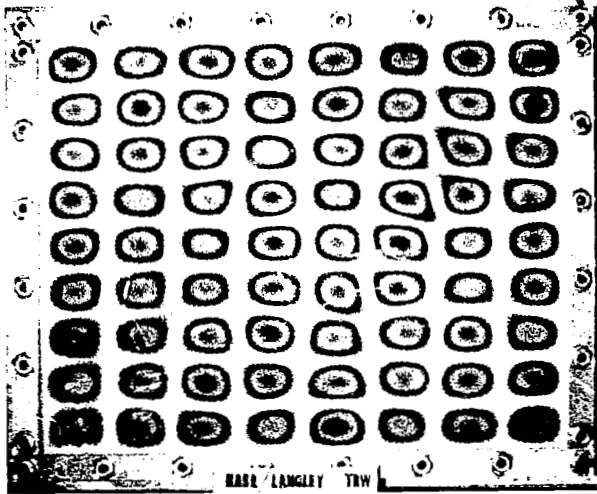
(a) m = 9, n = 8, f = 11,295 cps
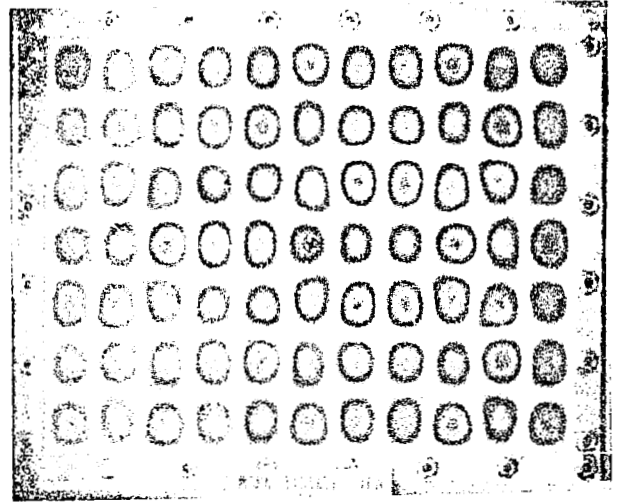
(b) m = 7, n = 11, f = 11,676 cps
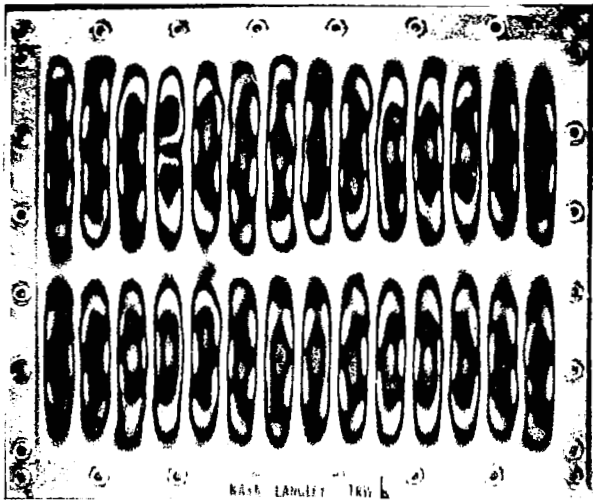
(c) m = 2, n = 4, f = 12,001 cps
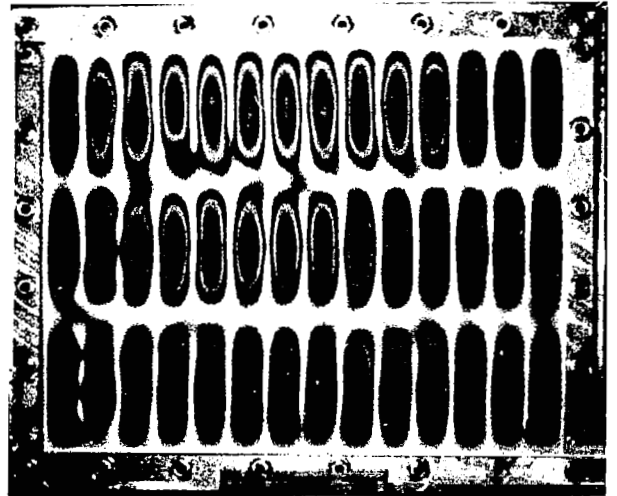
(d) m = 3, n = 14, f = 12,428 cps

Figure C13 - Plate Vibration Modes
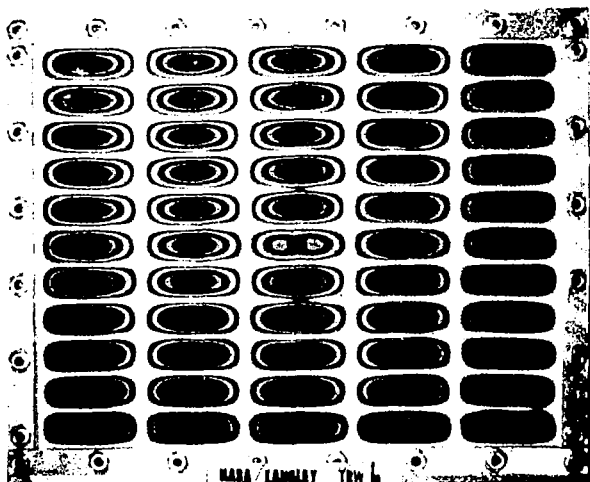
(a) m = 11, n = 5, f = 12,670 cps

(b) m = 6, n = 13, f = 13,238 cps
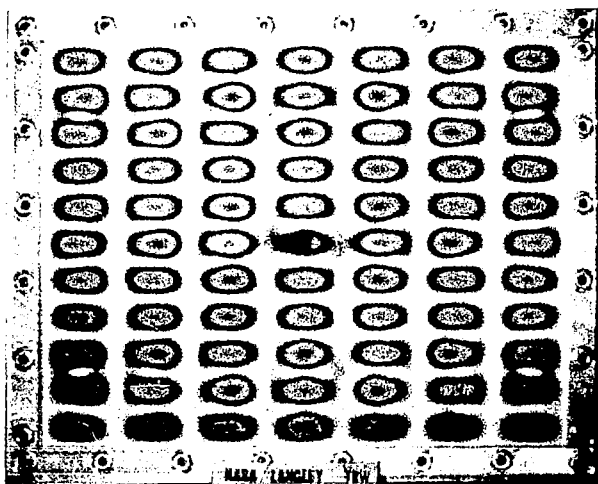
(c) m = 11, n = 7, f = 14,053 cps
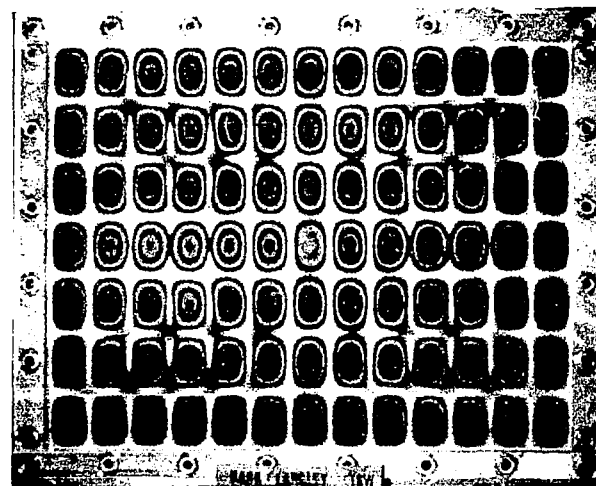
(d) m = 7, n = 13, f = 14,464 cps

Figure C14 - Plate Vibration Modes

133
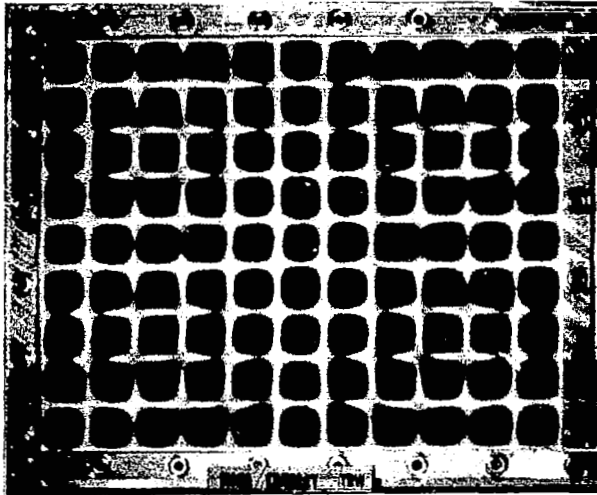
(a) m = 9, n = 11, f = 14,566 cps
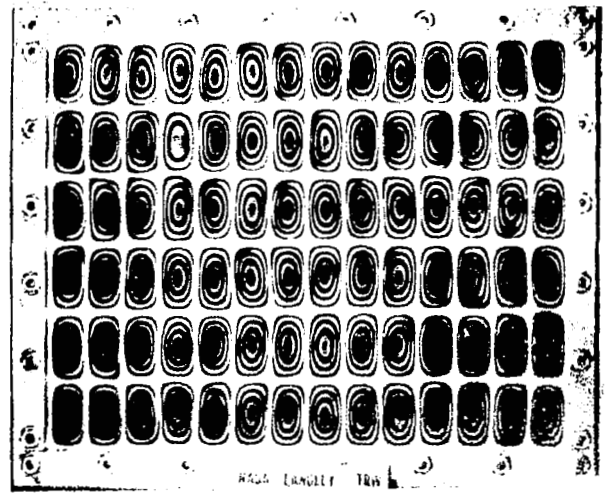
(b) m = 6, n = 14, f = 14,789 cps
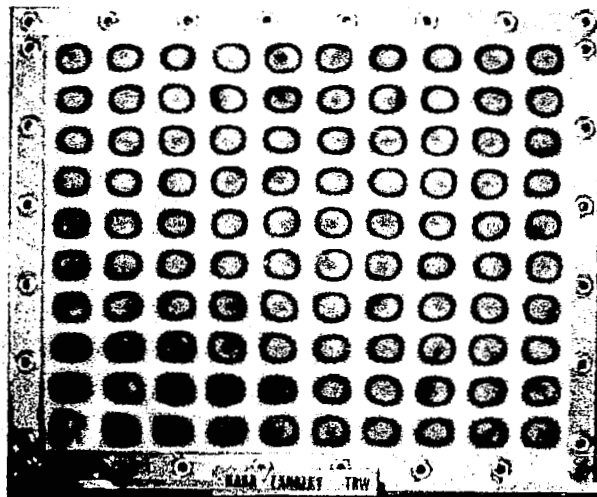
(c) m = 10, n = 10, f = 15,080 cps
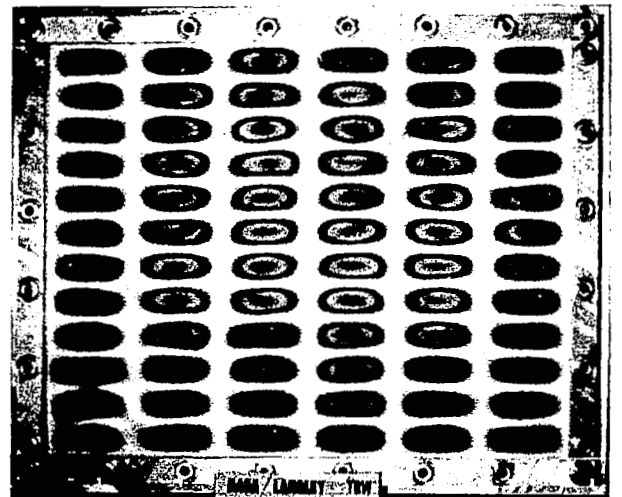
(d) m = 12, n = 6, f = 15,360 cps

Figure C15 - Plate Vibration Modes

134
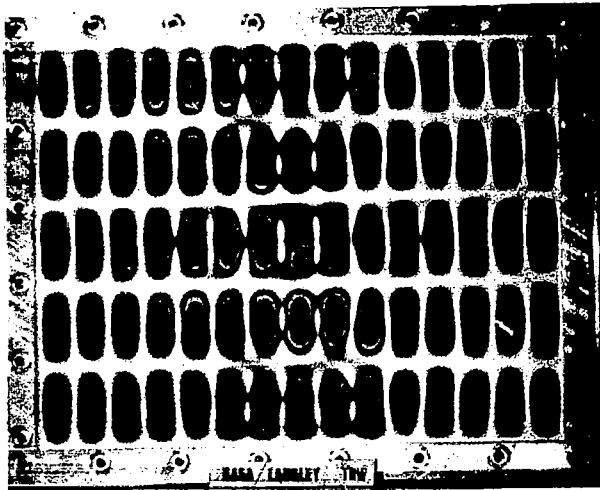
(a) m = 5, n = 15, f = 15,558 cps
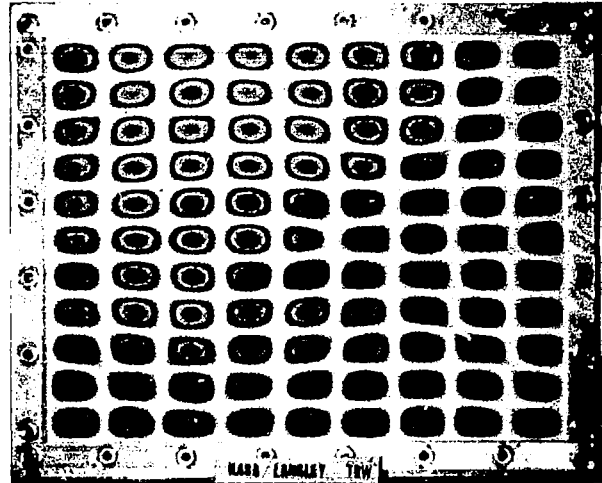
(b) m = 11, n = 9, f = 15,871 cps
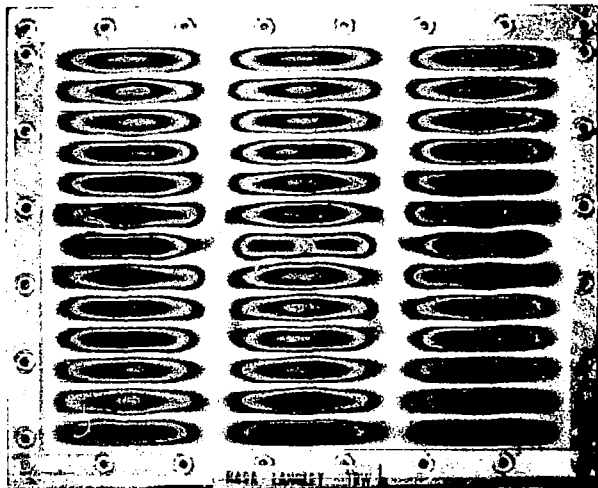
(c) m = 13, n = 3, f = 16,099 cps
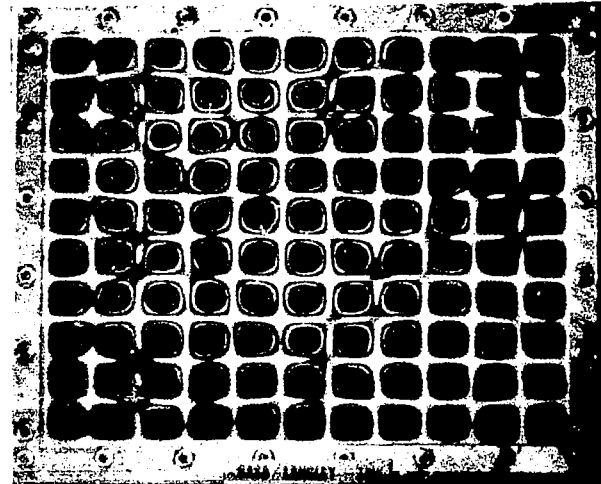
(d) m = 10, n = 11, f = 16, 276 cps

Figure C16 - Plate Vibration Modes

135

(a) m = 6, n = 15, f = 16,502 cps
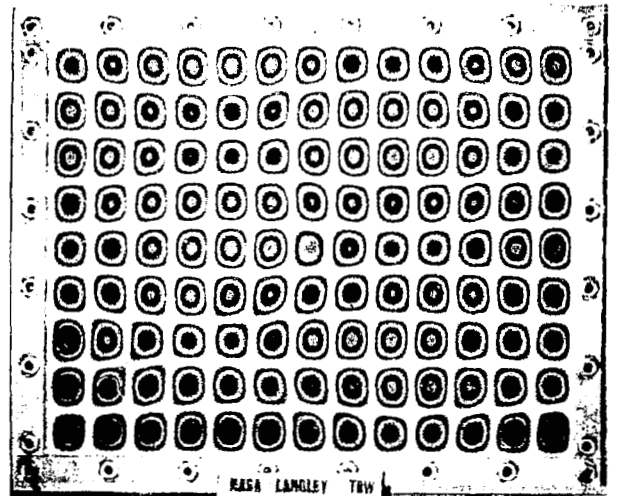
(b) m = 9, n = 13, f = 17,327 cps
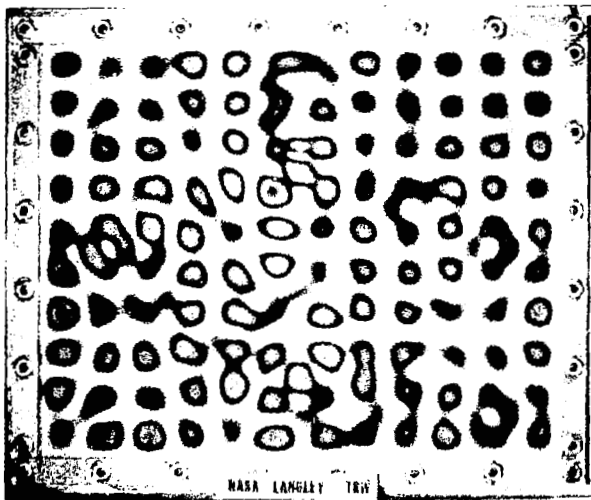
(c) m = 10, n = 12, f = 17,577 cps
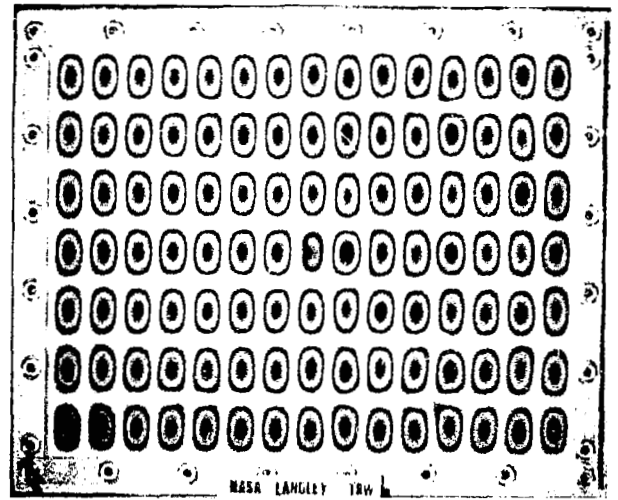
(d) m = 7, n = 15, f = 17,676 cps

Figure C17 - Plate Vibration Modes
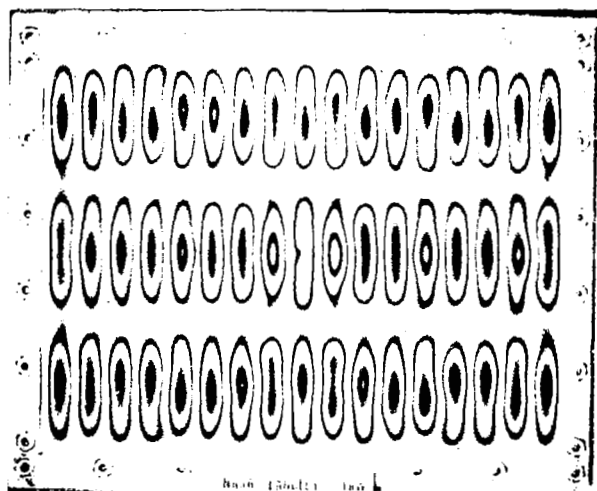
(a)   m = 3, n = 17,   f = 17,787 cps
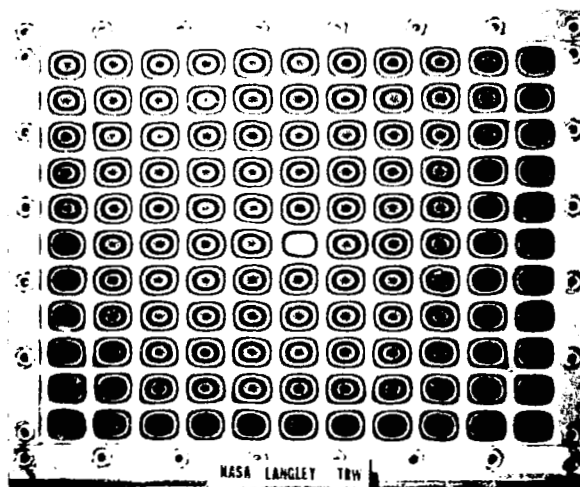
(b)   m = 11, n = 11,   f = 18,158 cps
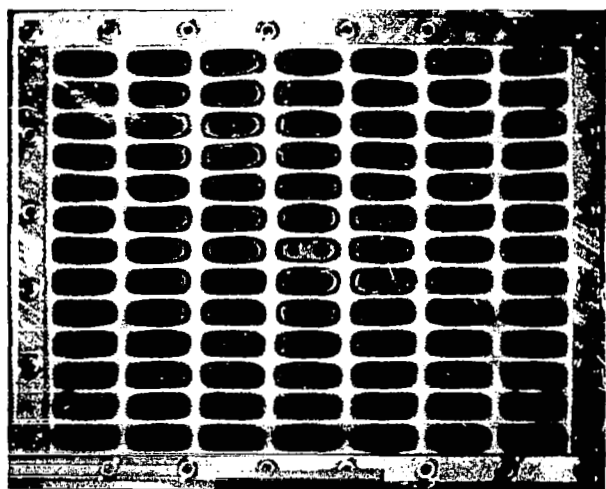
(c)   m = 13, n = 7,   f = 18,362 cps
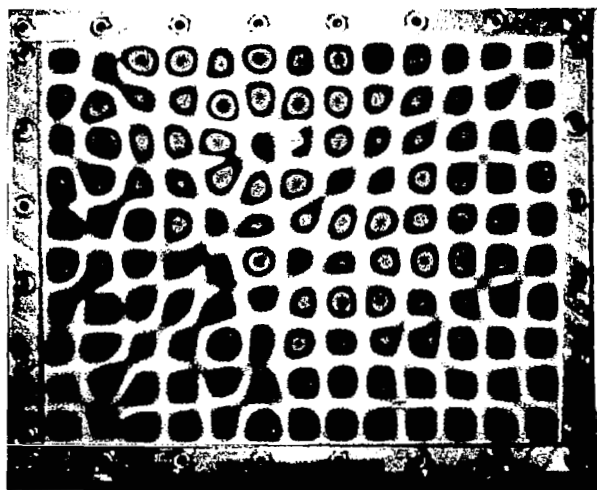
(d)   m = 10, n = 13,   f = 18,997 cps

Figure C18 - Plate Vibration Modes

137
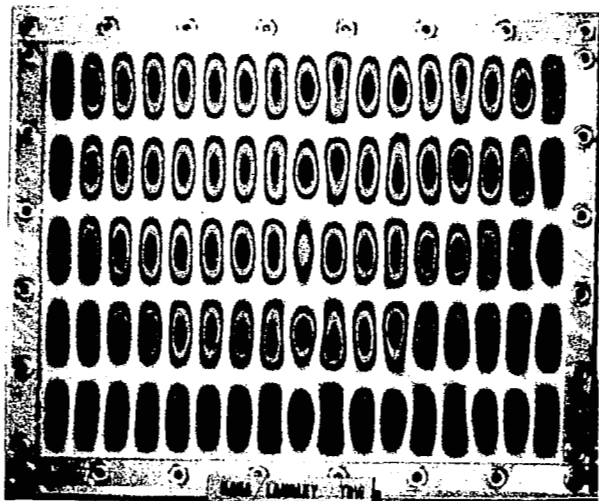
(a) m = 5, n = 17, f = 19,181 cps
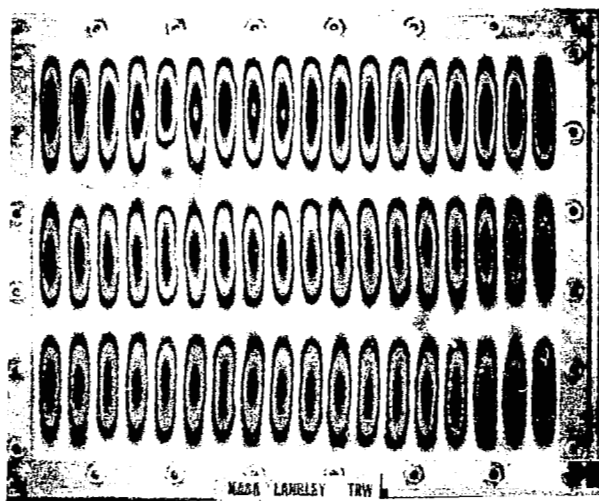
(b) m = 3, n = 18, f = 19,788 cps
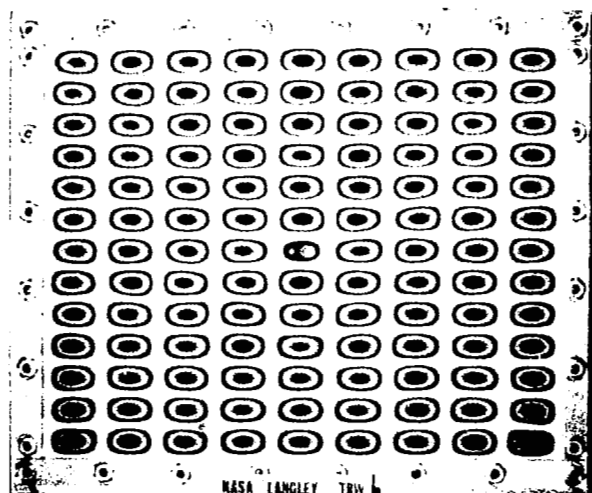
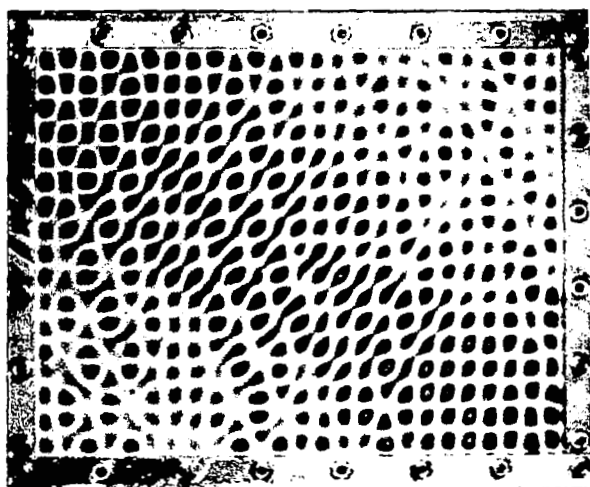(c) m = 13, n = 9, f = 20,164 cps
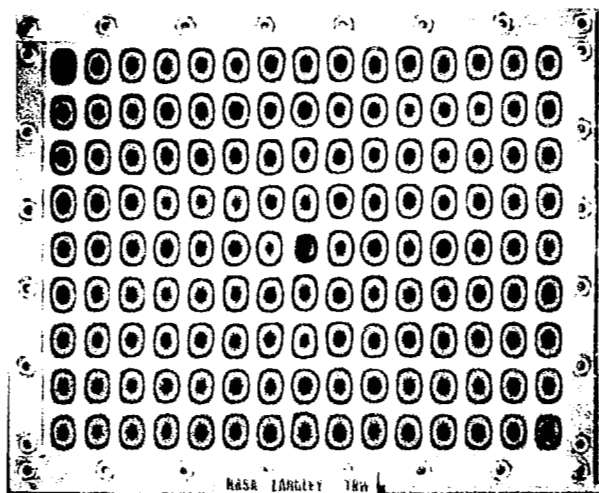
(d) m = 9, n = 15, f = 20,524 cps

Figure C19 - Plate Vibration Modes
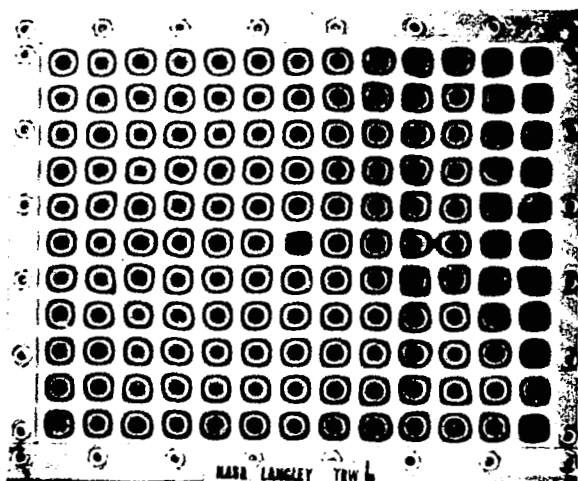
(a) m ≈ 11, n = 13, f = 20,892 cps
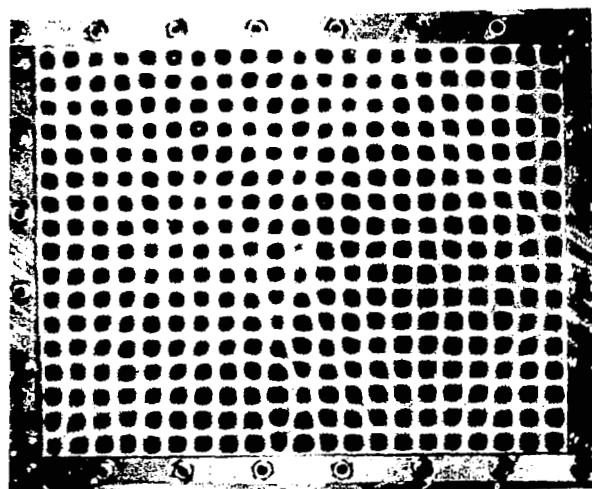
(b) m = 17, n = 21, f = 50,104 cps

(c) m = 17, n = 25, f ≈ 59,682 cps

Figure C20 - Plate Vibration Modes

139

APPENDIX D

TRANSVERSE WAVE TESTS
(1/4 – inch Steel Pendulum Ball)

This appendix contains the results of wave propagation tests made using a 1/4 – inch steel pendulum ball. This small ball was used to reduce the duration of impact (time in contact) to 30 μsec. The associated impulse imparted to the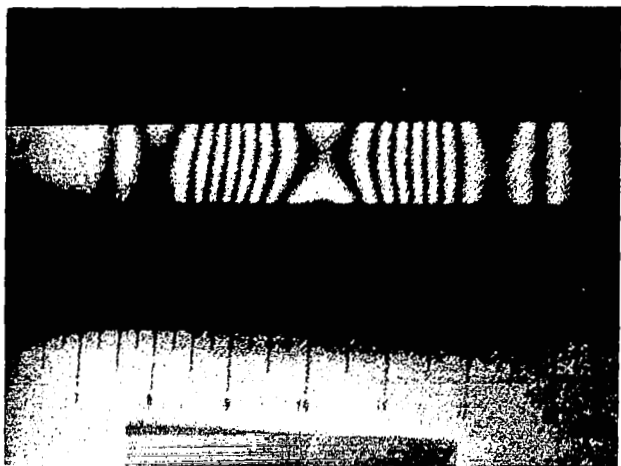 beam was approximately $I_o = 2.92 \times 10^{-4}$ lb-sec. The accompanying photographs were made from interferograms taken at times of 12.5, 25, 50 and 70 μsec after impact. These results are intended to supplement Figures 40, 41, and 42, which are discussed in the body of the report.
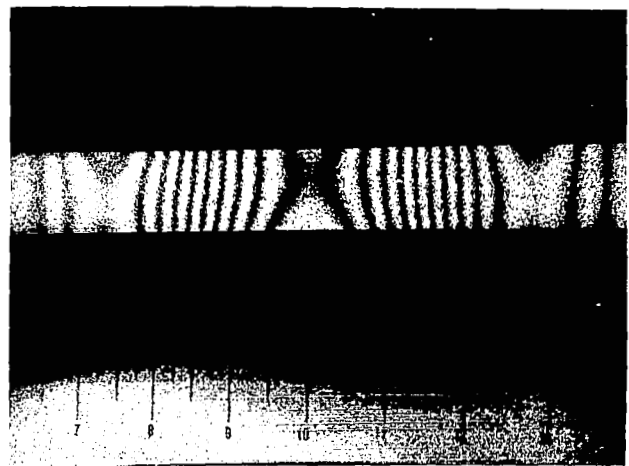
(a) 12.5 µsec after impact
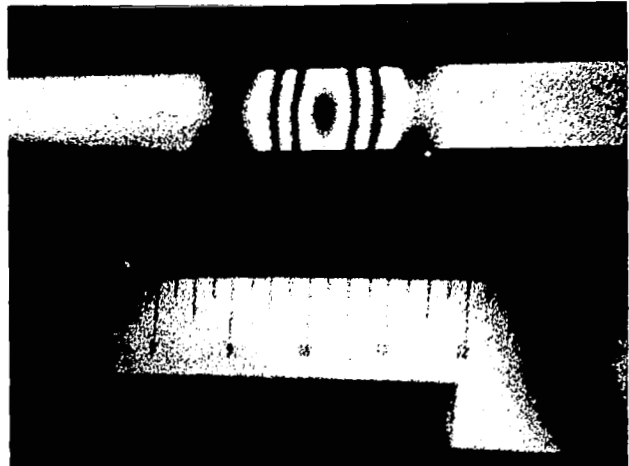
(b) 25 µsec after impact

(c) 50 µsec after impact

(d) 70 µsec after impact

Figure D1 - Bending Wave in a Long Beam
(1/4" - Diameter Pendulum Ball)